Electromagnetic Interrogation of Dielectric Materials [1]

H.T. Banks M.W. Buksas

Center for Research in Scientific Computation
North Carolina State University
Raleigh, NC

[1]Research supported in part by the U.S. Air Force Office of Scientific Research under grants AFSOR F49620-95-1-0236, AFSOR F49620-98-1-0180, AFSOR F49620-95-1-0375 and in part by the US Depertment of Education under a GAANN Fellowship through grant P200A40730.

Abstract

We investigate time domain based electromagnetic inverse problems. This is done in the context of general polarization models (which include the familiar Debye and Lorentz models as special cases) for dielectric materials. A one-dimensional model based on time-windowed pulsed inputs is formulated and well-posedness results are given for the simulation problem. Numerical investigations of problems involving estimation of dielectric parameters in a slab geometry are carried out. We also present results for use of secondary reflections to estimate geometry of the slab.

1 Background

A survey of the mathematical literature reveals considerable interest in the identification of material parameters describing electromagnetic phenomenon. For our purposes, we categorize the materials and the models employed to describe them as either dispersive or non-dispersive, where dispersive materials are those in which electromagnetic waves of different frequencies have different phase velocities. When modeled in the frequency domain, this is manifested as parameters which depend explicitly on frequency. In time domain models, the same phenomenon can be captured with constitutive laws in which the electric and/or the magnetic polarizations are expressed in terms of the convolution of the history of the electric and magnetic fields. The equivalence of the two in the case of electric polarization dispersion is shown by Jackson [Jac, pp.306]

Forward problems in this field are dominated by one dimensional scattering problems where planar electromagnetic waves impinge on dielectric slabs. In a series of four papers [KK, KK2, KK3, KK4] Kristenson and Krueger examine this problem with a wave splitting technique and the derivation of scattering operators which satisfy imbedding equations. The reconstruction of the functions representing the physical parameters proceeds from the imbedding equations and a scheme is presented which is shown to be robust in the presence of noise. The physical model covers stratified media, meaning that the material is inhomogeneous in the direction of the propagation of the waves.

A similar approach is applied to a slightly different model by Weston [Wes] who considers a dissipative wave equation equivalent to the the problem of planar waves in stratified media. These results are extended by Krueger [Kru, Kru2, Kru3] to cover media in multiple slabs, thus containing multiple discontunities in the material parameters. Corones and Sun [CS] use the same method of wave splitting and invariant imbedding to reconstruct coefficients in a one dimensional wave equation with a source term. In another paper, He and Ström [HS] also consider the scattering problem for stratified materials illuminated with waves generated by a magnetic dipole.

Some progress has also been made into more general geometries, largely due to the increasing sophistication of wave splitting techniques in higher dimensions. In a paper by Weston [Wes2] a decomposition of solutions of the dissipative wave equation in $\mathbb{R}^3$ is given and integro-differential equations are derived for the reflection operator. The reconstruction of the velocity and dissipation coefficients from the kernel of this operator are demonstrated.

Inverse problems involving dissipative materials follow a similar pattern of development in moving from one dimensional scattering with planar waves to more general settings. Beezley and Krueger [BK] began investigation into these problems by employing a method similar to the non-dispersive case in one dimension. Imbedding equations are derived for the reflection operator relating the incident and scattered parts of the split wave solution. The dielectric response kernel is reconstructed from the imbedding equations derived for homogeneous semi-infinite and finite slabs. The reconstruction is also carried out numerically in the presence of noise applied to the reflection kernel.

Well-posedness results for these problems are demonstrated by Bui [Bui] in which a time domain model involving both conductivity and electric polarization are considered. Theorems governing the existence, uniqueness and continuous dependence of solutions for both the forward and inverse problems are given.

In a different setting Sun [Sun] identifies the source current embedded inside a dispersive material using a time-domain approach. In a paper by Lerche [Ler] a different integral equation is derived relating the dielectric response function to an operator representing the frequency domain absorption characteristics of a material.

Wolfersdorf [Wol] extends these results to finite and semi-infinite slabs and derives exact solutions to the integral equations for the dielectric response.

A different geometry is considered by Kreider [Kri] who poses the problem of electromagnetic scattering in a stratified cylinder. The problem is also made one dimensional through angular symmetry of the cylinder and the fields. Unlike other problems with dispersive media, the material is inhomogeneous in space, although the dielectric parameter is restricted to functions which are separable between the variables of space and frequency: $\epsilon(x, \omega) = \epsilon_1(x)\epsilon_2(\omega)$.

Another problem which allows for spatially inhomogeneous dispersive materials is considered in [HFL]. Here an optimization approach is applied to match simulations to real and synthetic data. The constitutive equations permit convolution terms in both the electric polarization and the conductivity. The limitations of simultaneous reconstruction of the spatial and time-varying parts of the kernel functions is considered when both transmission and reflection data are available.

Another inhomogeneous two dimensional problem is considered by Colton and Monk [CM] who use a frequency domain approach in modeling the interaction of electromagnetic waves with human tissue for the detection of leukemia in bone marrow. The geometry of the medium is presumed known and the two dimensional domain is further partitioned into sub-domains of known geometry. The only unknowns are the constitutive parameters describing the bone marrow, and these are considered functions of space as well. The reconstruction of the bone marrow parameters is demonstrated and is shown to be robust in the presence of relative noise with magnitude as high as 1%.

Another problem motivated by an application is given in [RGKM] where models for the penetration of radar waves in soil are given. The ground is represented by a stratified semi-infinite slab and electromagnetic signals are generated by a circular loop of current. Well-posedness results are given for the inverse problem.

In summary, we note the differences between the physical models and the solution methods employed in these papers and our results which follow. A number of these papers differ from ours in that they deal with non-dispersive materials. This eliminates the need to reconstruct parameters which are functions of frequency or history kernels which are functions of time. These papers do consider materials which are inhomogeneous in the space variable, however, and while the model formulation is in the time domain, the forward and inverse problems are solved by wave-splitting and invariant imbedding techniques. A number of these papers consider physical problems similar to ours, in which planar electromagnetic waves impinge normally on slabs of material but progress has also been made into three dimensional settings for non-dispersive problems.

Among the papers which employ dispersive models, many differ from ours by using a frequency domain approach which is best suited for physical problems involving time-harmonic solutions. Among those treatments which use time-domain models, most use the wave splitting approach popular with the non-dispersive materials to formulate the forward and inverse problems. Only one paper [HFL] used an optimization approach and formulated an inverse problem using the time domain data itself. While this paper and others considered inhomogeneous materials, the geometry of the material slab is considered to be known. This differs from our problem in that we do not assume the thickness of the material slab is known *a priori* and attempt to identify this dimension along with the parameters describing the electromagnetic behavior.

2 Introduction and Problem Formulation

2.1 Motivation and the General Inverse Problem

The ability to interrogate the interior of tissues and other materials has applications to medical imaging and the early detection of anomalies. For example, the results we will present here suggest that the use of a metal tip catheter, threaded into a target organ such as the colon or arterial system, will provide the necessary localization of interrogating probes to allow practical diagnostics involving geometry. Furthermore, is it hoped that the *in vivo* dielectric properties of tissues and organs can be correlated with metabolic functioning. Hence the accurate determination of these dielectric properties can be employed in the evaluation of functional integrity of tissues and organs in subjects.

Other suggested applications for the technology developed here are non-destructive damage detection in aircraft, mine, ordinance and camouflage detection and subsurface and atmospheric environmental monitoring.

The goals of electromagnetic interrogation as presented here are twofold: the determination of both the geometry and dielectric properties of the materials under investigation. We consider the generalized problem depicted schematically in Figure 1. The domain Ω of the object under consideration has both a known and unknown portion of the boundary. The unknown portion $\Gamma(q)$ is presumed to be backed by a supraconductive material with an effectively infinite conductivity. On this boundary with outer normal $\hat{n}$, we thus have $\vec{E} \times \hat{n} = 0$ and $\vec{B} \cdot \hat{n} = 0$. Note that the unknown nature of the boundary is represented by its dependence on a set of parameters q which are to be determined to establish the geometry of the object.

The electric and magnetic fields inside Ω and exterior to Ω (this region will be denoted Ω_0) are governed by the macroscopic Maxwell's equations [Jac, Bal, St]. To

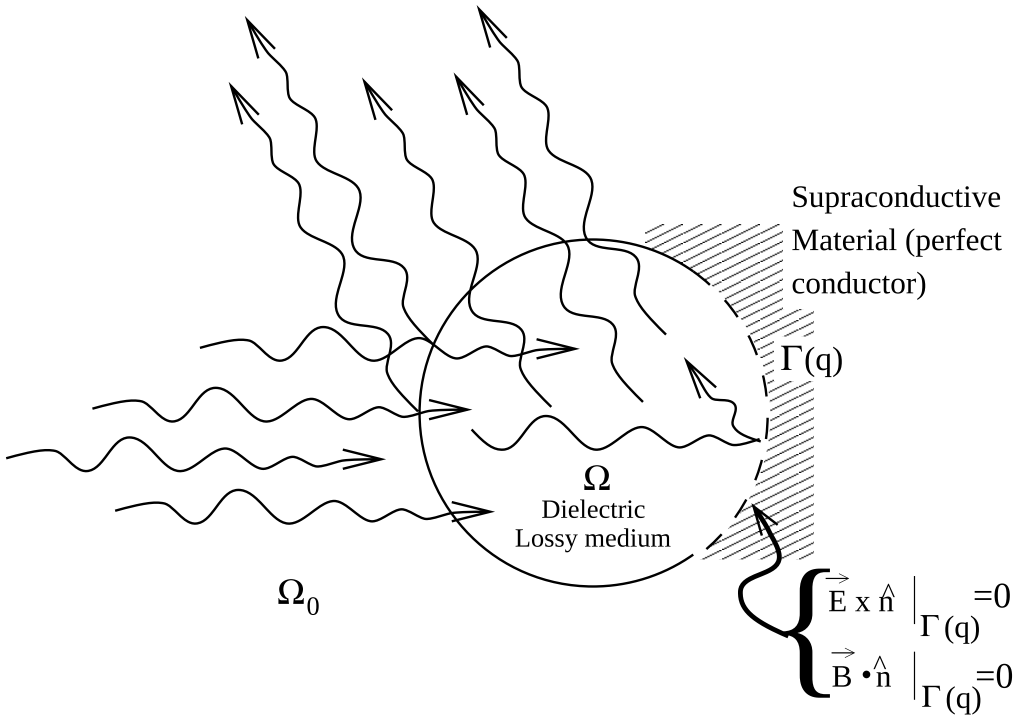

Figure 1: Schematic Diagram of Geometry

describe the electromagnetic behavior of complex materials, we express Maxwell's equations in a general form which includes terms for electric and magnetic polarization. We have

$$
\begin{aligned}
\nabla\times\vec{E} &= -\frac{\partial\vec{B}}{\partial t} & \qquad \vec{D} &= \epsilon_0\vec{E}+\vec{P}\\
\nabla\times\vec{H} &= \frac{\partial\vec{D}}{\partial t}+\vec{J} & \vec{B} &= \mu_0\vec{H}+\mu_0\vec{M}\\
\nabla\cdot\vec{D} &= \rho & \vec{J} &= \vec{J}_c+\vec{J}_s\\
\nabla\cdot\vec{B} &= 0.
\end{aligned}
$$

The vector-valued functions $\vec{E}$ and $\vec{H}$ represent the strengths of the electric and magnetic fields respectively, while $\vec{D}$ and $\vec{B}$ are the electric and magnetic flux densities respectively. The two current contributions are denoted by $\vec{J}_c$, the conduction current density, and $\vec{J}_s$, a source current density. The electric and magnetic polarizations are represented by $\vec{P}$ and $\vec{M}$, respectively . The scalar quantity ρ represents the density of electric charges unaccounted for in the electric polarization.

The three quantities $\vec{M}, \vec{P}$ and $\vec{J}_c$ embody the behavior of the material in response to the electromagnetic fields. Additional material-dependent equations (constitutive laws) are required to determine their dependence on the components of the fields $\vec{E}$ and $\vec{H}$. The dependence of these equations on the material is reflected both in the choice of a mathematical model and in the parameters (possibly functions) appearing in the model. Estimation of these parameters are the goals in the inverse problems we formulate below.

The region Ω_0 external to the medium is treated as empty space and is devoid of conductivity or polarization effects, hence $\vec{M} = 0, \vec{P} = 0$ and $\vec{J}_c = 0$ in Ω_0, and all of the necessary parameters for the determination of the fields are assumed known in this domain. The source current density term $\vec{J}_s$ will also be non-zero only at points in Ω_0. The presence of an alternating current source will generate the electromagnetic waves in this domain which illuminate the target medium Ω.

We make certain assumptions about the material which are reflected in the constitutive relations in the domain Ω. For the biological media of interest to us, we can neglect magnetic effects; we also assume that Ohm's law governs the electric conductivity. Hence for $\vec{x} \in \Omega$

$$\begin{aligned}\vec{M}(\vec{x}) &= 0 \\ \vec{J}_c(\vec{x}) &= \sigma \vec{E}(\vec{x}).\end{aligned}$$

The parameter σ is among those which need to be identified to determine the dielectric properties of the media. We note that for biomedical applications, the assumption of Ohm's law may not be appropriate (e.g., see [APM]) and one might need to also include a hysteretic dependency (in terms of a conductivity susceptibility kernel similar to the polarization kernel in (1) below). While such a more general conductivity relationship would add to the computational requirements, the ideas and techniques presented in this paper could readily be used to treat such an assumption. For simplicity we restrict ourselves to Ohmic conductivity in our discussion here.

To describe the behavior of the media's electric polarization, we employ a general integral equation model in which the polarization explicitly depends on the past history of the electric field. The resulting constitutive law can be given in terms of a *polarization or displacement susceptibility kernel* g by

$$\vec{P}(t,\vec{x}) = \int_0^t g(t-s,\vec{x})\vec{E}(s,\vec{x})ds. \tag{1}$$

We note that this model presupposes that $\vec{P}(0,\vec{x}) = 0$. In the electromagnetic literature, e.g., see [Jac, BK, APM], the relationship is often expressed as

$$\vec{P}(t,\vec{x}) = \int_0^\infty G(\xi,\vec{x})\vec{E}(t-\xi,\vec{x})d\xi$$

or as

$$\vec{P}(t,\vec{x}) = \int_0^t G(\xi,\vec{x})\vec{E}(t-\xi,\vec{x})d\xi$$

in the case of $\vec{E}(t,\vec{x}) = 0$ for $t < 0$ which is of interest here. These are both related to our formulation by the simple change of variables: $s = t - \xi$. We prefer our form of the equation since then any time derivatives are borne by the kernel function g and not the variable E. Specifically, under (1) the term $\frac{\partial^2\vec{P}}{\partial t^2}(t,\vec{x}) = \ddot{\vec{P}}(t,\vec{x})$, which will appear in subsequent equations, is given by

$$\ddot{\vec{P}}(t,\vec{x}) = \int_0^t \ddot{g}(t-s,\vec{x})\vec{E}(s,\vec{x})ds + g(0,\vec{x})\dot{\vec{E}}(t,\vec{x}) + \dot{g}(0,\vec{x})\vec{E}(t,\vec{x}) \tag{2}$$

while the more traditional representation leads to

$$\ddot{\vec{P}}(t,\vec{x}) = \int_0^t G(\xi,\vec{x})\ddot{\vec{E}}(t-\xi,\vec{x})ds + G(t,\vec{x})\vec{E}(0,\vec{x}) + \dot{G}(t,\vec{x})\vec{E}(0,\vec{x}). \tag{3}$$

The presence of $\ddot{\vec{E}}$ under the integral term in equation (3) complicates the analysis and solution of the Maxwell's equations considerably. Although the first formulation leads to the additional terms $g(0,\vec{x})\dot{\vec{E}}(t,\vec{x})$ and $\dot{g}(0,\vec{x})\dot{\vec{E}}(t,\vec{x})$, as we shall see below, these terms cause no increase in the complexity of the problem analysis or computation.

We note that an attempt to include a component of the polarization which depends on the instantaneous value of the electric field would add a delta function in the time variable to the kernel function $g(s,\vec{x})$. This introduces some mathematical complexities which, for simplicity, we avoid by treating instantaneous polarization when it arises in a different, but completely equivalent, manner (i.e., by modifying the first term in the displacement/electric field relationship). The equation relating the electric flux density to the electric field can be readily replaced by

$$\vec{D} = \epsilon_r\epsilon_0\vec{E} + \vec{P}$$

where $\epsilon_r \geq 1$ is defined as the relative permittivity. This formulation, which is standard in the electromagnetic literature, introduces another parameter ϵ_r which can be treated as a spatially dependent parameter to allow for instantaneous effects on displacement in Ω due to the electric field originating in Ω_0.

The constitutive law in equation (1) is also sufficiently general to include models based on differential equations and systems of differential equations, or delay differential equations, (see [BJ]) whose solutions can be expressed through fundamental solutions (in general variation-of-parameters representations). For example, the choice of kernel function $g(t) = e^{-t\tau}(\epsilon_s - \epsilon_\infty)/\tau$ in Ω corresponds to the differential equation of the Debye model in Ω given by

$$\begin{aligned} \tau\dot{\vec{P}} + \vec{P} &= \epsilon_0(\epsilon_s - \epsilon_\infty)\vec{E} \\ \vec{D} &= \epsilon_\infty\epsilon_0\vec{E} + \vec{P}. \end{aligned} \tag{4}$$

The presence of instantaneous polarization is accounted for in this case by the coefficient ϵ_∞ in the electric flux equation. That is, $\epsilon_r = \epsilon_\infty$ in $\Omega, \epsilon_r = 1$ in Ω_0. The remainder of the electric polarization is seen to be a decaying exponential, driven by the electric field, less the part included in the instantaneous polarization. This model was first proposed by Debye in [Deb, VH] to model the behavior of materials whose molecules have permanent dipole moments. The magnitude of the polarization term P represents the degree of alignment of these individual moments.

We will also consider the Lorentz model of electric polarization which, in differential form, is represented with the second order equation:

$$\begin{aligned}\ddot{\vec{P}} + \frac{1}{\tau}\dot{\vec{P}} + \omega_0^2\vec{P} &= \epsilon_0\omega_p^2\vec{E} \\ \vec{D} &= \epsilon_\infty\epsilon_0\vec{E} + \vec{P}.\end{aligned} \tag{5}$$

The so-called plasma frequency is defined to be $\omega_p = \omega_0\sqrt{\epsilon_s - \epsilon_\infty}$. A simple variation of constants solution yields the correct kernel function

$$g(t) = \frac{\epsilon_0\omega_p^2}{\nu_0}e^{-\frac{1}{2\tau}t}\sin(\nu_0 t)$$

where $\nu_0 = \sqrt{\omega_0^2 - \frac{1}{4\tau^2}}$.

2.2 Estimation Methodology

Adapting a rather standard approach, we propose to identify the unknown parameters in a given model of polarization and a geometric representation by attempting to minimize the difference between simulations and observations of time-domain data. The data are measurements of the electric field at points in the exterior domain Ω_0 at discrete times. The simulation is a computed solution to Maxwell's Equations with the constitutive laws for polarization, using candidate values of the geometric and material parameters. The criterion for optimization is the minimization of a least-squares measurement of the difference between the simulation and the observed data given by

$$J(\vec{q}) = \sum_{i=1}^{N} |\vec{E}(t_i, \vec{x}_i; \vec{q}) - \hat{E}_i|^2.$$

The $\hat{E}_i$ are measurements of the electric field taken at specific locations and times. The $\vec{E}(t_i, \vec{x}_i; \vec{q})$ are solutions evaluated at the same locations and times from the simulation using the full set of parameter values $\vec{q}$.

We note two nontrivial difficulties with this approach and propose solutions, the efficiency of which will be demonstrated in the particular implementation discussed in this paper.

The unknown location of part of the boundary creates computational challenges. During the course of an iterative optimization procedure, simulations will be repeated many times for different locations of the unknown part of the boundary of Ω. That is, iterative based methods generally will involve changing domains and hence changing discretization grids in the usual finite element or finite difference approximation schemes. Any associated computational scheme (with domain changing with each iterative step) will be prohibitive in effort and time.

We address this difficulty by employing the "method of mappings", [BKo, Pi, BKoW] and transforming the problem on $\Omega \bigcup \Omega_0$ with unknown geometry to one with known geometry (a reference domain $\tilde{\Omega}$) at the expense of introducing additional unknowns into the equations that must be solved on this new domain. Generally, we cannot expect these mappings to be C^2, or even C^1, which precludes finding classical solutions of the transformed system. For this and other reasons discussed below, we consider a weak formulation of the problem. The effect of the mapping is seen in additional coefficients appearing in the equations. The values of these coefficients must be interpreted through the inverse map to determine the geometric parameters.

Another difficulty arises from the oscillatory nature of the time domain data. Varying some parameters in the model has the effect of changing the time at which reflected signals are detected by varying the distance the propagated waves travel (to and from the unknown boundary $\Gamma(q)$) and their speed of propagation. This causes the simulated data to move in and out of phase with observations as these parameters are changed, producing in the cost function J an oscillatory character with respect to these parameters. Thus, local minima of J can (and do) arise at values for which the simulation moves partially back into phase with the data (this is illustrated in Section 4).

We choose to avoid the resulting difficult optimization problem by employing a multi-step approach which separates the identification of geometric and physical parameters. (Other approaches are possible, e.g., use of an optimization algorithm that obtains global minima even in the presence of multiple local minima.) The data set is truncated in time to a period which contains only partial reflections from initial penetrations of the interrogating signal on the surface of the material, eliminating the dependence on geometry. This generates an estimate of the dielectric parameters which is used in a second step which attempts to recover the geometry. To avoid the oscillatory nature of the objective function, a different optimization criterion is used in the second step. This criterion compares the secondary return times (i.e., return times after the pulse has reflected back from the unknown supraconductive-backed part of the boundary) of pulsed signals through mediums of varying geometry with the observed data secondary return times. A global optimization for improved estimated of all parameters is then attempted, in a third step using the estimates of the geometry and the prior estimate of the dielectric parameters as initial estimates.

2.3 Reduction to a Specific Problem

The choice of an interrogating input signal (in our case, a windowed microwave pulse from an exterior antenna in Ω_0) has profound implications on both theoretical and computational aspects of the inverse problem for estimation of dielectric and geometric parameters. A very popular (and readily implemented) choice consists of a *polarized* planar wave. This produces a signal with the $\vec{E}$ and $\vec{H}$ fields possessing

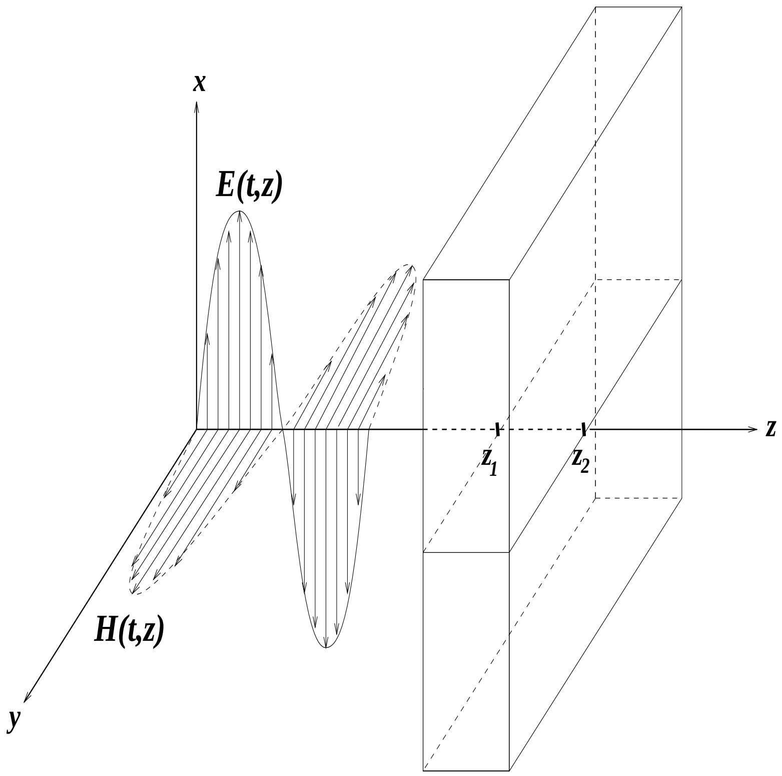

Figure 2: Geometry of Physical Problem

nontrivial components in only one dimension in Ω_0. If the interrogated medium Ω has some homogeneity (in planes parallel to that of the interrogating planar wave), a similar reduction of the $\vec{E}$ and $\vec{H}$ fields occurs in the body Ω.

To discuss our inverse problem ideas, we consider in this paper the problem of interrogating an infinite slab of homogeneous (in the directions orthogonal to the direction of propagation of the plane wave) material by a polarized plane wave windowed microwave pulse. Specifically, as depicted in Figure 2, the interrogating signal is assumed to be a planar electro-magnetic wave normally incident on an infinite slab of material contained in the interval $[z_1, z_2]$ with faces parallel to the xy plane. The electric field is polarized with oscillations in the xz plane only.

Under these assumptions, it is easy to argue that the electric field is parallel to the $\hat{\imath}$ axis at all points in Ω_0 (the region external to the slab) and that the magnetic field is always parallel to $\hat{\jmath}$. Furthermore, these fields are homogeneous in intensity in the x and y directions. Thus $\vec{E}(t, \vec{x}) = \hat{\imath}E(t, z), \vec{H}(t, \vec{x}) = \hat{\jmath}H(t, z)$ as shown in Figure 2.

The electric flux density $\vec{D}$ and polarization $\vec{P}$ inherit this uniform directional property from $\vec{E}$ and hence will be denoted hereafter by their scalar magnitudes D and P in the $\hat{\imath}$ direction. Since we have assumed that the material properties are homogeneous in the x and y variables, the propagating waves in Ω are also reduced to one nontrivial component. Thus the problem's dependence on x and y disappears since the resulting fields are necessarily homogeneous in these variables. This makes it possible to represent the fields in Ω and Ω_0 with the scalar functions $E(t,z)$ and $H(t,z)$. Under these assumptions, the differential operation $\nabla \times \vec{A}$ reduces to $-\hat{\imath}\frac{\partial A_y}{\partial z} + \hat{\jmath}\frac{\partial A_x}{\partial z}$ and the Maxwell's Equations from Section 2.1 become

$$\frac{\partial E}{\partial z} = -\mu_o \frac{\partial H}{\partial t} \tag{6}$$

$$-\frac{\partial H}{\partial z} = \frac{\partial D}{\partial t} + \sigma E + J_s. \tag{7}$$

We eliminate the magnetic field from the equations by taking the space derivative of equation (6), the time derivative of equation (7) and using the equation for electric flux density $D = \epsilon E + P$ where $\epsilon = \epsilon_0(1 + (\epsilon_r - 1)I_\Omega)$ to obtain

$$\mu_0 \epsilon \ddot{E} + \mu_0 \ddot{P} + \mu_0 \sigma \dot{E} - E'' = -\mu_0 \dot{J}_s. \tag{8}$$

Here and throughout, I_A will denote the indicator function for a set A and $' = \frac{\partial}{\partial z}$, $\dot{} = \frac{\partial}{\partial t}$.

This is the differential equation of concern for both our simulations and inverse problem calculations. We also define the domain of the computation (after the method of mappings has been applied) to be the interval $\tilde{\Omega} = [0,1]$ which contains Ω_0. An absorbing boundary condition is placed at the $z = 0$ boundary of the interval to prevent the reflection of waves. This can be expressed by

$$\left[\frac{1}{c}\frac{\partial E}{\partial t} - \frac{\partial E}{\partial z}\right]_{z=0} = 0 \tag{9}$$

where $c^2 \equiv 1/\epsilon_0 \mu_0$.

For our formulation we assume that the location of the boundary at $z = z_1$ is known, while the location of the *original* back boundary at $z = z_2$ (equivalently, the depth of the slab) is unknown, i.e., $\Gamma(q) = \{\vec{x} \in \mathbb{R}^3 | z = z_2\}$. Thus we have a supraconductive backing on the slab at $z = z_2$. The boundary conditions on this supra-conductive reflector can now be determined explicitly, again assuming that the method of maps had been applied and therefore the back boundary of the material is now found at $z = 1$, the edge of the computational domain. (The precise map will be discussed momentarily below.) The vector normal to the surface is $\hat{n} = \hat{k}$ and the condition $\vec{B} \cdot \hat{n}$ is satisfied automatically since $\vec{B} = B\hat{\jmath}$. The condition $\vec{E} \times \hat{n} = 0$ becomes $[E_y\hat{\imath} - E_x\hat{\jmath}]_\Gamma = 0$ and hence the condition $E_x = E_y = 0$. Since $\vec{E} = (E_x, 0, 0) = \hat{\imath}E$ this the equivalent to the condition that E(t,1)=0.

Substituting the expression for $\ddot{P}$ derived in equation (2) we obtain the strong form of the equation

$$\begin{aligned}
&\tilde{\epsilon}_r\ddot{E}(t,z) + \frac{1}{\epsilon_0}I_\Omega(z)(\sigma(z) + g(0,z))\dot{E}(t,z) \\
&\quad + \frac{1}{\epsilon_0}I_\Omega\dot{g}(0,z)E(t,z) + \int_0^t I_\Omega\frac{1}{\epsilon_0}\ddot{g}(t-s,z)E(s,z)ds \\
&\quad - c^2E''(t,z) = -\frac{1}{\epsilon_0}\dot{J}_s,
\end{aligned} \tag{10}$$

where indicator functions I_Ω have been added to explicitly enforce the restriction of polarization and conductivity to the interior of the transformed medium $\Omega = [z_1, 1]$ and $\tilde{\epsilon}_r = \epsilon/\epsilon_0 = 1 + (\epsilon_r - 1)I_\Omega \geq 1$ throughout $\Omega_0 \bigcup \Omega$.

Alternatively, we can apply integration by parts to the integral term and arrive at a different form of the equation

$$\begin{aligned}
&\tilde{\epsilon}_r\ddot{E}(t,x) + \frac{1}{\epsilon_0}I_\Omega(z)(\sigma(z) + g(0,z))\dot{E}(t,z) \\
&\quad + \frac{1}{\epsilon_0}I_\Omega\dot{g}(t,z)E(0,z) + \int_0^t \frac{1}{\epsilon_0}I_\Omega\dot{g}(t-s,z)\dot{E}(s,z)ds \\
&\quad - c^2E''(t,z) = -\frac{1}{\epsilon_0}\dot{J}_s(t,z).
\end{aligned} \tag{11}$$

This form of the equation has the advantage of requiring less continuity in the hysteresis function $g(s,z)$. Furthermore, one of its terms disappears when $E(0,z) = 0$, which is the case of interest in the simulations. We shall use the weak form of this equation in our computational investigations in Section 4.5 below. Analysis of the well posedness of equation (11) in weak form is carried out in [Buk].

Due to the forms of the interrogating inputs, the dielectrically discontinuous medium interfaces, and the possible lack of smoothness in mapping the original domain $\Omega_0 \bigcup \Omega = [0, z_2]$ to the reference domain $\tilde{\Omega} = [0,1]$, one should not expect classical solutions to Maxwell's equations in strong form. For both theoretical and computational purposes, it is therefore desirable to write the system equations in weak or variational form. Using the spaces $H = L_2(0,1)$ and $V = H^1_R(0,1) = \{\phi \in H^1(0,1) | \phi(1) = 0\}$, we can write equation (10) in weak form as

$$\begin{aligned} \langle \tilde{\epsilon}_r \ddot{E}, \phi \rangle + \langle \gamma \dot{E}, \phi \rangle + \langle \beta E, \phi \rangle + \langle \int_0^t \alpha(t-s,\cdot) E(s,\cdot) ds, \phi \rangle \\ + \langle c^2 E', \phi' \rangle + c\dot{E}(t,0)\phi(0) = \langle \mathcal{J}(t,\cdot), \phi \rangle \end{aligned} \tag{12}$$

with initial conditions

$$E(0,z) = \Phi(z) \quad \dot{E}(0,z) = \Psi(z).$$

The coefficients in (12) are given by

$$\alpha(t,z) = I_\Omega \ddot{g}(t,z), \quad \beta(z) = \frac{1}{\epsilon_0} I_\Omega \dot{g}(0,z),$$
$$\gamma(z) = \frac{1}{\epsilon_0} I_\Omega(z)(\sigma(z) + g(0,z)), \quad \mathcal{J}(t,z) = -\frac{1}{\epsilon_0} \dot{J}_s(t,z)$$

and $\langle \cdot, \cdot \rangle$ is the L^2 inner product (or equivalently, any appropriately chosen topologically equivalent inner product - the relevance of this remark will be clearer after our discussion below of the method of maps for this example). The functions α, β and γ are dependent on parameters which must be identified. These are assumed to be in L^∞ but may lack any additional regularity.

The source current is under our control, so we can and do choose its form precisely. For example, we may use

$$J_s(t,z) = \delta(z)\sin(\omega t) I_{(0,t_f)}(t). \tag{13}$$

Here, ω is a specified angular frequency of the input signal (and the carrier frequency of the resulting planar wave) and $\delta(z)$ is the Dirac distribution which has infinite mass at $z = 0$. The signal is truncated at a finite time t_f by the indicator function $I_{(0,t_f)}(t)$. We avoid the complications arising from a discontinuous (in t) input signal by requiring that the sinusoid be zero at t_f. Hence $\omega t_f = n\pi$ for some positive integer n. This is equivalent to requiring that the end of the signal occur after a integral number of half-periods. We note that this windowed signal can be equivalently chosen with additional smoothness in t by replacing the indicator $I_{(0,t_f)}$ with a slightly smoother (continuous or even differentiable) truncating function.

This windowed pulse input signal is most helpful in identifying the physical and geometric parameters separately. Since it has a finite duration, the wave's reflection off the surface of the media and its subsequent reflection off the back surface will not necessarily overlap for a sufficiently short pulse. This makes it possible to split the resulting data and perform the two estimation steps described above separately.

We turn to the details of the method of maps for this example. The application of the method of mappings is quite straightforward in this particular case. The value of z_1 is presumed known, while the surface at z_2 is inaccessible and therefore its location (i.e., the value of z_2) is not known. We use a piece-wise linear mapping which leaves the interval $(0, z_1)$ invariant and maps (z_1, z_2) to $(z_1, 1)$, thus mapping the original domain $\Omega_0 \bigcup \Omega = [0, z_2]$ to the reference domain $\tilde{\Omega} = [0,1]$. The new coordinate variable $\tilde{z}$ in $\tilde{\Omega} = [0,1]$ is defined by

$$\tilde{z} = f(z) = \begin{cases} z & 0 < z < z_1 \\ z_1 + (z - z_1)\frac{1-z_1}{z_2 - z_1} & z_1 \leq z \leq z_2 \end{cases}$$

We can express the function as

$$f(z) = z + (\zeta - 1)(z - z_1)I_{[z_1,z_2]}(z)$$

where $\zeta = \frac{1-z_1}{z_2-z_1}$ and

$$f'(z) = 1 + (\zeta - 1)I_\Omega(z).$$

The parameter ζ appearing the equations can be identified in lieu of the depth $z_2 - z_1$ which of course can be recovered from it. Wherever spatial derivatives appear in the equations, we must replace these with the derivatives with respect to the new variable $\tilde{z}$ using the chain rule

$$\frac{\partial}{\partial z} = \frac{\partial \tilde{z}}{\partial z}\frac{\partial}{\partial \tilde{z}} = f'(z)\frac{\partial}{\partial \tilde{z}}.$$

Hence $d\tilde{z} = f'(z)dz$ and the expressions for the inner products in the weak form are modified accordingly to

$$\begin{aligned}
\langle \phi, \psi \rangle &= \int_0^{z_2} \phi(z)\psi(z)dz \\
&= \int_0^1 \tilde{\phi}(\tilde{z})\tilde{\psi}(\tilde{z})\frac{d\tilde{z}}{\tilde{f}'(\tilde{z})} \\
&= \int_0^1 \frac{\tilde{\phi}(\tilde{z})\tilde{\psi}(\tilde{z})}{1 + (\zeta - 1)I_\Omega} d\tilde{z} \\
&= \int_0^{z_1} \tilde{\phi}(\tilde{z})\tilde{\psi}(\tilde{z})d\tilde{z} + \frac{1}{\zeta}\int_{z_1}^1 \tilde{\phi}(\tilde{z})\tilde{\psi}(\tilde{z})d\tilde{z} \qquad (14)
\end{aligned}$$

$$\begin{aligned}
\langle \phi', \psi' \rangle &= \int_0^{z_2} \phi'(z)\psi'(z)dz \\
&= \int_0^1 \tilde{\phi}'(\tilde{z})\tilde{f}'(\tilde{z})\tilde{\psi}'(\tilde{z})\tilde{f}'(\tilde{z})\frac{d\tilde{z}}{\tilde{f}'(\tilde{z})} \\
&= \int_0^1 \tilde{\phi}'(\tilde{z})\tilde{\psi}'(\tilde{z})\tilde{f}'(\tilde{z})d\tilde{z} \\
&= \int_0^1 (1 + (\zeta - 1)I_\Omega)\tilde{\phi}'(\tilde{z})\tilde{\psi}'(\tilde{z})d\tilde{z} \\
&= \int_0^{z_1} \tilde{\phi}'(\tilde{z})\tilde{\psi}'(\tilde{z})d\tilde{z} + \zeta\int_{z_1}^1 \tilde{\phi}'(\tilde{z})\tilde{\psi}'(\tilde{z})d\tilde{z}. \qquad (15)
\end{aligned}$$

Here the functions ϕ and ψ have been expressed in terms of the new variables $\phi(z) = \tilde{\phi}(\tilde{z}), \psi(z) = \tilde{\psi}(\tilde{z})$. For convenience, we will drop the over tilde notation in subsequent discussion.

Returning to equation (12) again, we see that in mapping the original Maxwell system on the domain $\Omega_0 \bigcup \Omega$ to the reference domain $\tilde{\Omega} = [0, 1]$, the $\langle \cdot, \cdot \rangle$ in (12) should be interpreted in the sense (14),(15) above. This will be done is all computational results presented in Section 4. Note that for the theoretical discussions of Section 3 we can without loss of generality use the usual inner products.

This one dimensional problem also permits a simple interpretation of the return time when identifying the geometry. Before the method of maps is applied, the unknown geometric quantity is the depth, $z_2 - z_1$, of the medium. After the mapping is applied, the actual depth of the medium is fixed, but the effects of changing geometry are reflected in the new coefficients, (actually the weighting parameter ζ in the inner products) which appears in the equation. Since there is only one path for the pulse to pass through the medium and be reflected back, the first return of the transmitted signal is a singular event and simple to identify.

To further clarify the identification of the return time, we restrict our attention to materials which are sufficiently thick and pulses which are sufficiently short so that the first reflection of the pulse off the surface at z_1 is completed before the transmitted signal has returned from the back surface. Using c, the speed of light in a vacuum, as an upper limit on the speed of propagation in the material, this condition requires that $t_f c < 2(z_2 - z_1)$.

3 Wellposedness

3.1 A Variational Formulation

In this section we consider wellposedness questions for the variational form (12) of Maxwell's equation with a general polarization term, absorbing left boundary conditions and supra-conductive right boundary conditions as discussed and formulated in the previous section. Without loss of generality, we may take $\tilde{\epsilon}_r = 1$ for our discussions in this section. That is, we are concerned with existence, uniqueness, continuous dependence and regularity of solutions to

$$\langle \ddot{E}, \phi\rangle + \langle \gamma \dot{E}, \phi\rangle + \langle \beta E, \phi\rangle + \langle \int_0^t \alpha(t-s)E(s)ds, \phi\rangle$$
$$+\langle c^2 E', \phi'\rangle + c\dot{E}(t,0)\phi(0) = \langle \mathcal{J}(t), \phi\rangle \tag{16}$$
$$E(0,z) = \Phi(z), \dot{E}(0,z) = \Psi(z). \tag{17}$$

We seek solutions $t \to E(t)$ with $E(t)$ in $V \equiv H^1_R(0,1) = \{\phi \in H^1(0,1) : \phi(1) = 0\}$ satisfying (17) and (16) for all $\phi \in V$. We shall do this in the context of a Gelfand triple setting $V \hookrightarrow H \hookrightarrow V^*$ where $H = L^2(0,1)$. We assume throughout this section that the slab region $\Omega = [z_1, z_2]$ has been mapped to $[z_1, 1]$ so that our domain of interest is $\tilde{\Omega} = [0,1]$ with γ, β and $\alpha(t)$ bounded on $[0,1]$ and vanishing outside $[z_1, 1]$. Thus, in (16) the inner products should be properly interpreted in the sense of (14),15). However, as explained in the last section, one can equivalently treat the well-posedness questions of this section using the unweighted L^2 inner product in (16) and we shall do this.

From a general theory presented in [BIW], [BSW, Chapter 4], one sees that (16) differs from the usual lightly damped second order systems of [BSW] only because of the presence of the terms $c\dot{E}(t,0)\phi(0)$ due to the absorbing left boundary condition and $\langle \int_0^t \alpha(t-s)E(s)ds, \phi\rangle$ resulting from the convolution representation for the polarization. From the general theory one might expect to seek solutions of (16) in the sense of $L^2(0,T;V)^* \simeq L^2(0,T;V^*)$ with $E \in L^2(0,T;V), \dot{E} \in L^2(0,T;H)$ and $\ddot{E} \in L^2(0,T;V^*)$ for appropriate interpretation of the $\langle\cdot,\cdot\rangle$ in (16) i.e., the duality product $\langle\cdot,\cdot\rangle_{V^*,V}$ which reduces to the $H = L^2$ inner product in all terms of (16) except the first and last. We recall from Section 2.3 that the input $\mathcal{J}(t)$ results from a point source (antenna) at $z = 0$ and hence $\mathcal{J}(t)$ has the form $g(t)\delta(z)$ for a windowed time signal $g(t)$. This motivates our desire for results allowing $\mathcal{J}(t)$ values in V^*.

In addition to differences one might encounter due to the polarization term, if one obtains as usual $\dot{E} \in L^2(0,T;H)$ where $H = L^2(0,1)$, then questions arise as to the interpretation of the boundary term $c\dot{E}(t,0)\phi(0)$ which has the appearance of pointwise evaluation of an $L^2(0,1)$ "function" at $z = 0$. Correct interpretation of this term will result from our arguments below.

We follow the general approach using sesquilinear forms as in [BIW],[BSW] which are standard in the research literature citeLions, [Wloka]. We first rewrite (16) by adding a term $\langle kE,\phi\rangle_H$ to both sides of the equation. The positive constant k is chosen so that $\hat{\beta} \equiv k+\beta$ satisfies $\hat{\beta} \geq \hat{\epsilon} > 0$ on $[0,1]$ for some constant $\hat{\epsilon}$; this is possible since by assumption $\beta \in L^\infty(0,1)$. We define a sesquilinear form $\sigma_1 : V \times V \longrightarrow \mathbb{C}$ by

$$\sigma_1(\phi,\psi) = \langle c^2\phi',\psi'\rangle_H + \langle\hat{\beta}\phi,\psi\rangle_H \quad \text{for } \phi,\psi \in V.$$

Equation (16) can then be rewritten as

$$\begin{aligned} \langle\ddot{E}(t),\phi\rangle_{V^*,V} + \langle\gamma\dot{E}(t),\phi\rangle + \langle\int_0^t \alpha(t-s)E(s)ds,\phi\rangle + \sigma_1(E(t),\phi) \\ +c\dot{E}(t,0)\phi(0) = \langle\mathcal{J}(t),\phi\rangle_{V^*,V} + \langle kE(t),\phi\rangle \end{aligned} \tag{18}$$

for all $\phi \in V$, where it is readily seen that σ_1 is V-continuous and V-elliptic. That is, there are positive constants c_1, c_2 such that

$$\begin{aligned} |\sigma_1(\phi,\psi)| &\leq c_2|\phi|_V|\psi|_V \quad \text{for all } \phi,\psi \in V, \\ \sigma_1(\phi,\phi) &\geq c_1|\phi|_V^2 \quad \text{for } \phi \in V. \end{aligned}$$

To establish existence of solutions (17), (18) where $\Phi \in V, \Psi \in H$, we follow the ideas in [BSW] and choose a subset $\{w_i\}_{i=1}^{\infty}$ spanning V (without loss of generality we may assume linear independence of these elements). Let $V^m \equiv \text{span}\{w_1, \ldots, w_m\}$ and define Galerkin "approximates"

$$E_m(t,z) = \sum_{i=1}^{m} e_i^m(t) w_i(z) \tag{19}$$

where the $\{e_i^m(t)\}_{i=1}^m$ are determined by substitution into (18) and requiring this system of ordinary differential equations to hold for $\phi = w_i, i = 1, 2, \ldots, m$. This m-dimensional system is solved with initial conditions

$$\begin{aligned} E_m(0) &= \Phi_m \\ \dot{E}_m(0) &= \Psi_m \end{aligned}$$

where the Φ_m, Ψ_m are chosen in V^m so that $\Phi_m \to \Phi$ in V, $\Psi_m \to \Psi$ in H. We thus find that $E_m(t)$ satisfies (18) with $\phi = \dot{E}_m(t) \in V$ so that for each t we have the system

$$\begin{aligned} &\frac{d}{dt}\frac{1}{2}|\dot{E}_m(t)|_H^2 + \langle \gamma \dot{E}_m(t), \dot{E}_m(t)\rangle_H \\ &\quad + \quad \langle \int_0^t \alpha(t-s)\dot{E}_m(s)ds, \dot{E}_m(t)\rangle_H + \sigma_1(E_m(t), \dot{E}_m(t)) + c|\dot{E}_m(t,0)|^2 \\ &\quad = \quad \langle \mathcal{J}(t), \dot{E}_m(t)\rangle_{V^*,V} + \langle kE_m(t), \dot{E}_m(t)\rangle_H, \qquad (20) \\ &E_m(0) = \Phi_m, \dot{E}_m(0) = \Psi_m. \end{aligned}$$

This system will allow us to obtain bounds for $\{E_m\}, \{\dot{E}_m\}$, and $\{\dot{E}_m(\cdot, 0)\}$ that are independent of m.

Using the fact that

$$\frac{1}{2}\frac{d}{dt}\sigma_1(E_m(t), E_m(t)) = \sigma_1(E_m(t), \dot{E}_m(t)),$$

we may rewrite (20) as

$$\frac{1}{2}\frac{d}{dt}\{|\dot{E}_m(t)|_H^2 + \sigma_1(E_m(t), E_m(t))\} + |\sqrt{\gamma}\dot{E}_m(t)|_H^2 + c|\dot{E}_m(t,0)|^2$$

$$= \langle -\int_0^t \alpha(t-s)E_m(s)ds, \dot{E}_m(t)\rangle_H + \langle kE_m(t), \dot{E}_m(t)\rangle_H$$
$$+ \langle \mathcal{J}(t), \dot{E}_m(t)\rangle_{V^*,V}.$$

Integration along with use of the V ellipticity of σ_1 yields

$$|\dot{E}_m(t)|_H^2 + c_1|E_m(t)|_V^2 + 2\int_0^t |\sqrt{\gamma}\dot{E}_m(s)|_H^2 ds + 2c|\dot{E}_m(\cdot,0)|^2_{L^2(0,t)}$$
$$\leq |\dot{E}_m(0)|_H^2 + c_2|E_m(0)|_V^2 + 2|\int_0^t F_m(\tau)d\tau| \qquad (21)$$

where

$$\begin{aligned} F_m(\tau) &= \langle -\int_0^\tau \alpha(\tau-s)E_m(s)ds, \dot{E}_m(\tau)\rangle + \langle kE_m(\tau), \dot{E}_m(\tau)\rangle \\ &\quad + \langle \mathcal{J}(\tau), \dot{E}_m(\tau)\rangle_{V^*,V} \\ &\equiv T_1(\tau) + T_2(\tau) + T_3(\tau). \end{aligned}$$

Assuming that α is bounded on $[0,T]\times[0,1]$ we have for $\tau \in [0,t]$

$$\begin{aligned} |T_1(\tau)| &\leq \int_0^\tau K|E_m(s)|_H ds|\dot{E}_m(\tau)|_H \\ &\leq \frac{1}{2}(\int_0^\tau K|E_m(s)|_H ds)^2 + \frac{1}{2}|\dot{E}_m(\tau)|_H^2 \\ &\leq \frac{1}{2}K^2 t\int_0^\tau |E_m(s)|_H^2 ds + \frac{1}{2}|\dot{E}_m(\tau)|_H^2 \\ &\leq \frac{1}{2}K^2 t\int_0^t |E_m(s)|_H^2 ds + \frac{1}{2}|\dot{E}_m(\tau)|_H^2. \end{aligned}$$

Thus we find

$$\int_0^t |T_1(\tau)|d\tau \leq K_1\int_0^t |E_m(s)|_H^2 ds + K_2\int_0^t |\dot{E}_m(\tau)|_H^2 d\tau. \qquad (22)$$

We also have

$$\int_0^t |T_2(\tau)|d\tau \leq \int_0^t \{\frac{1}{2}k^2|E_m(\tau)|_H^2 + \frac{1}{2}|\dot{E}_m(\tau)|_H^2\}d\tau. \qquad (23)$$

Finally to consider the term T_3, we use (assuming that $\dot{\mathcal{J}} \in L^2(0,T;V^*)$)

$$\frac{d}{dt}\langle \mathcal{J}(t), E_m(t)\rangle_{V^*,V} = \langle \dot{\mathcal{J}}(t), E_m(t)\rangle_{V^*,V} + \langle \mathcal{J}(t), \dot{E}_m(t)\rangle_{V^*,V}.$$

We obtain

$$
\begin{aligned}
\Big|\int_0^t T_3(\tau)d\tau\Big| &= \Big|\int_0^t \{\frac{d}{d\tau}\langle \mathcal{J}(\tau), E_m(\tau)\rangle_{V^*,V} - \langle \dot{\mathcal{J}}(\tau), E_m(\tau)\rangle_{V^*,V}\}d\tau\Big| \\
&= \Big|\langle \mathcal{J}(t), E_m(t)\rangle_{V^*,V} - \langle \mathcal{J}(0), E_m(0)\rangle_{V^*,V} - \int_0^t \langle \dot{\mathcal{J}}(\tau), E_m(\tau)\rangle_{V^*,V} d\tau\Big| \\
&\leq \frac{1}{4\epsilon}|\mathcal{J}(t)|_{V^*}^2 + \epsilon|E_m(t)|_V^2 + \frac{1}{2}|\mathcal{J}(0)|_{V^*}^2 + \frac{1}{2}|E_m(0)|_V^2 \\
&\quad + \int_0^t \Big\{\frac{1}{2}|\dot{\mathcal{J}}(\tau)|_{V^*}^2 + \frac{1}{2}|E_m(\tau)|_V^2\Big\}d\tau. \qquad (24)
\end{aligned}
$$

Combining (21), (22), (23), and (24), we obtain

$$
\begin{aligned}
&|\dot{E}_m(t)|_H^2 + (c_1 - 2\epsilon)|E_m(t)|_V^2 + 2\int_0^t |\sqrt{\gamma}\dot{E}_m(s)|_H^2 ds + 2c|\dot{E}_m(\cdot,0)|_{L^2(0,t)}^2 \\
&\leq |\dot{E}_m(0)|_H^2 + (c_2+1)|E_m(0)|_V^2 + \frac{1}{2\epsilon}|\mathcal{J}(t)|_{V^*}^2 + |\mathcal{J}(0)|_{V^*}^2 + \int_0^t |\dot{\mathcal{J}}(s)|_{V^*}^2 ds \\
&+ \int_0^t \{C_1|E_m(s)|_H^2 + C_2|\dot{E}_m(s)|_H^2 + C_3|E_m(s)|_V^2\}ds. \qquad (25)
\end{aligned}
$$

Assuming that $\mathcal{J} \in H^1(0,T;V^*)$ and using the boundedness of $\{E_m(0)\}$ in V and $\{\dot{E}_m(0)\}$ in H (which follows from the convergences of $\{\Phi_m\}$ and $\{\Psi_m\}$ respectively), we may employ Gronwall's inequality along with the inequality (25) to conclude that $\{\dot{E}_m\}$ is bounded in $C(0,T;H)$, $\{E_m\}$ is bounded in $C(0,T;V)$ and $\{\dot{E}_m(\cdot,0)\}$ is bounded in $L^2(0,T)$. Thus we find (extracting subsequences and reindexing as usual) there exist $E \in L^2(0,T;V)$, $\tilde{E} \in L^2(0,T;H)$ and $z_0 \in L^2(0,T)$ such that

$$
\begin{aligned}
E_m &\to E \quad \text{weakly in} \quad L^2(0,T;V) \\
\dot{E}_m &\to \tilde{E} \quad \text{weakly in} \quad L^2(0,T;H) \\
\dot{E}_m(\cdot,0) &\to z_0 \quad \text{weakly in} \quad L^2(0,T).
\end{aligned}
$$

The limit function E is a candidate for solution of (17), (18) and we must verify that $\tilde{E} = \dot{E}$, $z_0 = \dot{E}(\cdot,0)$ in some sense and that we may pass to the limit in the version of (18) for E_m to obtain (18) for the limit function. First we note that for each m

$$
E_m(t) = E_m(0) + \int_0^t \dot{E}_m(s)ds \qquad (26)
$$

and

$$E_m(t,0) = E_m(0,0) + \int_0^t \dot{E}_m(s,0)ds. \tag{27}$$

Passing to the limit (in the weak H sense in (26)) we obtain

$$\begin{aligned} E(t) &= \Phi + \int_0^t \tilde{E}(s)ds & (28)\\ E(t,0) &= \Phi(0) + \int_0^t z_0(s)ds. & (29) \end{aligned}$$

We find that (28) holds in the H sense for each $t \in [0,T]$ and hence $\dot{E} = \tilde{E}$ while (29) yields that $E(t,0)$ exists and is continuous in t. In actuality we have $E(t,0)$ is absolutely continuous with $\dot{E}(t,0) = z_0(t)$ for almost every t.

We note, in fact, that the same arguments used in [BSGII, Lemma 5.1(b)] can be used to establish that E_m also converges weakly in $C(0,T;H)$ to E so that $E \in C(0,T;H) \cap L^2(0,T;V)$.

Thus we have that our candidate E for solution of (17), (18) satisfies

$$\begin{aligned} E_m \to E &\quad \text{weakly in} \quad L^2(0,T;V) & (30)\\ \dot{E}_m \to \dot{E} &\quad \text{weakly in} \quad L^2(0,T;H) & (31)\\ \dot{E}_m(\cdot,0) \to \dot{E}(\cdot,0) &\quad \text{weakly in} \quad L^2(0,T). & (32) \end{aligned}$$

We must show that E satisfies (18). For this we follow directly the arguments of pp.100-101 in [BSW]. Taking $\psi \in C^1[0,T]$ with $\psi(T) = 0$ and choosing $\psi_j(t) \equiv \psi(t)w_j$ where the $\{w_j\}_{j=1}^{\infty}$ are as chosen before, we have, fixing j, that for all $m > j$, E_m must satisfy

$$\begin{aligned} &\int_0^T \{\langle \ddot{E}_m(t), \psi_j(t)\rangle + \langle \gamma \dot{E}_m(t), \psi_j(t)\rangle + \langle \int_0^t \alpha(t-s)E_m(s)ds, \psi_j(t)\rangle \\ &+ \ \sigma_1(E_m(t), \psi_j(t)) + c\dot{E}_m(t,0)\psi_j(t)(0)\}dt \\ &= \ \int_0^T \{\langle \mathcal{J}(t), \psi_j(t)\rangle_{V^*,V} + \langle kE_m(t), \psi_j(t)\rangle\}dt. \end{aligned}$$

Integrating by parts in the first term and then taking the limit as $m \to \infty$, with the convergences of (30)-(32) we obtain

$$\begin{aligned}
&\int_0^T \{-\langle \dot{E}(t), \dot{\psi}_j(t)\rangle + \langle \gamma \dot{E}(t), \psi_j(t)\rangle + \langle \int_0^t \alpha(t-s)E(s)ds, \psi_j(t)\rangle \\
&+ \quad \sigma_1(E(t), \psi_j(t)) + c\dot{E}(t,0)\psi_j(t)(0)\}dt \\
&= \quad \int_0^T \{\langle \mathcal{J}(t), \psi_j(t)\rangle_{V^*,V} + \langle kE(t), \psi_j(t)\rangle\}dt + \langle \Psi, \psi_j(0)\rangle.
\end{aligned}$$

It follows that for every w_j we have in the $L^2(0,T)$ sense

$$\begin{aligned}
&\frac{d}{dt}\langle \dot{E}(t), w_j\rangle + \langle \gamma \dot{E}(t), w_j\rangle + \langle \int_o^t \alpha(t-s)E(s)ds, w_j\rangle \\
&+\sigma_1(E(t), w_j) + cE(t,0)w_j(0) = \langle \mathcal{J}(t), w_j\rangle_{V^*,V} + \langle kE(t), w_j\rangle.
\end{aligned}$$

Since $\{w_j\}_{j=1}^{\infty}$ was chosen total in V we thus obtain that $\ddot{E} \in L^2(0,T;V^*)$ and that E satisfies (18). From (28) we know that $E(0) = \Phi$ and the arguments that $\dot{E} = \Psi$ follow exactly as those on p.101 of [BSW]. Hence we find that E is a solution of (17),(18).

Continuous dependence of solutions to (17), (18) on Φ, Ψ and $\mathcal{J}$ follow readily from the inequality (25) and some standard arguments. Noting that $|\cdot|_H \le \mu|\cdot|_V$ for some constant μ and letting

$$\begin{aligned}
K_m \quad &\equiv \quad |\dot{E}_m(0)|_H^2 + (c_2+1)|E_m(0)|_V^2 + \frac{1}{2\epsilon}|\mathcal{J}|^2_{L^\infty(0,T;V^*)} \\
&+ \quad |\mathcal{J}(0)|^2_{V^*} + \int_0^T |\dot{\mathcal{J}}(s)|^2_{V^*}ds, \qquad (33)
\end{aligned}$$

we observe that (25) implies

$$|\dot{E}_m(t)|_H^2 + |E_m(t)|_V^2 \le \nu K_m + \int_0^t \nu\Big\{|E_m(\tau)|_V^2 + |\dot{E}_m(\tau)|_H^2\Big\}d\tau$$

for some positive constant ν independent of m. Using Gronwall's inequality again, we obtain

$$|\dot{E}_m(t)|_H^2 + |E_m(t)|_V^2 \le \nu K_m e^{\nu T} \quad \text{for } t \in [0,T]. \qquad (34)$$

Recalling that $E_m(0) = \Phi_m \to \Phi$ in V and $\dot{E}_m(0) = \Psi_m \to \Psi$ in H so that from (33) we have $\lim K_m \le K$ where $K \equiv |\Psi|_H^2 + (c_2+1)|\Phi|_V^2 + \mathcal{K}|\mathcal{J}|^2_{H^1(0,T;V^*)}$, we may use weak lower semicontinuity of norms, the convergences of (30) and (31), and (34) to conclude

$$|\dot{E}|^2_{L^2(0,T;H)} + |E|^2_{L^2(0,T;V)} \leq \nu K e^{\nu T} \tag{35}$$

Since the mapping $(\Phi, \Psi, \mathcal{J}) \to (E, \dot{E})$ is linear from $V \times H \times H^1(0,T;V^*)$ to $L^2(0,T;V) \times L^2(0,T;H)$ we see that (35) yields continuous dependence of solutions $(E, \dot{E})$ of (17), (18) on initial data (Φ, Ψ) and input $\mathcal{J}$.

For uniqueness of solutions to (17), (18), we again follow the standard arguments given in p.102-103 of [BSW]. In this case the details are tedious but rather straightforward. As usual, it suffices to show that the only solution of (18) corresponding to zero initial data ($\Phi = \Psi = 0$ in (17)) and zero input ($\mathcal{J} = 0$) is the trivial solution. Let E be a solution corresponding to $\Phi = \Psi = \mathcal{J} = 0$ and for arbitrary s in $(0,T)$ define

$$\psi_s(t) = \begin{cases} -\int_t^s E(\xi)d\xi & t < s \\ 0 & t \geq s \end{cases}$$

so that $\psi_s(T) = 0$ and $\psi_s(t) \in V$ for each t. We then find that

$$\int_0^s \{\langle \ddot{E}(t), \psi_s(t)\rangle_{V^*,V} + \langle \dot{E}(t), E(t)\rangle_H\}dt = 0.$$

Hence, choosing $\phi = \psi_s(t)$ in (18) and integrating over t from 0 to s, we have

$$\begin{aligned} &\int_0^s \{\langle \dot{E}(t), E(t)\rangle_H - \langle \gamma \dot{E}(t), \psi_s(t)\rangle_H - \langle \int_0^t \alpha(t-\tau)E(\tau)d\tau, \psi_s(t)\rangle_H \\ &- \quad \sigma_1(E(t), \psi_s(t)) - c\dot{E}(t,0)\psi_s(t)(0) + \langle kE(t), \psi_s(t)\rangle_H\}dt = 0. \end{aligned} \tag{36}$$

Observing that

$$\int_0^s \{\langle \gamma \dot{E}, \psi_s\rangle + \langle \gamma E, E\rangle\}dt = \int_0^s \frac{d}{dt}\langle \gamma E, \psi_s\rangle dt = 0,$$

$$\frac{d}{dt}\sigma_1(\psi_s(t), \psi_s(t)) = 2\mathrm{Re}\sigma_1(E(t), \psi_s(t)),$$

$$\int_0^s \{c\dot{E}(t,0)\psi_s(t)(0) + cE(t,0)^2\}dt = \int_0^s \frac{d}{dt}\{cE(t,0)\psi_s(t)(0)\}dt = 0$$

and

$$\frac{d}{dt}\langle k\psi_s(t),\psi_s(t)\rangle_H = 2\mathrm{Re}\langle kE(t),\psi_s(t)\rangle,$$

we may use (36) to obtain

$$\begin{aligned}
&\frac{1}{2}|E(s)|_H^2 + \frac{1}{2}\sigma_1(\psi_s(0)\psi_s(0)) + \frac{1}{2}\langle k\psi_s(0),\psi_s(0)\rangle \\
&+ \quad \int_0^s \{\langle\gamma E(t),E(t)\rangle + cE(t,0)^2 \\
&\qquad -\mathrm{Re}\langle\int_0^t \alpha(t-\tau)E(\tau)d\tau,\psi_s(t)\rangle\}dt = 0. \qquad (37)
\end{aligned}$$

It follows immediately that

$$\begin{aligned}
&\frac{1}{2}|E(s)|_H^2 \le \frac{1}{2}|\langle k\psi_s(0),\psi_s(0)\rangle| \\
&+ \quad \int_0^s \{|\langle\gamma E(t),E(t)\rangle| + |\langle\int_0^t \alpha(t-\tau)E(\tau)d\tau,\psi_s(t)\rangle|\}dt. \qquad (38)
\end{aligned}$$

From the definition of ψ_s we have for each $t\in[0,T]$

$$|\psi_s(t)|_H^2 \le (\int_0^s |E(\xi)|_H d\xi)^2 \le T\int_0^s |E(\xi)|_H^2 d\xi \qquad (39)$$

so that

$$\begin{aligned}
|\langle k\psi_s(0),\psi_s(0)\rangle_H| &= |\int_0^1 k(\int_0^s E(\xi,z)d\xi)^2 dz| \\
&\le |\int_0^1 kT\int_0^s |E(\xi,z)|^2 d\xi dz| \\
&= kT\int_0^s |E(\xi)|_H^2 d\xi. \qquad (40)
\end{aligned}$$

Using (39) and arguments exactly like those behind the estimate (22) for $T_1(\tau)$ we find for $t<s$

$$\begin{aligned}
|\langle\int_0^t \alpha(t-\tau)E(\tau)d\tau,\psi_s(t)\rangle| &\le (\int_0^t K|E(\tau)|_H d\tau)|\psi_s(t)|_H \\
&\le \frac{1}{2}(\int_0^t K|E(\tau)|_H d\tau)^2 + \frac{1}{2}|\psi_s(t)|_H^2 \\
&\le K_3\int_0^s |E(\xi)|_H^2 d\xi. \qquad (41)
\end{aligned}$$

Using (40) and (41) we thus obtain

$$\frac{1}{2}|E(s)|_H^2 \leq \{\frac{1}{2}kT + |\gamma|_\infty + K_3\} \int_0^s |E(\xi)|_H^2 d\xi \tag{42}$$

or

$$|E(s)|_H^2 \leq \mathcal{K} \int_0^s |E(\xi)|_H^2 d\xi \tag{43}$$

for arbitrary $s \in (0, T]$. Invoking the Gronwall inequality once again, we conclude that $E(\xi) \equiv 0$ on $(0, T)$ and solutions of (17), (18) are unique.

Summarizing our discussions in this section, we see that we have proved the following result.

Theorem 1 *Suppose that $\mathcal{J} \in H^1(0, T; V^*)$, $\gamma, \beta \in L^\infty(0, 1)$, $\alpha \in L^\infty(0, T; L^\infty(0, 1))$ with α, β, γ vanishing outside $[z_1, 1]$. Then for $\Phi \in V = H_R^1(0, 1), \Psi \in H = L^2(0, 1)$, we have that solutions to (17), (18) exist and are unique. These solutions satisfy $E \in L^2(0, T; V) \cap C(0, T; H), \dot{E} \in L^2(0, T; H)$, and $\ddot{E} \in L^2(0, T; V^*)$. Moreover, $t \to E(t, 0)$ is absolutely continuous with $\dot{E}(\cdot, 0) \in L^2(0, T)$. The solutions depend continuously on $(\Phi, \Psi, \mathcal{J})$ as maps from $V \times H \times H^1(0, T; V^*)$ to $L^2(0, T; V) \times L^2(0, T; H)$.*

3.2 A Semigroup Formulation

While the variational formulation of the previous section provides adequate well-posedness results for our subsequent discussions, it is of some mathematical interest as to whether the integro-partial differential system (16), (17) has a semigroup based formulation. For the sake of completeness, we present such a formulation next while noting that for this particular problem, improved regularity results over our theorem in Section 3.1 will not be obtained using semi-group methods.

For this section we assume that as before $\alpha, \beta \in L^\infty(0, 1)$ and vanish outside Ω while $\gamma \in L^\infty((0, 1) \times (0, 1))$ and also vanishes outside Ω. We further assume that

$t \mapsto \alpha(t,\cdot)$ is positive in Ω and and monotone decreasing to zero so that $\dot{\alpha}(t,\cdot) \leq 0$ whenever $\alpha \in H^1(0,T)$. This monoticity assumption is typical of the usual assumptions in displacement susceptibility kernels (e.g., see [Blo, p.102] or [Hop, 1887]). We further assume for this section that $\alpha(t,\cdot)$ is constant in Ω so that $\alpha(t,x) = \chi_\Omega(z)\hat{\alpha}(t)$ for some monotone decreasing function $\hat{\alpha}$.

We consider the term (tacitly assuming $E(s) = 0$ for $s < 0$)

$$\int_0^t \alpha(t-s)E(s)ds = \int_{-\infty}^t \alpha(t-s)E(s)ds$$

from (16) and note that it can be equivalently written

$$\begin{aligned}\int_{-\infty}^t \alpha(t-s)E(s)ds &= \int_{-\infty}^0 \alpha(-\xi)E(t+s)d\xi \\ \approx \quad \int_{-r}^0 \alpha(-\xi)E(t+\xi)d\xi &= \int_{-r}^0 G(\xi)E(t+\xi)d\xi\end{aligned}$$

where $G(\xi) = \alpha(-\xi)$. We denote $\hat{G}\xi = \hat{\alpha}(-\xi)$ so that $G(\xi) = \chi\hat{G}(-\xi)$.

The approximation is valid for r sufficiently large ($r = \infty$ is permitted) so that $\alpha(t) \approx 0$ for $t > r$. We observe at this point that $\hat{G}(\xi) \geq 0$ with $\hat{G}(\xi) > 0$ on $(-r, 0]$.

As in the previous section, we take $V = H_R^1(0,1), H = L^2(0,1)$ and assume that $\Omega = [z_1, 1] \subset [0,1]$ is the region of interest. We shall have use of $\hat{H} = L^2(\Omega)$ and shall denote the restriction of functions ϕ in $L^2(0,1)$ to Ω again by ϕ and write $\phi \in L^2(\Omega)$ whenever no confusion will result.

Motivated by the "strong" form of (16), i.e., see equation (10) with $\epsilon_r = 1$, and using the above definitions and approximating, we may write (16) as

$$\ddot{E}(t) + \gamma\dot{E}(t) + \beta E(t) + \int_{-r}^0 G(\xi)E(t+\xi)d\xi - c^2E''(t) = \mathcal{J}(t) \tag{44}$$

where, of course, the derivatives must be interpreted in a weak or distributional sense. Following [BFW1, 1987], [BFW2, 1989], [FI, 1990] and [BMZ, 1996], we define an auxiliary variable $w(t)$ in $W \equiv L^2(-r,0;H)$ by $w(t)(\theta) = E(t) - E(t+\theta), -r \leq \theta \leq 0$.

Since $G(\theta, z) = \hat{G}(\theta, z) > 0$ for $\theta \in (-r, 0], z \in \Omega$ and G is constant in Ω, we may take as an inner product for W the weighted L^2 inner product

$$\langle \eta, w \rangle \equiv \int_{-r}^{0} \hat{G}(\theta) \langle \eta(\theta), w(\theta) \rangle_{\hat{H}} d\theta$$

under which W is a Hilbert Space. We note that by our notational convention explained above, we have $w(t) \in W$ for any $E(t, z)$ with $E(\cdot, \cdot) \in L^2_G(-r, 0; H)$ using a standard shift notation, we may write $w(t) = E(t) - E(t + \theta) = E(t) - E^t(\theta)$ where $E^t(\theta) \equiv E(t + \theta)$ for $-r \leq \theta \leq 0$. Adding and subtracting appropriate terms in (44), we find

$$\ddot{E}(t) + \gamma \dot{E}(t) + \beta E(t) + \int_{-r}^{0} G(\xi) E(t) d\xi - \int_{-r}^{0} G(\xi)[E(t) - E^t(\xi)] d\xi - c^2 E''(t) = \mathcal{J}(t)$$

or, equivalently

$$\ddot{E}(t) + \gamma \dot{E} + (\beta + G_{11}) E(t) - \int_{-r}^{0} G(\xi) w(t)(\xi) d\xi - c^2 E''(t) = \mathcal{J} \tag{45}$$

where $G_{11} \equiv \int_{-r}^{0} G(\xi) d\xi$ and $w(t)(\xi) = E(t) - E^t(\xi)$.

For our semigroup formulation, we consider (45) in the state space $Z = V \times H \times W = H^1_R(0, 1) \times L^2(0, 1) \times L^2_G(-r, 0, \hat{H})$ with states $(\phi, \psi, \eta) = (E(t), \dot{E}(t), w(t)) = (E(t), \dot{E}(t), E(t) - E^t(\cdot))$. To define an infinitesimal generator we begin by defining a fundamental set of component operators. Let $\hat{A} \in \mathcal{L}(V, V^*)$ be defined by

$$\hat{A}\phi \equiv c^2 \phi'' - (\beta + G_{11}) + c^2 \phi'(\cdot) \delta_0 \tag{46}$$

where δ_0 is the Dirac operator $\delta_0 \phi = \phi(0)$. then we find

$$\langle -\hat{A}\phi, \psi >_{V^*, V} = \langle c^2 \phi', \psi' \rangle_H + \langle (\beta + G_{11}) \phi, \psi \rangle_H \tag{47}$$

so that it is readily seen that $\hat{\sigma}_1 : V \times V \mapsto \mathbb{C}$ defined by

$$\hat{\sigma}_1(\phi, \psi) = \langle -\hat{A}\phi, \psi \rangle_{V^*, V} \tag{48}$$

is symmetric, V continuous and V coercive (i.e. $\hat{\sigma}_1(\phi,\phi) \geq c_1|\phi|_V^2 - \lambda_0|\phi|_H^2$ for constants λ_0 and $c_1 > 0$).

We also define operators $B\mathcal{L}(V,V^*)$ and $\hat{K} \in (W,H)$ by

$$B\phi = -\gamma\phi - c\phi(0)\delta_0 \tag{49}$$

so that

$$\langle -B\phi,\psi\rangle_{V^*,V} = \langle\gamma\phi,\psi\rangle_H + c\phi(0)\psi(0) \tag{50}$$

and, for $\eta \in W = L_G^2(-r,0;\hat{H})$,

$$(\hat{K}\eta)(z) = \begin{cases} 0 & z \in (0,1)\backslash\Omega \\ \int_{-r}^0 G(\xi)\eta(\xi)d\xi & z \in \Omega. \end{cases} \tag{51}$$

Since $G(\xi,z) = 0$ for $z \in (0,1)\backslash\Omega$, we abuse notation and write this as

$$\hat{K}\eta = \int_{-r}^0 G(\xi)\eta(\xi)d\xi$$

even though, strictly speaking, $\eta(\xi,z)$ is only defined for $x \in \Omega$.

With these definitions and notations, equation (45) can then be written as

$$\begin{aligned}\langle\ddot{E},\phi\rangle_{V^*,V} + \langle -\hat{A}E,\phi\rangle_{V^*,V} + \langle -B\dot{E},\phi\rangle_{V^*,V}& \\ + \quad \langle -\hat{K}(E-E^t),\phi\rangle_{V^*,V} &= \langle\mathcal{J},\phi\rangle_{V^*,V}\end{aligned}$$

or

$$\ddot{E}(t) = \hat{A}E(t) + B\dot{E}(t) + \hat{K}(E(t)-E^t) + \mathcal{J}(t) \quad \text{in } V^*. \tag{52}$$

We rewrite equation (52) as a first order system in the state $\zeta(t) = (E(t),\dot{E}(t),w(t))$ where $w(t) = E(t) - E^t$. To aid in this we introduce another operator

$$D : \text{dom } D \subset W \mapsto W$$

defined on dom $D = \{\eta \in H^1(-r,0;\hat{H}) | \eta(0) = 0\}$ by

$$D\eta(\theta) = \frac{\partial}{\partial\theta}\eta(\theta).$$

We then observe that $w(t) = E(t) - E^t$ satisfies

$$\begin{aligned} \dot{w}(t)(\theta) &= \dot{E}(t) - \dot{E}(t+\theta) = \dot{E}(t) - DE^t(\theta) \\ &= \dot{E}(t) + D(E(t) - E^t(\theta)) = \dot{E}(t) + Dw(t)(\theta). \end{aligned}$$

Thus we may formally require (52) as a first order system and adjoin it to the equation

$$\dot{w}(t) = Dw(t) + \dot{E}(t). \tag{53}$$

We then obtain the first order system for $\zeta(t)$ given by

$$\dot{\zeta}(t) = \mathcal{A}\zeta(t) + \mathcal{F}(t) \tag{54}$$

where $\mathcal{A}$ given by

$$\mathcal{A} = \begin{pmatrix} 0 & I & 0 \\ \hat{A} & B & \hat{K} \\ 0 & I & D \end{pmatrix}$$

is defined on

$$\text{dom } \mathcal{A} = \{(\phi, \psi, \eta)\ inZ | \psi \in V, \eta \in \text{dom } D, \hat{A}\phi + B\psi \in H\}.$$

That is, $\mathcal{A}\Phi = (\phi, \hat{A}\phi + B\psi + \hat{K}\eta, \phi + D\eta)$ for $\Phi = (\phi, \psi, \eta)$. The forcing function $\mathcal{F}$ in (54) is given by $\mathcal{F} = \text{col}(0, \mathcal{J}, 0)$. To argue that $\mathcal{A}$ is the infinitesimal generator of a C_0-semigroup, we actually consider the system (54) on an equivlaent space $Z_1 = V_1 \times H \times W$ where V_1 is the space V with equivalent inner product $\langle \phi_1, \phi_2 \rangle_{V_1} = \hat{\sigma}_1(\phi_1, \phi_2)$ where $\hat{\sigma}_1$ is the sesquilinear form given in (48). Recall that $\hat{\sigma}_1$ is symmetric, V continuous and V coercive so that it is topologically equivalent to the V inner product.

Under the assumptions on α, β, γ listed in the beginning of this section, we can establish the following.

Theorem 2 *The operator $\mathcal{A}$ is the infinitesimal generator of a C_0-semigroup on Z_1 and hence on the equivalent space Z.*

To prove this theorem, we use the Lumer-phillips theorem ([Paz, p.14]). Since Z_1 is a Hilbert space, it suffices to to argue that for some λ_0, $\mathcal{A} - \lambda_0 I$ is dissipative in Z_1 and $\mathcal{R}(\lambda I - \mathcal{A}) = Z_1$ for some $\lambda > 0$, where $\mathcal{R}(\lambda I - \mathcal{A})$ is the range of $\lambda I - A$. We first argue dissipativeness.

Let $\Phi = (\phi, \psi, \eta) \in \text{dom } \mathcal{A}$. Then

$$\begin{aligned}
\langle A\Phi, \Phi\rangle_{Z_1} &= \langle \psi, \phi\rangle_{V_1} + \langle \hat{A}\phi + B\psi + \hat{K}\eta, \phi\rangle_H + \langle \psi + D\eta, \eta\rangle_W \\
&= \langle \phi, \psi\rangle_{V_1} + \langle \hat{A}\phi + B\psi, \psi\rangle_{V^*,V} + \langle \hat{K}\eta, \psi\rangle_H + \langle \psi + D\eta, \eta\rangle_W \\
&= \hat{\sigma}_1(\psi, \phi) - \hat{\sigma}_1(\phi, \psi) + \langle B\phi, \phi\rangle_H + \langle \hat{K}\eta, \psi\rangle_H + \langle \psi + D\eta, \eta\rangle_W \\
&= - < \gamma\psi, \psi\rangle_H - c|\psi(0)|^2 + \langle \hat{K}\eta, \psi\rangle_H + \langle \psi + D\eta, \eta\rangle_W \\
&\leq |\gamma|_\infty |\psi|_H^2 + |\langle \hat{K}\eta, \psi\rangle| + |\langle \phi + D\eta, \eta\rangle_W|. \qquad (55)
\end{aligned}$$

We consider estimates for the last two terms in (55) separately. From (51) we have

$$\begin{aligned}
|\langle \hat{K}\eta, \phi\rangle_H| &= |\int_{-r}^0 \hat{G}(\theta)\langle \eta(\theta), \phi\rangle_{\hat{H}} d\theta| \\
&\leq \int_{-r}^0 \hat{G}(\theta)|\eta(\theta)|_{\hat{H}}|\phi|_H d\theta \\
&\leq \frac{1}{2}\int_{-r}^0 \hat{G}(\theta)\{|\eta(\theta)|_{\hat{H}}^2 + |\phi|_H^2\} d\theta \\
&\leq k_1|\eta|_W^2 + k_2|\phi|_H^2.
\end{aligned}$$

Moreover,

$$\begin{aligned}
|\langle \psi, \eta\rangle_W| &\leq \int_{-r}^0 \hat{G}(\theta)|\langle \psi, \eta(\theta)\rangle_{\hat{H}}| d\theta \\
&\leq \int -r^0 \hat{G}(\theta)\{\frac{1}{2}|\psi|_H^2 + \frac{1}{2}|\eta(\theta)|_{\hat{H}}\} d\theta \\
&\leq k_3|\psi|_H^2 + k_4|\eta|_W^2.
\end{aligned}$$

Finally, since $\hat{G}(\theta) \geq 0, \dot{\hat{G}} \geq 0$, and $\eta \in \text{dom } D$ requires $\eta(0) = 0$ we may argue

$$\langle D\eta, \eta\rangle_W = \int_{-r}^0 \hat{G}(\theta)\langle D\eta(\theta), \eta(\theta)\rangle_{\hat{H}} d\theta$$

$$
\begin{aligned}
&= \int_{-r}^{0} \hat{G}(\theta)\frac{\partial}{\partial\theta}\frac{1}{2}|\eta(\theta)|_{\hat{h}}^{2}d\theta \\
&= \int_{-r}^{0} \frac{\partial}{\partial\theta}(\hat{G}(\theta)\frac{1}{2}|\eta(\theta)|_{\hat{H}}^{2})d\theta \\
&= \hat{G}(0)\frac{1}{2}|\eta(\theta)|_{\hat{H}}^{2} - \hat{G}(-r)\frac{1}{2}|\eta(-r)|_{\hat{H}}^{2} - \frac{1}{2}\int_{-r}^{0} \dot{\hat{G}}(\theta)|\eta(\theta)|_{\hat{H}}^{2}d\theta \\
&\leq 0.
\end{aligned}
$$

Combining these estimates with (55), we obtain for $\Phi \in \mathrm{dom}\ \mathcal{A}$

$$
\begin{aligned}
\langle \mathcal{A}\Phi, \Phi\rangle_{Z_1} &\leq |\gamma|_\infty|\psi|_H^2 + (k_1+k_4)|\eta|_W^2 + (k_2+k_3)|\psi|_H^2 \\
&\leq \lambda_0|\Phi|_{Z_1}^2,
\end{aligned}
$$

which yields the desired dissapativeness in Z_1.

To establish the range statement, we must argue there exists some $\lambda > 0$ such that for any given $\Psi = (\mu, \nu, \xi)$ in Z, there exists Φ in dom $\mathcal{A}$ satisfying

$$
(\lambda I - \mathcal{A})\Phi = \Psi. \tag{56}
$$

In view of the definition of $\mathcal{A}$, the equation 56 is equivalent to the system

$$
\begin{aligned}
\lambda\phi - \psi &= \mu \\
\hat{A}\phi + (\lambda - B)\psi - \hat{K}\eta &= \nu \\
\psi + (\lambda - D)\eta &= \xi
\end{aligned} \tag{57}
$$

for $(\phi,\psi,\eta) \in \mathrm{dom}\ \mathcal{A}, (\mu,\nu,\xi) \in Z = V \times H \times W$. The first equation us the same as $\psi = \lambda\phi + \mu$ while the third can be written as $\eta = (\lambda - D)^{-1}(\xi+\psi) = (\lambda-D)^{-1}(\xi+\lambda\phi+\mu)$. These two equations can be substituted in the second for $\phi \in V$, to attain an equation for ϕ. If this equation can be solved for $\phi \in V$, then the first and third can be solved for ϕ and η respectively. the equation for ϕ that must be solved is given by

$$
-\hat{A}\phi + (\lambda + B)(\lambda\phi + \mu) - \hat{K}(\lambda - D)^{-1}(\xi + \lambda\phi + \mu) = \nu
$$

or

$$\left[\lambda^2 - \lambda B - \hat{A} - \hat{K}(\lambda - D)^{-1}\lambda\right]\phi = (B - \lambda)\mu + \nu + \hat{K}(\lambda - D)^{-1}(\xi + \mu). \tag{58}$$

If we can invert (58) for $\phi \in V$, then $\psi = \lambda\psi + \mu$ is in V, $\eta = (\lambda - D)^{-1}[\xi + \lambda\phi\mu]$ is in dom $D \subset W$ and

$$\begin{aligned} \hat{A}\phi + B\psi &= \lambda^2\phi + \lambda\phi + \lambda\mu - \nu - \hat{K}(\lambda - D)^{-1}(\xi + \lambda\phi + \mu) \\ &= \lambda\phi - \nu - \hat{K}\eta \end{aligned}$$

is in H so that (ϕ, ψ, η) is in dom $\mathcal{A}$ and solves (57).

Thus the range statement reduces to solving (58) for $\phi \in V$. This in turn reduces to invertability of the operator $\lambda^2 - \lambda B - \hat{A} - \hat{K}(\lambda - D)^{-1}\lambda$.

We first observe that $(\lambda - D)^{-1} = (1 - e^{\lambda\cdot})/\lambda$ since $(\lambda - D)(1 - e^{\lambda\cdot}) = \lambda$ while $\eta(\theta) = \frac{1 - e^{\lambda\theta}}{\lambda}[\xi + \lambda\phi + \mu]$ satisfies $\eta(0) = 0$ and hence is in dom D.

Thus, for $\phi \in H, \hat{K}(\lambda - D)^{-1}\lambda$ satisfies

$$\begin{aligned} \langle \hat{K}(1 - e^{\lambda\theta})\phi, \phi\rangle_H &= \int_{-r}^{0} \hat{G}(\theta)(1 - e^{\lambda\theta})\langle\phi, \phi\rangle_{\hat{H}} d\theta \\ &\leq k_5|\phi|^2_{\hat{h}} \end{aligned}$$

and

$$\begin{aligned} \langle(\lambda^2 - \lambda B)\phi, \phi\rangle &= \langle(\lambda^2 + \lambda\gamma)\phi, \phi\rangle_H + \lambda c|\phi(0)|^2 \\ &\geq k_6|\phi|^2_H \quad \text{for } \lambda \text{ sufficiently large.} \end{aligned}$$

Hence for λ sufficiently large we have

$$\begin{aligned} &\langle(\lambda^2 - \lambda B - \hat{A} - \hat{K}(\lambda - D)^{-1}\lambda)\phi, \phi\rangle_{V^*,V} \\ &\quad = \langle(\lambda^2 - \lambda B)\phi, \phi\rangle_{V^*,V} + \hat{\sigma}_1(\phi, \phi) - \langle\hat{K}(\lambda - D)^{-1}\lambda\phi, \phi\rangle_H \\ &\quad \geq k_6|\phi|^2_H + c_1|\phi|^2_V - \lambda_0|\phi|^2_H - k_5|\phi|^2_H \\ &\quad = c_1|\phi|^2_V + (k_6 - \lambda_0 - k_5)|\phi|^2_H. \end{aligned}$$

Thus is we define the sesquilinear form

$$\sigma_\lambda(\phi,\psi) \equiv \langle(\lambda^2 - \lambda B - \hat{A} - \hat{K}(\lambda - D)^{-1})\phi, \psi\rangle_{V^*,V}$$

we see that for λ sufficiently large, σ_λ is V coercive and hence, by the Lax-Milgram lemma [Wloka], it is invertible. It follows immediately that (58) is invertible for $\phi \in V$. This completes the arguments to prove Theorem 2.

Let $S(t)$ denote the semigroup generated by $\mathcal{A}$ so that solutions to (54) are given by

$$\zeta(t) = S(t)\zeta_0 + \int_0^t S(t-s)\mathcal{F}(s)ds. \tag{59}$$

Solutions are clearly continuously dependent on initial data ζ_0 and the nonhomogeneous perturbation $\mathcal{F}$. The first component of $\zeta(t)$ is a solution $E(t)$ of (44). To argue that the solution agrees with that obtained in Section 3.1, one can now see the arguments in Chapter 4.4 of [BSW]. In summary, one argues equivalence for sufficiently regular initial data and nonhomogeneous perturbation. Then density along with continuous dependence is used to extend the equivalence to more general data (see [BSW] for details).

4 Computational Methods and Results

4.1 The Forward or Simulation Problem for the Debye Polarization Model

In this section we present computational results for both forward problem simulations and inverse problems based on the general formulation for the 1-dimensional geometry given in Section 2.3. We are concerned here with numerical results for the special case of a Debye medium Ω with $\epsilon_r(z) = \epsilon_\infty$, defining the instantaneous polarization in Ω. We first, however, formulate a Galerkin finite element approximation scheme for the system with general polarization.

We return to the differential equation (8) and express it in weak form by

$$\begin{aligned} &\langle \mu_0 \epsilon \ddot{E}, \phi \rangle + \langle \mu_0 \sigma \dot{E}, \phi \rangle + \langle \mu_0 \ddot{P}, \phi \rangle \\ &\quad + \langle E', \phi' \rangle + \frac{1}{c} \dot{E}(t,0)\phi(0) = -\langle \mu_0 \dot{J}_s(t,\cdot), \phi \rangle \end{aligned}$$

where the polarization P is for the moment of the form given in (1) and the mapping to $\tilde{\Omega} = [0,1]$ has already been carried out. The term $\frac{1}{c}\dot{E}(t,0)\phi(0)$ is part of the weak form of the absorbing boundary condition.

To facilitate the computations, we scale the time variable by a factor of $c = 1/\sqrt{\epsilon_0 \mu_0}$ and polarization P by a factor of $1/\epsilon_0$ (i.e., $\tilde{t} = ct$, $\tilde{P} = P/\epsilon_0$). Furthermore, we assume that the permittivity of the medium Ω is a constant. The new equation in the scaled variables (where we have dropped the overtildas on the scaled variables) is

$$\begin{aligned} &\langle \epsilon_r \ddot{E}, \phi \rangle + \eta_0 \langle \sigma \dot{E}, \phi \rangle + \langle \ddot{P}, \phi \rangle \\ &\quad + \langle E', \phi' \rangle + \dot{E}(t,0)\phi(0) = -\eta_0 \langle \dot{J}_s, \phi \rangle \quad \text{for } \phi \in V. \end{aligned} \tag{60}$$

where $\epsilon_r(z) = 1 + I_\Omega(z)(\epsilon_\infty - 1)$ is the relative electric permittivity so that $\epsilon = \epsilon_r \epsilon_0$ and the impedance of free space is defined $\eta_0 = \sqrt{\mu_0/\epsilon_0} \approx 376.73$ Ohms. Moreover, the $\langle \cdot, \cdot \rangle$ are the weighted inner products discussed in Section 2.3.

We employ a first order Galerkin finite element approximation to discretize the problem in the space variable, yielding piecewise linear approximations for $E(\cdot, z)$ and $P(\cdot, z)$. We partition the interval $[0,1]$ uniformly at the points $\bar{z}_i^N = ih$ where $h = 1/N$ and $i = 0, \ldots, N$ and construct the standard piecewise linear spline functions $\phi_i^N(z)$ such that $\phi_i^N(\bar{z}_j^N) = \delta_{ij}$ for $i, j = 0, \ldots, N$. We omit ϕ_N^N in constructing our finite dimensional approximating subspaces $V^N = \text{span}\{\phi_0^N, \phi_1^N, \ldots, \phi_{N-1}^N\}$ so that for all the basis functions we have the essential boundary conditions $\phi_i^N(1) = 0$. The computations reported on here are also simplified by the further requirement that the material boundaries of the slab $\Omega = [z_1, 1]$ coincide with grid points. We denote the index of the left boundary z_1 of Ω by $j = L$, i.e., $\bar{z}_L^N = z_1$. Since the right edge of the material has been mapped to $z = 1$, this corresponds to the grid point $\bar{z}_N^N$.

We seek an approximate solution of (60) in the space $V^N \subset V = H_R^1(0,1)$. Let E_N and P_N denote the the approximations of E and P in this space so that

$$E(t,z) \approx E_N(t,z) \;=\; \sum_{j=0}^{N-1} e_i^N(t)\phi_i^N(z) \tag{61}$$

$$P(t,z) \approx P_N(t,z) \;=\; \sum_{j=0}^{N-1} p_i^N(t)\phi_i^N(z). \tag{62}$$

By allowing both the space of solutions and space of test functions in (60) to be V^N in the weak form of the equation, we obtain in the usual way the Galerkin finite dimensional system of equations given by

$$(M + M_\Omega(\epsilon_\infty - 1))\ddot{e} + M_\Omega \ddot{p} + (\eta_0 \sigma M_\Omega + B)\dot{e} + Ke = \eta_0 \mathcal{J}. \tag{63}$$

for $e = (e_0^N, e_1^N, \ldots, e_{N-1}^N)$ and $p = (p_0^N, p_1^N, \ldots, p_{N-1}^N)$.

The elements of the resulting $N \times N$ finite element matrices are computed in the usual manner (for $i, j = 1, 2, \ldots, N$) by

$$M_{ij} \;=\; \langle \phi_{i-1}, \phi_{j-1} \rangle = \int_0^1 \frac{\bar{\phi}_{i-1}\bar{\phi}_{j-1}}{1 + (\zeta - 1)I_\Omega} d\bar{z}$$

$$
\begin{aligned}
M_{\Omega ij} &= \langle \phi_{i-1}, I_\Omega \phi_{j-1} \rangle = \int_0^1 \frac{I_\Omega}{1+(\zeta-1)I_\Omega} \bar{\phi}_{i-1} \bar{\phi}_{j-1} d\bar{z} \\
K_{ij} &= \langle \phi'_{i-1}, \phi'_{j-1} \rangle = \int_0^1 (1+(\zeta-1)I_\Omega) \bar{\phi}'_{i-1} \bar{\phi}'_{j-1} d\bar{z} \\
B_{ij} &= \phi_{i-1}(0)\phi_{j-1}(0),
\end{aligned} \tag{64}
$$

while

$$
\mathcal{J}_i = -\langle \dot{J}_s, \phi_{i-1} \rangle = -\int_0^1 \frac{\dot{J}_s \bar{\phi}_{i-1}}{1+(\zeta-1)I_\Omega} d\bar{z},
$$

where the integrals are expressed in the scaled variables described in Section 2.3. We note that the variables e, p as well as the coefficient matrices should carry the index N, i.e., p^N, e^N, M^N, K^N, etc. But since this is well understood, we shall drop the notation to that given in (63) and (64) in our subsequent discussions, reminding the reader that as usual all these quantities depend on the spatial discretization index N in the obvious ways.

We have not yet imposed a particular constitutive law to govern polarization in the above formulation. We now restrict our consideration to the Debye model given in equation (4). Applying the same scaling in time and to P as above, (i.e., $\tilde{P} = P/\epsilon_0, \tilde{t} = ct$) we obtain the scaled Debye polarization law

$$
\dot{P} + \lambda P = \epsilon_d \lambda E \quad \text{in } \Omega \tag{65}
$$

where $\epsilon_d = \epsilon_s - \epsilon_\infty$ and $\lambda = 1/c\tau$. Since this equation only holds inside the material domain, we can equivalently multiply the entire equation by $I_\Omega(z)$ and then the Galerkin approximation results in the system of equations

$$
M_\Omega \dot{p} + M_\Omega \lambda p - M_\Omega \lambda \epsilon_d e = 0. \tag{66}
$$

The matrix M_Ω is singular (the first $L-1$ rows and the first $L-1$ columns vanish identically), so in actual computations we solve this equation for the nontrivial variables $p_i, i = L, L+1, \ldots N$ (i.e., $p_0 = p_1 = \cdots = p_{L-1} = 0$). This is equivalent to considering only the Lth through Nth elements of each vector (p, e) in the Galerkin approximation equation for P. With this tacit understanding, we may write the entire system of equations (63),(66) as

$$\begin{aligned}(M + M_\Omega(\epsilon_\infty - 1))\ddot{e} + M_\Omega\ddot{p} \\ + (\eta_0\sigma M_\Omega + B)\dot{e} + Ke &= \eta_0\mathcal{J} \qquad (67)\\ \dot{p} + \lambda p - \lambda\epsilon_d e &= 0. \qquad (68)\end{aligned}$$

By substituting equation (68) and its derivative into equation (67) we obtain an equivalent system of equations

$$\begin{aligned}(M + (\epsilon_\infty - 1)M_\Omega)\,\ddot{e} + (\lambda\epsilon_d M_\Omega + \eta_0\sigma M_\Omega + B)\dot{e} \\ + (-\lambda^2\epsilon_d M_\Omega + K)e + \lambda^2 M_\Omega p &= \eta_0\mathcal{J} \qquad (69)\\ \dot{p} + \lambda p - \lambda\epsilon_d e &= 0.\end{aligned}$$

This can be written as a first order system in the composite variable $x = (e, p, \dot{e})$ as

$$\bar{M}\dot{x} + \bar{K}x = F$$

or,

$$\begin{bmatrix} I & & \\ & I & \\ & & M_1 \end{bmatrix} \dot{\begin{bmatrix} e \\ p \\ \dot{e} \end{bmatrix}} + \begin{bmatrix} 0 & 0 & -I \\ -\lambda\epsilon_d I_{LR} & \lambda I_{LR} & 0 \\ M_2 & M_3 & M_4 \end{bmatrix} \begin{bmatrix} e \\ p \\ \dot{e} \end{bmatrix} = \begin{bmatrix} 0 \\ 0 \\ \eta_0\mathcal{J} \end{bmatrix} \qquad (70)$$

where

$$\begin{aligned} M_1 &= M + (\epsilon_\infty - 1)M_\Omega \\ M_2 &= -\lambda^2\epsilon_d M_\Omega + K \\ M_3 &= \lambda^2 M_\Omega \\ M_4 &= M_\Omega(\lambda\epsilon_d + \eta_0\sigma) + B \end{aligned}$$

and I_{LR} is the $N \times N$ identity matrix where the ones have been replaced with zeros in rows 1 through $L-1$.

We compute an approximate solution to this differential system with the standard Crank-Nicholson scheme, which is a member of a single parameter (θ) family of schemes. Briefly, this can be summarized as follows. For a given value of θ and a step size k, the family of schemes applied to the differential equation: $\dot{x} = f(t,x)$ yields the sequence of iterates $x_n \approx x(t_n) = x(nk)$ where

$$x_{n+1} = x_n + kf_{n+\theta} \tag{71}$$

and

$$f_{n+\theta} = (1-\theta)f(t_n, x_n) + \theta f(t_{n+1}, x_{n+1}).$$

This family includes the Euler scheme when $\theta = 0$, the Crank-Nicholson scheme when $\theta = 1/2$ and the implicit Euler when $\theta = 1$. Since x_{n+1} appears on both sides of equation (71), the method is implicit unless $\theta = 0$. Since our system is linear, it can be solved directly for the value of x_{n+1} even in the case $\theta \neq 0$. Applying this to our matrix system, we obtain another matrix problem for the iterations

$$x_{n+1} = x_n + ky_n$$

where

$$(\bar{M} + k\theta\bar{K})y_n = -\bar{K}x_n + F_{n+\theta} \tag{72}$$

and $x_0 = 0$, since the material is assumed to be initially electrically inactive. Equation (72) is reduced through block-Gaussian elimination to a block upper-triangular system of size $3N - L + 1$, in which only a single block of size N needs to be factored. The LU factorization of this block can be computed once and used throughout the computation. Computational experiments with different values of θ did not produce any substantial improvement in accuracy over $\theta = 1/2$ for our particular systems.

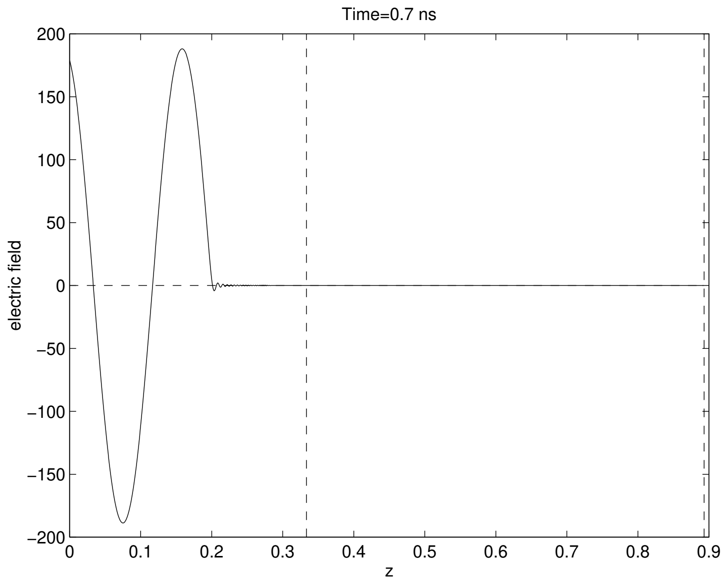

Figure 3: Debye model simulation ($t = 0.7$ ns)

Hence in the numerical results described below all calculations were carried out with the standard Crank-Nicholson time stepping scheme.

We report graphically a sample of results from our forward simulations for the model with Debye polarization. Figures 3 through 6 depict (through time snapshots at $t = 0.7, 5.0, 7.0, 10.0$ ns) the propagation of an electromagnetic wave through a material slab lying in $z \in (.33, .89)$. The material parameters are: $\sigma = 1.0 \times 10^{-2}$ Ohm^{-1}, $\tau = 1.0 \times 10^{-11}$ seconds, $\epsilon_s = 35, \epsilon_\infty = 5, \omega = 2\pi \times 1.8$ GHz. The numerical method is as described above, with the results depicted in the unscaled (i.e., in the original scales) spatial (z) and time (t) axes.

In Figure 3 the incoming wave generated by the current source at $z = 0$ has yet to reach the left edge of the material at $z_1 = 1/3$. In Figure 4 the signal has subsequently been partially reflected and partially transmitted. The reflected part of the field is the first part to be measured in the inverse problems discussed in the next

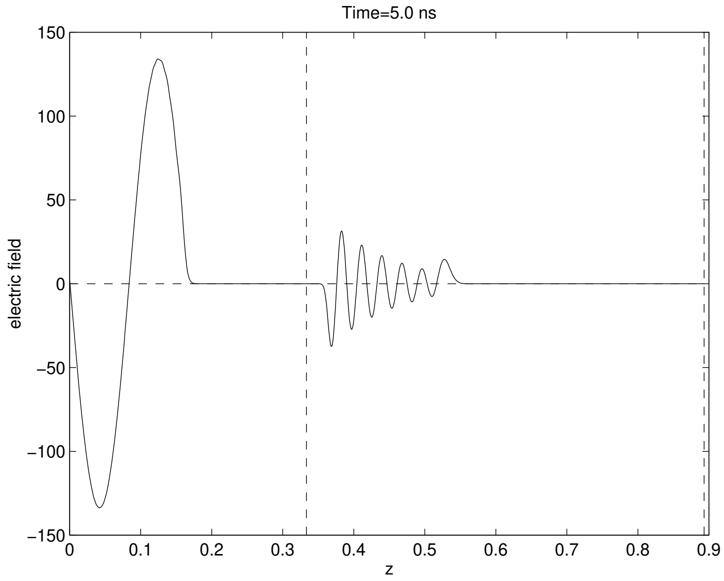

Figure 4: Debye model simulation ($t = 5.0$ ns)

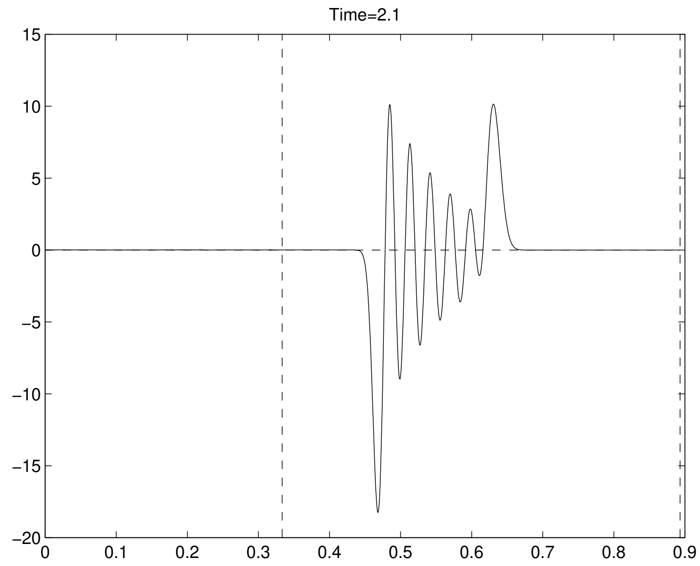

Figure 5: Debye model simulation ($t = 7.0$ ns)

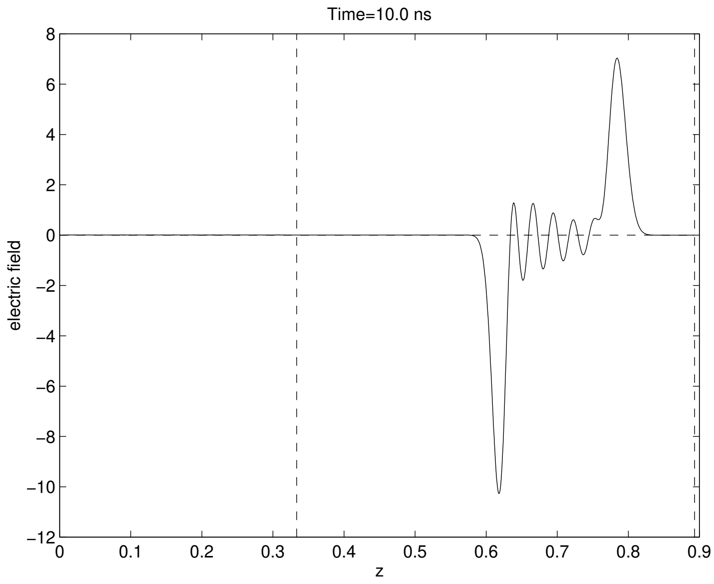

Figure 6: Debye model simulation ($t = 10.0$ ns)

section. In the transmitted part we see the formation of the signal precursor (the Brillion precursors— see [APM, Bri]), which becomes more pronounced in Figures 5 and 6. These simulations were performed on an interval of length 1 with $N = 450$ and the time step was $k = 1 \times 10^{-4}$. Comparison of these (and other simulations) with independently generated solutions (finite difference and Fourier series) demonstrated the general accuracy and efficiency of the piecewise linear/Crank-Nicholson approximation methods in forward simulations and we turned next to the use of these ideas in inverse problem techniques.

4.2 The Inverse or Estimation Problem with the Debye Model

The objective of the inverse problem is the reconstruction of the values of the parameters in the polarization model and the boundary geometry using information obtained through a scattering experiment of the type described in Section 2.1. Observations from the experiment are limited to sampled values of the electric field at selected points outside the material domain Ω. The estimation problem is to minimize a suitable measure of the difference between the simulated prediction and a set of data taken from experienments. The goal of our investigation here is the test the feasibility of this approach for the identification of dielectric and geometric parameters.

We use the same physical problem as in the forward problem described in Section 2.3; this involves a homogeneous slab obeying the Debye model of polarization and a planar electromagnetic interrogating signal. Therefore our observations and data consist of scalar values representing the $\hat{\imath}$ component of the electric field. The experimental observations, consist of the value of the electric field at $z = 0$ at uniform intervals in time $\bar{t}_i = \Delta T i$. Let E_i denote the data we seek to reconstruct and $E(t, z; \vec{q})$ be the electric field arising from a scattering experiment with dielectric and geometric parameters $\vec{q}$. The inverse problem is performed by minimizing the l^2 difference between the data and the simulation results.

$$\min_{\vec{q} \in Q} J(\vec{q}) \quad \text{where} \quad J(\vec{q}) = \sum_{i=1}^{S} |E(\bar{t}_i, 0; \vec{q}) - E_i|^2$$

where S is the number of sample data points. The set of admissible parameters Q is chosen to enforce limitations on the parameters that arise from physical or geometric considerations. The formulation of physical problems generally requires that physical parameters be non-negative. Geometric bounds will be determined according to how the boundary is represented by the parameters, and will reflect both mathematical constraints and physical limitations on the boundary. This set can be made compact by providing both upper and lower bounds for each member.

To test the feasibility of the estimation approach we produce synthetic data for the observations E_i by adding random noise to the results of the simulation with a known set of parameters. The absolute magnitude of the noise is relative to the size of the signal, reflecting the relative nature of uncertainties in measurements. Letting E_i

be the data sampled from the solution with the true parameters, i.e., $E_i = E(\bar{t}_i, 0; \vec{q}^*)$, we define $\bar{E}_i = E_i(1+\chi\eta_i)$ where the η_i are independent normally distributed random variables with mean zero and variance one. The coefficient χ is chosen to adjust the relative magnitude of the noise. We express the magnitude of the noise as a percentage of the size of the signal by taking two times the variance as the size of the random variable. Hence $\chi = 0.05$ corresponds to 10% noise and $\chi = 0.025$ to 5% noise.

The feasibility of the inverse problem is measured by how successful it is at recovering the original values $\vec{q}^*$ and the sensitivity of the results with respect to the magnitude of the noise χ. In the absence of noise, an exact match for the parameter values has an error of zero (or roughly machine precision, allowing for non-essential differences in the method of computation). Minimizing $J(\vec{q})$ is performed though an l_∞ trust region adaptation of Newton's method, using a BFGS secant update for the approximation of the Hessian of the objective function $\frac{\partial^2}{\partial q_i \partial q_j} J(\vec{q})$.

The parameters arising in the Debye model of polarization are the conductivity σ, the infinite and static limits of the dielectric permittivity $\epsilon_\infty, \epsilon_s$ and the relaxation time τ. (Strictly speaking, the conductivity σ is not part of the polarization model, but for convenience we will always group it with the other parameters which describe the dielectric properties of the material.) We will directly identify the related set of parameters $\vec{q} = (\sigma, \epsilon_s, \epsilon_d, \lambda)$ where $\epsilon_d = \epsilon_s - \epsilon_\infty$ and $\lambda = 1/c\tau$. These parameters appear as coefficients in the scaled version of the equations and early simulation results indicated that the optimization problem is better posed when expressed in terms of λ rather than τ. In a subsequent problem we will add the identification of the thickness of the slab $d = z_2 - z_1$. In the scaled version of the equations this is done through identifying the scaling parameter $\zeta = (1 - z_1)/(z_2 - z_1)$ which appears in the definition of the weighted inner products.

Sample Results We present results from the inverse problem of identifying the dielectric parameters in the Debye model. The data to be identified are generated with the Debye model using the following ("true") parameter values:

$$\begin{aligned} \sigma &= 1 \times 10^{-5} \\ \tau &= 8.1 \times 10^{-12} \\ \epsilon_s &= 80.1 \\ \epsilon_\infty &= 5.5 \end{aligned}$$

These parameters are considered reasonable for modeling the polarization behavior of water. The carrier frequency of the interrogating signal is 1.2GHz (hence the angular frequency is $\omega = 2\pi \times 1.2 \times 10^9 = 7.54 \times 10^9$ rad/s) and the duration of the window is 1.67 ns, which is two complete periods. The data consist of 100 measurements of the electric field taken at $z = 0$ every 0.06 ns from $t = 0.06$ ns to $t = 6$ ns. The width of the slab is a fixed quantity sufficient to ensure that the portion of the interrogating signal transmitted through the surface at $z = z_1$ has not returned to $z = 0$ after a subsequent reflection off the back boundary.

Eight different attempts are made at the inverse problem, each with a different level of random noise added to the data. The initial values of parameters used in all of the inverse problems are $\sigma_0 = 1.5 \times 10^{-5}, \tau_0 = 10.0 \times 10^{-12}, \epsilon_{s0} = 73.1, \epsilon_{\infty 0} = 6.0$. The results are summarized in Table 1.

We note that only the parameter ϵ_s is consistently recovered in this inverse problem. While some of the values of τ are close, the converged values of σ and ϵ_∞ are substantially off at all levels of noise. A partial explanation for the differing sensitivities can be found by examining the equations which give rise to the wave equation and polarization equation. Consider the polarization equation,

$$\tau \dot{P} + P = \epsilon_0(\epsilon_s - \epsilon_\infty)E. \tag{73}$$

Test	% Noise	σ	τ	ϵ_s	ϵ_∞	residual
True values:		1.0×10^{-5}	8.1×10^{-12}	80.1	5.5	
1	0.0	9.96×10^{-6}	8.10×10^{-12}	80.10	5.51	8.152×10^{-10}
2	0.5	0.00	1.23×10^{-11}	80.20	29.74	2.180×10^{-2}
3	1.0	0.00	9.18×10^{-12}	80.15	13.89	1.284×10^{-1}
4	1.5	1.14×10^{-2}	2.89×10^{-11}	81.18	60.02	2.631×10^{-1}
5	2.0	0.00	6.49×10^{-12}	80.46	1.00	4.748×10^{-1}
6	2.5	7.34×10^{-3}	1.93×10^{-11}	80.04	48.68	5.752×10^{-1}
7	3.0	0.00	1.30×10^{-11}	79.95	31.10	8.347×10^{-1}
8	5.0	5.56×10^{-2}	3.77×10^{-12}	78.82	28.07	2.034

Table 1: Estimated Parameters in Debye Inverse Problem. Test 1

The small magnitude of τ suggests that $P \approx \epsilon_0(\epsilon_s - \epsilon_\infty)E$. We use this as the basis of an approximation to P. Let $P_s = \epsilon_0(\epsilon_s - \epsilon_\infty)E$ and $P = P_s + P_\tau$. The remaining polarization P_τ satisfies the new differential equation

$$\tau \dot{P}_\tau + P_\tau = -\tau\epsilon_0(\epsilon_s - \epsilon_\infty)\dot{E}. \tag{74}$$

Note that this is the same equation as for the original polarization with a different driving function. We substitute into the equation for the electric flux density and find

$$\begin{aligned} D &= \epsilon_0\epsilon_\infty E + P \\ &= \epsilon_0\epsilon_s E + P_\tau \end{aligned}$$

When the wave equation is derived from this new expression for D, ϵ_s replaces ϵ_∞ as the coefficient of the $\ddot{E}$ term and the parameter ϵ_∞ only appears in the differential equation for P_τ. It remains to argue that the magnitude of this polarization term is much smaller than that of the original P. We make an argument for this based on the roughly periodic nature of the electric field. At any point, when the electric field is not zero (i.e., outside the windowed pulse) the electric field is approximately periodic with a known angular frequency ω. From this we conclude, very approximately, that

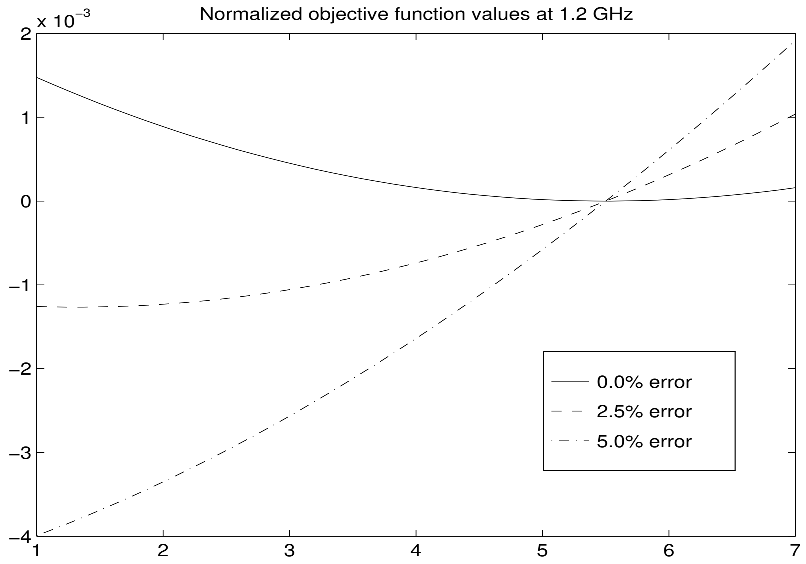

Figure 7: Plot of $J(\vec{q}) - J(\vec{q}^*)$ versus ϵ_∞

$|\dot{E}| \approx |\omega E|$. Comparing the magnitudes of the driving terms in the original (for P) and new (for P_τ) polarization equations we have $|E|/|\tau\dot{E}| \approx 1/\omega\tau$. For the parameter values $\tau = 8.1\times10^{-12}s$ and $\omega = 7.54\times10^9$ rad/s we would expect that that magnitude of P is about 16 times as great as P_τ. Furthermore, ϵ_∞ is many times smaller than ϵ_s and therefore affects the coefficient of the driving term less. This suggests that the effect on the solutions to the forward problem of the parameter ϵ_∞ is dwarfed by that of ϵ_s.

We illustrate this idea graphically by plotting the objective function $J(\vec{q})$ as a function of ϵ_∞ alone. The plots of the objective functions in Figures 7 and 8 are normalized by subtracting the value of $J(\vec{q}^*)$. When no noise in present in the data, this value is zero. The values when noise is present are given in Table 2.

Comparing the two figures, we can see that the objective function is more sensitive to ϵ_∞ for the larger frequency and that the minimizing value of ϵ_∞ is closer to the

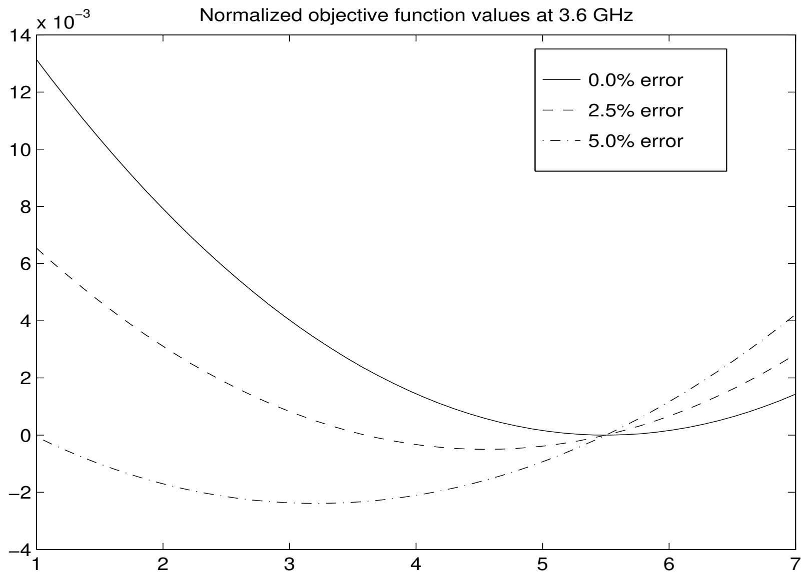

Figure 8: Plot of $J(\vec{q}) - J(\vec{q}^*)$ versus ϵ_∞

	frequency (GHz)	
Noise level	1.2	3.6
2.5%	0.772	5.30
5.0%	3.01	21.20

Table 2: $J(\vec{q}^*)$ in the presence of noise

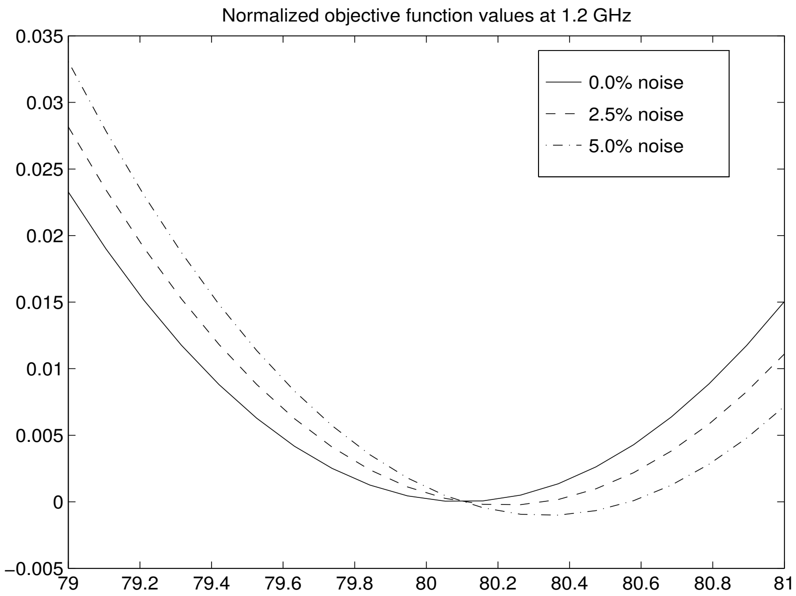

Figure 9: Plot of $J(\vec{q}) - J(\vec{q}^*)$ versus ϵ_s

true value. For the case of 5% noise and $\omega = 2\pi \times 1.2$ rad/s the minimizing value of ϵ_∞ has apparently slipped below the minimum value of $\epsilon_\infty = 1$, the lowest value of ϵ_∞ allowable on physical grounds. For comparison, we also show the dependence of the objective function on the parameters ϵ_s in Figure 9 and σ in Figure 10. Even in a comparatively small range of values for ϵ_s, we see that the dependence is much stronger and that the minimum value is not perturbed as far as ϵ_∞. On the other hand, the dependence of the objective function on σ is moderate for a range of values which is several orders of magnitude larger than the value of σ itself. Hence, we expect that σ is a difficult parameter to recover accurately, when accuracy is measured relative to the size of the parameter.

The new polarization equation (74) also suggests that it may be difficult to separate the parameters τ from ϵ_∞, since the same analysis as before leads us to conclude that $P_\tau \approx -\tau\epsilon_0(\epsilon_s - \epsilon_\infty)E$. Here, τ and ϵ_∞ appear together in the coefficient of the

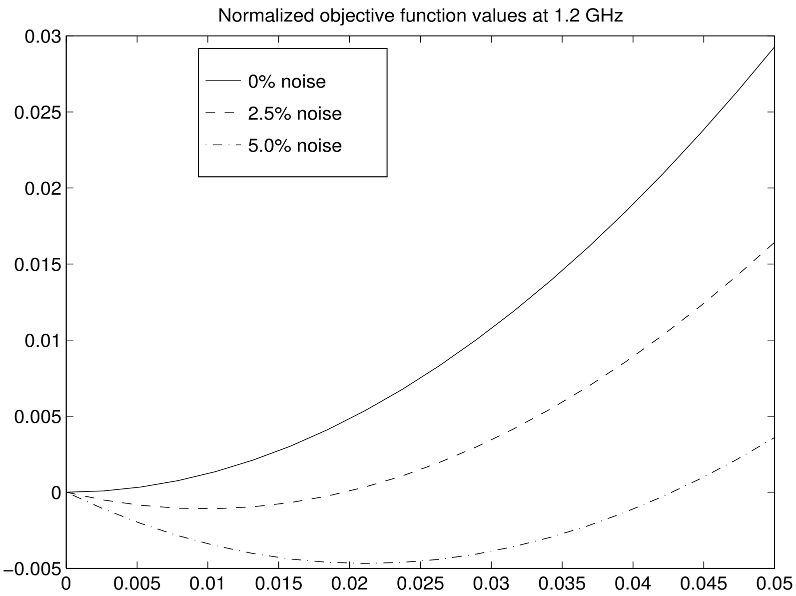

Figure 10: Plot of $J(\vec{q}) - J(\vec{q}^*)$ versus σ

driving term and any other influence of τ on the solution has been ruled out by this approximation. While it should be possible to estimate the size of the driving term's coefficient, it would not be possible to identify particular values for ϵ_∞ and τ. (The parameter ϵ_s, which is also present in the coefficient, is distinguished by its appearance in the wave equation.) This observation is borne out by results from another inverse problem in which the values σ and ϵ_∞ are held fixed. The conductivity σ is fixed at zero and the interrogating frequency is 3.6 GHz. Performing the zero-noise inverse problem, we obtain different values of τ according to the fixed value of ϵ_∞. These results are summarized in Table 3.

The residual column of Table 3 indicates that it is possible to get an acceptably low residual value with parameters far from the "true" values which generated the data. The last column shows that the coefficient of the driving term in the polarization equation (74) is being accurately reconstructed each time, even if the particular

fixed ϵ_∞	estimated τ	estimated ϵ_s	residual	$\tau(\epsilon_s - \epsilon_\infty)$
1.0	7.62×10^{-12}	79.96	3.94×10^{-4}	6.02×10^{-10}
5.5	8.10×10^{-12}	80.10	6.36×10^{-11}	6.04×10^{-10}
10.0	8.64×10^{-12}	80.26	1.61×10^{-4}	6.07×10^{-10}

Table 3: Parameters resulting from incorrect ϵ_∞

Test	% Noise	σ (fixed)	τ	ϵ_s	ϵ_∞ (fixed)	residual
True values:		1.0×10^{-5}	8.1×10^{-12}	80.1	5.5	
1	0.0	0.00	7.62×10^{-12}	79.96	1.00	3.942×10^{-3}
2	0.5	0.00	7.64×10^{-12}	80.37	1.00	0.208
3	1.0	0.00	7.65×10^{-12}	80.79	1.00	0.834
4	1.5	0.00	7.66×10^{-12}	81.21	1.00	1.877
5	2.0	0.00	7.67×10^{-12}	81.63	1.00	3.338
6	2.5	0.00	7.68×10^{-12}	82.06	1.00	5.217
7	3.0	0.00	7.70×10^{-12}	82.49	1.00	7.513
8	5.0	0.00	7.74×10^{-12}	84.24	1.00	20.87

Table 4: Estimated Parameters in Debye Inverse Problem. Test 2

parameter values are wrong. This suggests that the difficulty surrounding the identification of the parameters ϵ_∞ and τ arises because these two parameters are strongly coupled together in their influence on the objective function. The relatively low sensitivity of the objective function to these parameters (compared to ϵ_s) further suggests that parameter values obtained by arbitrarily fixing one of the parameters and identifying a corresponding value for the other will yield parameters which capture the dynamics of the problem accurately (i.e., yield a small residual). To test this approach we perform the optimization problem with the parameter ϵ_∞ fixed at the value 1.0 and the conductivity σ fixed at zero. The results are summarized in Table 4.

In the event that the exact value of ϵ_∞ is known, we can fix the parameter at this value in the optimizations. The results of performing the inverse problem with ϵ_∞ fixed at its correct value of 5.5 are shown in Table 5. We notice that except in the case of zero noise that the residuals are slightly *higher* when the correct value of ϵ_∞

Test	% Noise	σ (fixed)	τ	ϵ_s	ϵ_∞ (fixed)	residual
True values:		1.0×10^{-5}	8.1×10^{-12}	80.1	5.5	
1	0.0	0.00	8.10×10^{-12}	80.10	5.5	6.364×10^{-10}
2	0.5	0.00	8.11×10^{-12}	80.5	5.5	0.209
3	1.0	0.00	8.12×10^{-12}	80.93	5.5	0.835
4	1.5	0.00	8.13×10^{-12}	81.35	5.5	1.879
5	2.0	0.00	8.14×10^{-12}	81.77	5.5	3.341
6	2.5	0.00	7.68×10^{-12}	82.06	5.5	5.220
7	3.0	0.00	8.15×10^{-12}	82.63	5.5	7.517
8	5.0	0.00	8.19×10^{-12}	84.39	5.5	20.88

Table 5: Estimated Parameters in Debye Inverse Problem. Test 3

is used than when $\epsilon_\infty = 1.0$ is used. This is explained by our observation in Figures 7 and 8 that the presence of noise uniformly lowers the optimal value of ϵ_∞.

Reconstruction with Inferior Accuracy As the data used in the above inverse problems is computed with the same numerical scheme which is used in the reconstruction process, we must we aware of the possibility that this positively affects the reliability of the reconstruction. Although we expect that the addition of random noise to the generated data would mask it's fine details well enough to prevent unusually good convergence, we nevertheless test for the possibility by performing the reconstruction with simulations that are less accurate than the one used to generate the data. This is done by generating the data in a simulation with larger values of N, smaller values of dt or both. The results of the inverse problem are summarized in Table 6.

The second row of Table 6 contains the result in which the parameters in the reconstruction match those in the generation of data, resulting in a low residual and accurate reconstruction of parameter values because no noise has been added to the data. The remaining rows indicate the results when different values of N and dt were used in the generation of the synthetic data while the same values of $N = 100$ and

N	dt	σ	τ	ϵ_s	ϵ_∞	residual
True values:		1.0×10^{-5}	8.1×10^{-12}	80.1	5.5	
100	3×10^{-4}	9.96×10^{-6}	8.10×10^{-12}	80.10	5.51	8.152×10^{-10}
400	3×10^{-4}	0.00	9.29×10^{-12}	80.21	14.98	1.530×10^{-3}
100	1×10^{-5}	0.00	1.07×10^{-11}	80.23	22.88	4.206×10^{-2}
400	1×10^{-5}	0.00	9.89×10^{-12}	80.28	17.67	4.430×10^{-2}

Table 6: Estimated Parameters in Debye inverse Problem with Inferior Accuracy

$dt = 3 \times 10^{-4}$ were used in the reconstruction. The results obtained are similar to adding a moderate amount of noise to the data, as seen by comparison with Table 1.

Identification of Material Depth Identifying the depth of the material with this method proved to be more difficult than identifying other parameters. We add the scaling parameter to the list of parameters to be identified, so $\vec{q} = (\sigma, \epsilon_d, \epsilon_\infty, \lambda, \zeta)$ and consider a slightly different inverse problem. In this case, the material is sufficiently thin and the duration of the data collection sufficiently long so that the part of the interrogating signal transmitted through the medium had returned after being reflected off the metallic back boundary. This is clearly necessary in any attempt to recover the depth of the sample.

We see in in Figure 11 the complicated dependence of $J(q,d)$ on d, owing to the oscillatory nature of the time domain data. (The results are presented in terms of the actual thickness d instead of the scaling parameter ζ). Here, $J(\vec{q}^*, d)$ is plotted for various values of d with the other parameters held fixed at their true values. The true depth of the material is $d = 0.05$, corresponding to the global minimum of $J(\vec{q})$. (This example uses the parameter values for water given above.)

Figure 12 depicts one cause of the multiple local minima apparent in Figure 11. With the incorrect value of d, the return of the transmitted and subsequently reflected part of the interrogating signal is delayed by two full periods of the input signal. This

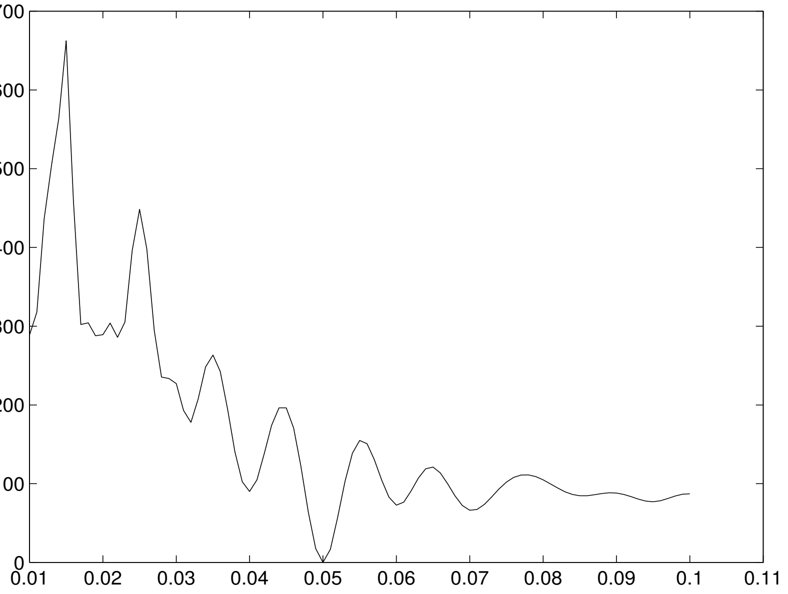

Figure 11: Error as a function of material depth.

brings it back into partial synchronization with the data, giving it a smaller error than nearby values where the data is out of phase. This produces a local minima as seen in Figure 11.

Optimization results using the function $J(\vec{q})$ where $\vec{q}$ includes the scaling parameter ζ were very poor, even when only attempting to identify the depth d. Solutions tended to incorrect local minima for all but a very narrow range of initial values of d. This led us to develop another procedure for identifying depth, based on identifying the return time of the transmitted part of the interrogation signal.

We separate the geometric parameter ζ from the rest of the parameters in $\vec{q}$ to clarify parts of the following discussion. Here, $\hat{q}$ contains just the physical (material) parameters and $\vec{q} = (\hat{q}, \zeta)$. We will interchangeably discuss estimation of the parameters ζ and d with the understanding that the actual optimization is always performed over ζ and that the two parameters are related through $\zeta = (1 - z_1)/d$.

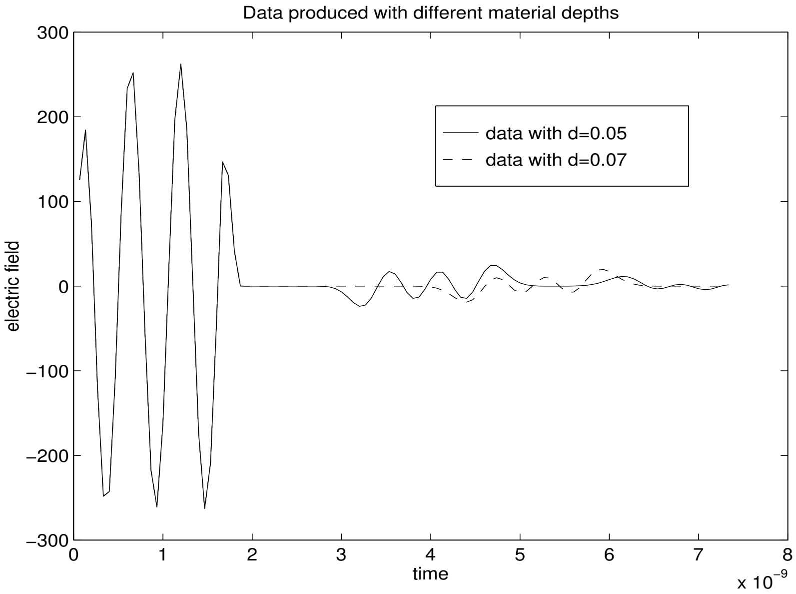

Figure 12: Illustration of local minima at $d = 0.07$

Let $t_r(\hat{q}, d)$ be the time at which the signal which penetrates Ω first returns to $z = 0$ after being transmitted through the medium and reflected off its back surface, expressed as a function of the material parameters and the depth of the sample. Let Δ and δ be positive constants with values to be determined and t_f^s be the duration of the interrogation signal. We approximate the return time by: $t_r(q, d) \approx \tilde{t}_r(q, d) = \bar{t}_{\bar{\imath}}$ where $\bar{\imath}$ is the first index such that:

$$E_i - E_{i-1} \geq \Delta(\bar{t}_i - \bar{t}_{i-1}) \tag{75}$$

$$t_i \geq (1+\delta)(2z_1 + t_f^s). \tag{76}$$

Equation (75) is satisfied when the finite difference approximation to $E_t(t, 0)$ is greater than the constant Δ. The constraint in equation (76) prevents the test from detecting the first reflection off the surface of Ω, which is over at $t = 2z_1 + t_f^s$. (Note that the time is expressed in the scaled variable.) The parameter δ is chosen to delay detection further in order to avoid detecting numerical noise or the decaying electric

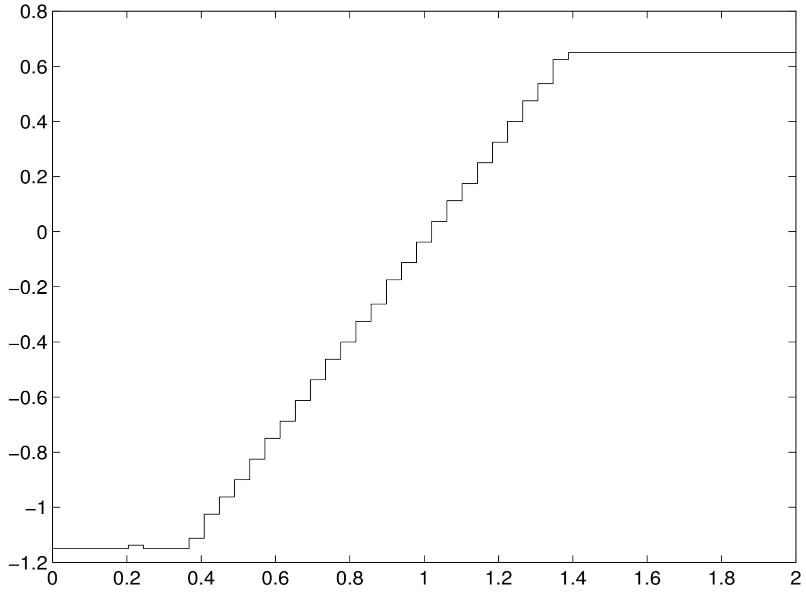

Figure 13: $f_t(d)$ for example problem.

field which trails behind the reflection when the value of the conductivity σ is large. Typical values of these parameters which give good results are $\Delta = 20.0$ and $\delta = 0.05$.

We use the estimated return time $\tilde{t}(\hat{q}, d)$ to identify the true material depth d^*. Let $\tilde{t}(\hat{q}^*, d^*)$ be the estimated return time (satisfying equations (75) and (76)) for the true data E_i, generated with the true parameter values $\hat{q}^*$ and material depth d^*. We then look for a root of the equation $f_t(d) = \tilde{t}(q^*, d) - \tilde{t}(q^*, d^*)$, which represents the difference in estimated return times between the simulation and the data.

The function $f_t(d)$ corresponding to the example given in detail below is plotted in Figure 13. The plateau of values for large d occurs because the deep reflection no longer returns before the end of the simulation and the detection algorithm returns t_f, yielding $f_t(d) = t_f - \tilde{t}_r(q^*, d^*)$

Because $f_t(d)$ is a discontinuous function of a single variable, we employ Brent's method [PTVF, p.352] to approximate the root, since it does not rely on derivative

Noise Level %	Converged to
0.5	0.099996
10.0	0.099926
20.0	0.09985
30.0	0.09978
40.0	0.09972
100.0	0.09934

Table 7: Results of depth estimation

information. The piecewise constant character of $f_t(d)$ also limits the accuracy available in the estimate of d. Therefore, we adopt a two-step approach to finding the final value of this parameter.

1. Use Brent's method to find an estimate d_1 of the root of $f_t(d)$.

2. Use $\zeta_1 = (1 - z_1)/d_1$ as an initial value for the continuous optimization of $J(q^*, d)$ over the single parameter ζ.

Results The two step approach described above is extremely effective. For a test problem using the physical parameters for water ($\sigma = 1.0 \times 10^{-5}, \epsilon_s = 80.1, \epsilon_\infty = 5.5, \tau = 8.1 \times 10^{-12}$) and $\omega = 2\pi \times 2.33$ GHz, $t_f^s = 1.66$ ns, $t_f = 8.33$ ns and $d^* = 0.1$ a wide variety of initial values of d in the range $(0, 1.0)$ lead to convergence to the correct value. In these simulations, $\Delta T = 4.66 \times 10^{-3}$ ns and the parameters in the signal return detection are $\Delta = 20.0, \delta = 0.05$.

The identification of the material depth is also very insensitive to noise in the data. We tested the sensitivity of the problem by adding normally distributed random noise of various magnitudes to the data set as in Section 4.2 and repeated the inverse problems using the initial value $d_0 = 0.02$, with the results obtained shown in Table 7.

Here we can see that noise as large as the amplitude of the original signal does not affect the depth estimation very much. This robustness of the depth estimate is due in part to the nature of the noise. Since it is relative noise, it has little effect on the data points between the surface reflection and the return of the signal which penetrated the material since these values are all nearly zero. Thus the return time of the signal is not effected, since the point at which the data has its first substantial jump is the same. Furthermore, the minimum of $J(\vec{q})$ is still attained by the value of d for which the penetrating part of the signal returns at the correct time, causing the zero and non-zero parts of the data to match.

Estimating Depth and Physical Parameters The method described above for estimating the depth d is limited by the need to know the exact values of the physical parameters $\hat{q}^*$ to form the function $f_t(d) = \tilde{t}(\hat{q}^*, d) - \tilde{t}(\hat{q}^*, d^*)$. We eliminate this requirement by modifying the algorithm and obtaining the following three step process.

1. Estimate the physical parameters by minimizing $J(\vec{q})$ over the physical parameters $\hat{q}$ only. Do this over a data set sufficiently short so that it only contains the exterior surface (i.e., $z = z_1$) reflection. Choose $\zeta_0 = (1 - z_1)/d_0$ such that the penetrating signal does not return from the back boundary in any of the simulations. To do this, choose $t_f' < t_r(\hat{q}^*, d^*)$ and $t_f' < t_r(\hat{q}, d_0)$ for a wide range of values of $\hat{q}$ and d_0. Estimate $\hat{q}_1$ only using the data E_i where $\bar{t}_i < t_f'$.

2. Using the estimate $\hat{q}_1$ from step 1, find the root of $f_t^1(d) = \tilde{t}(\hat{q}_1, d) - \tilde{t}(\hat{q}^*, d^*)$. Call this estimate d_1

3. Use the estimated value $\zeta_1 = (1 - z_1)/d_1$ from step 2 and the estimate $\hat{q}_1$ from step one as an initial estimate for minimizing $J(\vec{q})$.

To accomplish step 1, we use the physical property that the speed of propagation of waves in the media cannot be any faster than is it in vacuum. Since the deep reflection must transverse the distance z_1 twice at speed one and the depth of the material twice at no more than speed one, $t_r(\hat{q}, d) > 2(z_1 + d)$ for all parameter values $\hat{q}$.

We need to choose the reduced test time t'_f so that it is after the end of the first reflection and before the beginning of the deep reflection. Hence,

$$2z_1 + t^s_f \le t'_f \le 2z_1 + 2d \tag{77}$$

Using this conservative estimate, we can guarantee the existence of a suitable test time t'_f where $d > t^s_f/2$ and where $t^s_f \in [2z_1 + t^f_s, 2z_1 + 2d]$. In practice, we can relax the constraint on d because the typical speed on propagation in these materials is much less than 1. This is the case in the example given in the next section.

Results Our example for this inverse problem uses the following physical parameters for the generation of data: $\sigma^* = 1.5 \times 10^{-5}$, $\tau^* = 8.1 \times 10^{-12}$, $\epsilon^*_s = 80.1$, $\epsilon^*_\infty = 5.5$, $d^* = 0.05$. These parameters will be estimated in the inverse problem. The leading edge of the material is at $z_1 = 0.25$ and the simulation is run until $t_f = 7.33$ ns, which is sufficient time for the transmitted part of the signal to return to $z = 0$ after subsequent reflections off the far boundary. The duration of the input signal is $t^s_f = 1.66$ ns and its frequency is $\omega = 2\pi \times 1.8$ GHz, yielding three full oscillations. The data is sampled 110 times over the duration of the simulation, hence $\Delta T = 0.0667$ ns. The resulting data collected at $z = 0$ is plotted in Figure 14. The transmitted pulse can be seen passing through $z = 0$ over the time span 4.3 ns to 6.7 ns.

Notice that the right inequality in equation (77) is not satisfied by this value of d. We can see from Figure 14 that the slow propagation of the signal through the medium nevertheless results in a gap between the end of the first reflection and the beginning of the transmitted signal.

The first stage of the optimization is carried out over half of the data up to the

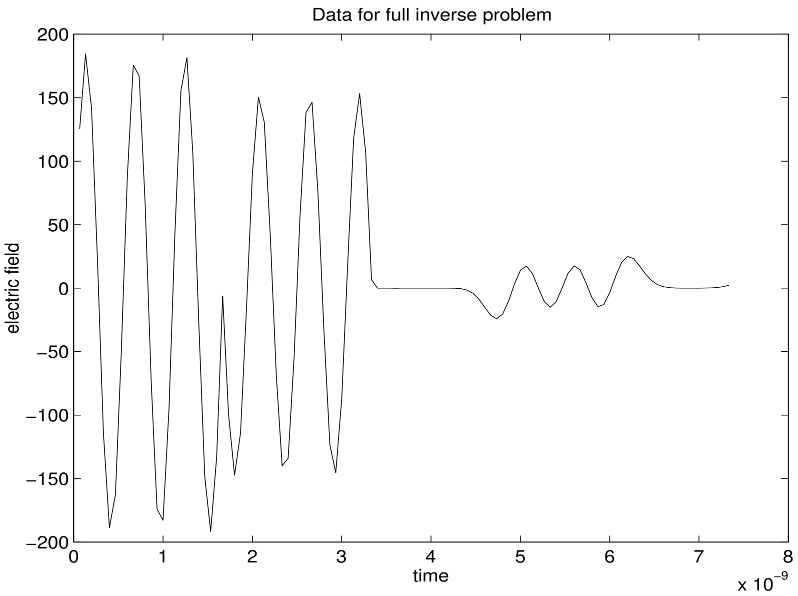

Figure 14: E_i for inverse problem.

time $t'_f = 1.1$. The data was generated numerically using 600 basis elements in the spatial (finite element) approximation. As before, random noise is added to the results of the forward problem to generate synthetic data for the inverse problem. Various initial values are used to test the range of convergence for the optimization problem. The results of one such test are given in Table 8.

As before, we see that the estimates of σ and ϵ_∞ are not very good, while ϵ_s and τ are comparatively robust with respect to noise in the data. Further, the estimated depth of the sample is largely insensitive to noise. Performing the experiment again with a different initial value yields similar results as given in Table 9.

Aside from the unreasonable values (underlined in Table 9) which appear in the case of 2.0% noise, these results resemble those in the previous trial, especially in the values of ϵ_s and τ. As before, the depth measurement is quite accurate. The results of the 2.0% trial indicate that the method as presented here is not perfectly robust,

% Noise	σ	τ	ϵ_s	ϵ_∞	d
True values:	1.0×10^{-5}	8.1×10^{-12}	80.1	5.5	0.05
Initial values:	1.0×10^{-5}	8.2×10^{-12}	81.0	5.3	0.055
0.0	2.0×10^{-5}	8.07×10^{-12}	80.09	5.19	0.0500
0.5	1.3×10^{-3}	7.86×10^{-12}	79.84	3.33	0.0501
1.0	0.0	7.76×10^{-12}	79.85	2.23	0.0501
1.5	3.70×10^{-3}	7.99×10^{-12}	78.94	4.37	0.0503
2.0	0.0	7.76×10^{-12}	80.31	2.38	0.0499
2.5	4.23×10^{-3}	7.52×10^{-12}	77.82	0.0	0.0503

Table 8: Simultaneous Estimation of Debye Parameters and Depth. Test 1

% Noise	σ	τ	ϵ_s	ϵ_∞	d
True values:	1.0×10^{-5}	8.1×10^{-12}	80.1	5.5	0.05
Initial values:	1.0×10^{-3}	10.0×10^{-12}	90.0	3.0	0.1
0.0	8.2×10^{-4}	8.11×10^{-12}	80.10	5.58	0.0500
0.5	1.3×10^{-2}	7.88×10^{-12}	79.84	3.48	0.0501
1.0	0.0	7.77×10^{-12}	79.85	2.29	0.0501
1.5	3.70×10^{-2}	7.99×10^{-12}	78.94	4.33	0.0504
2.0	8.00×10^{-2}	$\underline{12.36 \times 10^{-12}}$	80.60	$\underline{41.72}$	$\underline{0.119}$
2.5	4.23×10^{-5}	7.52×10^{-12}	78.82	0.0	0.0504

Table 9: Simultaneous Estimation. Test 2

and some caution interpreting results is called for.

4.3 Forward or Simulation Problem with the Lorentz Model

The underlying numerical formulation for simulations using the Lorentz model is the same as that for the Debye model up to and including the the finite dimensional system of differential equations in (63) and the matrix definition in (64). We depart from the previous formulation in the choice of constitutive law to govern polarization. We use the Lorentz equation discussed in Section 2.1. Applying the same scaling as before, we obtain the scaled Lorentz polarization law

$$\ddot{P} + 2\lambda\dot{P} + \hat{\omega}_0^2 P = \hat{\omega}_p^2 E \tag{78}$$

where $\hat{\omega}_0 = \omega_0/c, \hat{\omega}_p = \omega_p/c$ and $\lambda = 1/2c\tau$. The derivation of the finite element equations for the polarization precedes exactly as in the Debye case, with the same provision that components of the variables p and $\dot{p}$ which are identically zero are dropped. (These are the ones corresponding to the exterior of the material domain Ω). The resulting system of equations is

$$\begin{aligned} (M + M_\Omega(\epsilon_\infty - 1))\ddot{e} + M_\Omega\ddot{p} & \\ + (\eta_0\sigma M_\Omega + B)\dot{e} + Ke &= \eta_0\mathcal{J} \qquad (79) \\ \ddot{p} + 2\lambda\dot{p} + \hat{\omega}_0^2 p - \hat{\omega}_p^2 e &= 0. \qquad (80) \end{aligned}$$

By substituting equation (80) into equation (79) we obtain an equivalent system of equations

$$\begin{aligned} (M + (\epsilon_\infty - 1)M_\Omega)\,\ddot{e} + (\eta_0\sigma M_\Omega + B)\dot{e} & \\ + (\hat{\omega}_p^2 M_\Omega + K)e - \hat{\omega}_0^2 M_\Omega p - 2\lambda^2 M_\Omega\dot{p} &= \eta_0\mathcal{J} \qquad (81) \\ \ddot{p} + 2\lambda\dot{p} + \hat{\omega}_0^2 p - \hat{\omega}_p^2 e &= 0. \qquad (82) \end{aligned}$$

This can also be written as a first order system in the composite variable $x = (e, p, \dot{e}, \dot{p})$ as

$$\bar{M}\dot{x} + \bar{K}x = F$$

where

$$\bar{M} = \begin{bmatrix} I & & & \\ & I & & \\ & & M_r & \\ & & & I \end{bmatrix} \tag{83}$$

$$\bar{K} = \begin{bmatrix} 0 & 0 & I & 0 \\ 0 & 0 & 0 & I \\ K_1 & K_2 & K_3 & K_4 \\ -\hat{\omega}_p^2 I & \hat{\omega}_0^2 I & 0 & 2\lambda I \end{bmatrix}$$

and the submatrices are

$$\begin{aligned} M_r &= M + (\epsilon_\infty - 1)M_\Omega \\ K_1 &= (\hat{\omega}_p^2 M_\Omega + K) \\ K_2 &= -\hat{\omega}_0^2 M_\Omega \\ K_3 &= (\eta_0 \sigma M_\Omega + B) \\ K_4 &= -2\lambda^2 M_\Omega \end{aligned} \tag{84}$$

In the implementation, a matrix-free method is used which avoids constructing the large and irregularly sparse matrices $\bar{M}$ and $\bar{K}$. The matrix-free implementation works by providing a function which computes the derivative of the composite state variable x to a software routine which performs the quadrature. The function for computing the derivative is made faster by re-using the computation of $\ddot{p}$, which is part the of the derivative of the state and also appears in equation (79) where it is used in the direct computation of $\ddot{e}$.

Difficulties arise in the computation of solutions to the above equation when using physically realistic values of the material parameters, as the resulting linear system of equations is exceedingly stiff. We use the parameter values $\epsilon_s = 2.25, \epsilon_\infty = 1.0, \omega_0 = 4.00 \times 10^{16}, \tau = 3.57 \times 10^{-16}$ and the corresponding plasma frequency is $\omega_p = 4.472 \times 10^{16}$. These are typical values in the study of physical optics [BF]. We perform the discretization described above on a grid of size $N = 100$ with the left edge of the material located at $z = 0.01$ and the right edge at $z = 0.1$. We computed the matrices $\bar{M}$ and $\bar{K}$ using Matlab and from this found the condition number of the linear system matrix $\kappa(\bar{M}^{-1}\bar{K}) = 3.23 \times 10^{19}$, making this an extremely stiff system to be integrated. In the fourth order Runga-Kutta methods applied to this equation, the largest step sizes which did not lead to the blowup of the system are generally around $k = 1 \times 10^{-8}$. To generate solutions to this system of equations, we must be content with very short simulations which observe the pulse propagating through a very short distance.

The following results are generated from a simulation where the material occupies the interval $(1.0 \times 10^{-6}, 1.0 \times 10^{-5})$, and with material parameters $\epsilon_s = 2.25, \epsilon_\infty = 1.0, \omega_0 = 1.779 \times 10^{16}, \tau = 7.14 \times 10^{-16}$. The frequency of the interrogation signal is taken to be 8×10^5 GHz and the duration of the signal is equal to twelve of its periods. (The high frequency is necessary in order to see the formation of the Brillion and Sommerfield precursors associated with the Lorentz model.) The resulting pulse train thus has twelve complete cycles. Solutions from the simulation are are displayed graphically in Figures 15, 16, 17, and 18.

In Figure 15 the pulse is traveling to the right after having just entered the material. In Figure 16 it has undergone two reflections, first off the supra-conducting back boundary followed by a partial reflection off the surface at z_1. Figure 17 is two reflections later again, and in Figure 18 the pulse is traveling to the left after another reflection off the back boundary. Here we can see that the pulse has resolved

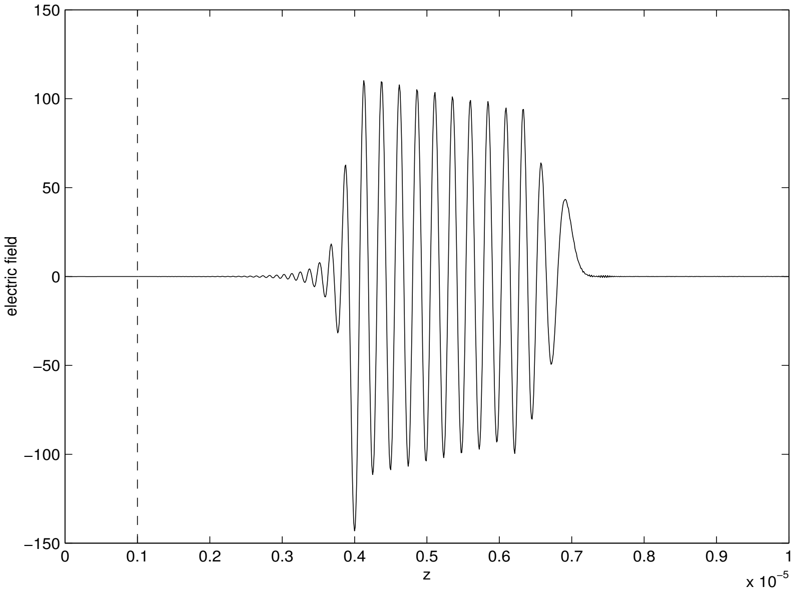

Figure 15: Lorentz model simulation ($t = 3.33 \times 10^{-5}$ ns)

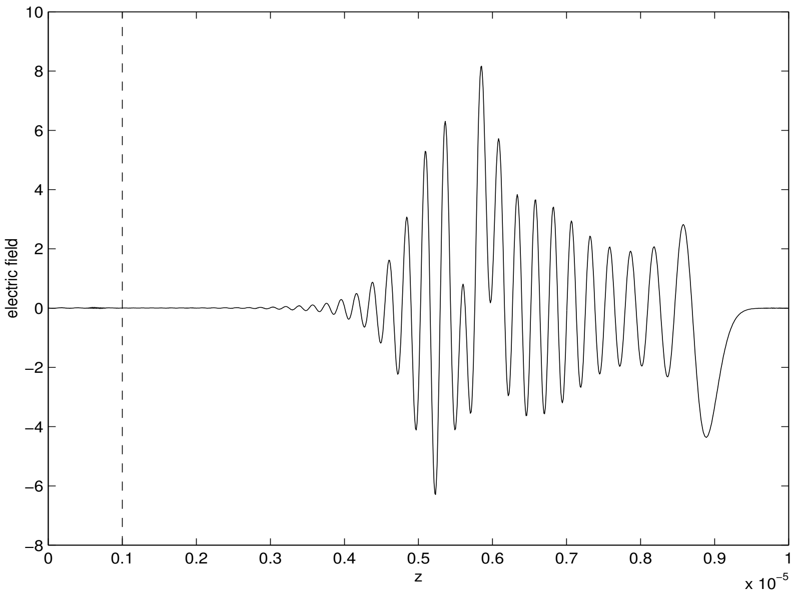

Figure 16: Lorentz model simulation ($t = 1.33 \times 10^{-4}$ ns)

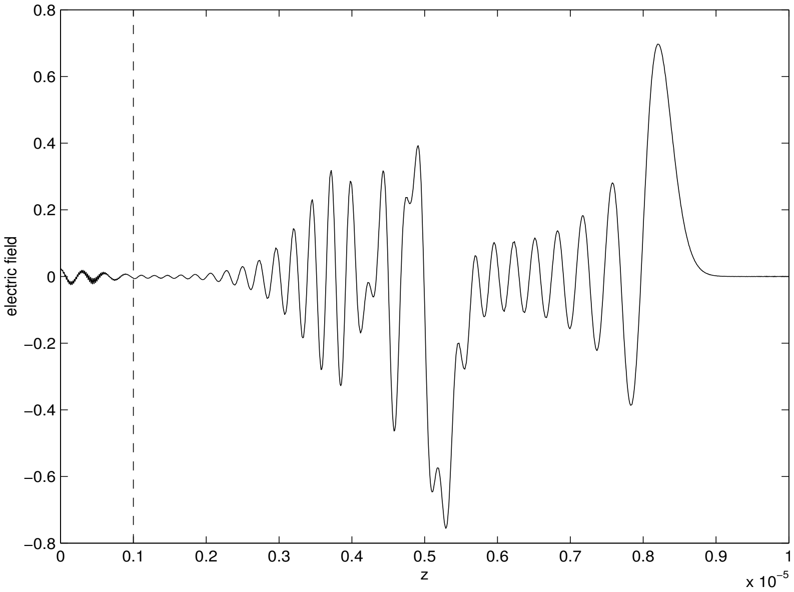

Figure 17: Lorentz model simulation ($t = 2.2 \times 10^{-4}$ ns)

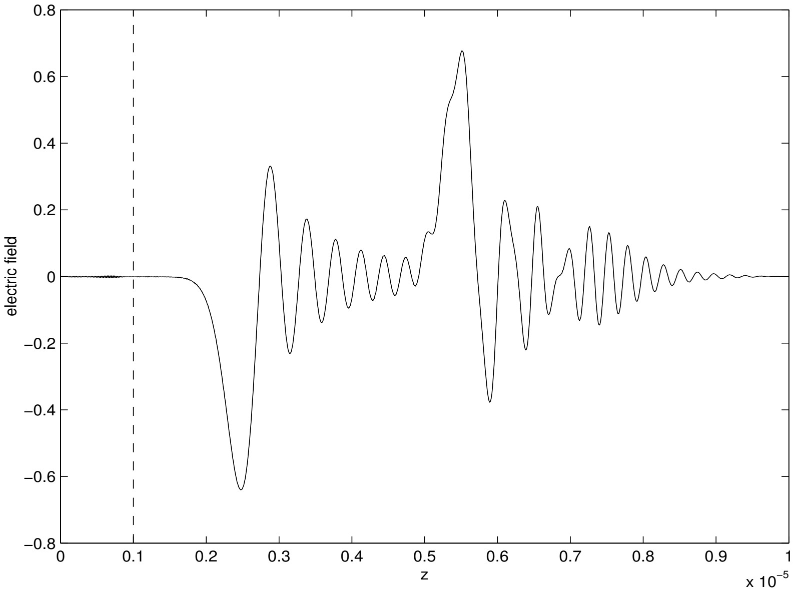

Figure 18: Lorentz model simulation ($t = 2.67 \times 10^{-4}$ ns)

into a part which resembles the Brillion precursors encountered in simulations of the Debye model, and another part associated with the Sommerfield precursors. These precursors are examined in detail in [BF] using a frequency domain approach.

These plots were made from a simulation using one thousand basis elements in the discretization of the space variable and with a step size of $k = 3.0 \times 10^{-9}$ in the scaled time variable. This represents an actual time step of 1.0×10^{-8} ns and over 26,000 steps are required to reach the state shown in Figure 18. Certain limitations of the accuracy of the simulation are also visible in Figures 15 through 18. The persistent distance of the solution from zero outside of the pulse is accumulated numerical error. Although this error appears negligible in Figure 15, the subsequent decay in the magnitude of the pulse continually increases the relative size of this error.

4.4 The Inverse or Estimation Problem with the Lorentz Model

Because of the long execution times of the forward simulations using the Lorentz model, we restrict our attention to the identification of parameters using the reflection of the interrogating signal off the surface of the material and do not attempt to identify the material's depth. Based on our experience with the Debye equation, we also do not attempt to identify the conductivity parameter σ. However, unlike the Debye problem, this problem is adequately sensitive to the parameter ϵ_∞. Our attempts at estimating the parameters in the Lorentz model take place in a test problem with a slightly different set of physical parameters than used in the example above (since those parameters were chosen to accent the precursor development for demonstration, we now choose parameters more representative of real materials [BF]). Here we use $\epsilon_s = 2.25, \epsilon_\infty = 1.0, \omega_0 = 4.0 \times 10^{16}, \tau = 3.57 \times 10^{-16}$ The interrogating signal is given a frequency of 1.2×10^{14} Hz and the signal is stopped after four complete periods of

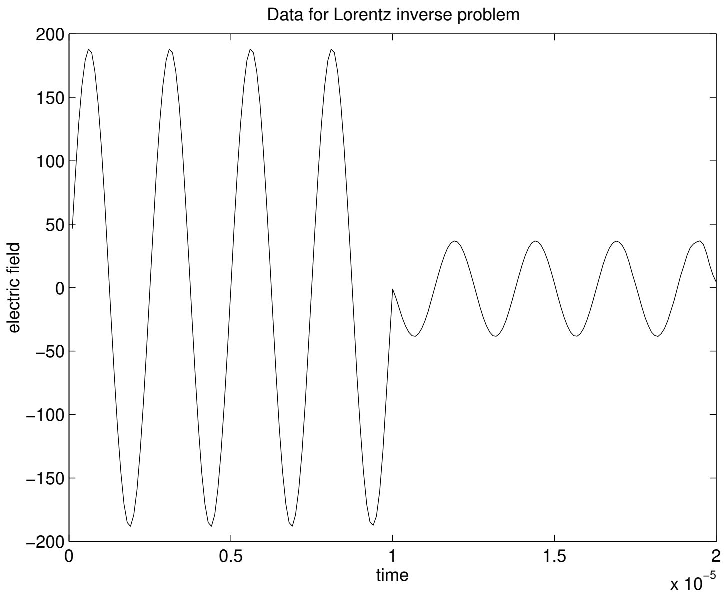

Figure 19: Data for Lorentz inverse problem

the input ($\frac{1}{3} \times 10^{-13}$ sec). The data for the inverse problem is depicted graphically in Figure 19.

The first trials of the inverse problem attempt to establish a rough radius of the acceptable initial values for the parameters to be successfully estimated. This optimization is attempted first over the two parameters ω_0 and ω_p and then over three parameters ω_0, ω_p and τ. Note that the optimization over τ is actually performed through the related parameter $\lambda = 1/2c\tau$. The initial values for the parameters are found by perturbing the "true" values by various relative values, i.e., $\omega_0^0 = (1+\chi)\omega_0^*$. A value of $\chi = 0.05$ yields a 5% perturbation of ω_0, for example.

The first attempts on the Lorentz model with the l_∞ trust region code used with the Debye model encountered difficulties arising from the scale and sensitivity to the parameters. The algorithm quickly became saddled with a trust region which was too small to allow sufficient progress to the minimum, or which caused successive steps

% Distance	ϵ_∞	ω_0	ω_p	τ	residual
True values:	1.0000	4.0000×10^{16}	4.4721×10^{16}	3.57×10^{-16}	0.0
20%	1.0001	3.9958×10^{16}	4.4675×10^{16}	3.57×10^{-16}	4.311×10^{-2}
30%	1.0001	4.0000×10^{16}	4.4720×10^{16}	3.55×10^{-16}	1.564×10^{-3}

Table 10: Convergence results over ω_0 and ω_p

% Noise	ϵ_∞	ω_0	ω_p	τ
True values:	1.0	4.000×10^{16}	4.472×10^{16}	3.570×10^{-16}
1.0%	1.00016	4.006×10^{16}	4.480×10^{16}	3.239×10^{-16}
2.0%	1.00000	4.019×10^{16}	4.496×10^{16}	3.238×10^{-16}
3.0%	1.00038	4.028×10^{16}	4.472×10^{16}	3.236×10^{-16}
4.0%	1.00012	4.034×10^{16}	4.516×10^{16}	3.233×10^{-16}
5.0%	1.79856	2.540×10^{16}	1.715×10^{16}	3.100×10^{-16}
6.0%	1.87854	2.356×10^{16}	1.445×10^{16}	2.976×10^{-16}

Table 11: Results of Lorentz Inverse Problem in the Presence of Noise

short enough to trigger the convergence criterion prematurely. This was remedied by switching to a line-search method and scaling the parameters to give them similar magnitudes. The scaling factors used with each parameter are 1 for ϵ_∞, 1×10^8 for ω_0 and ω_∞ and 1×10^6 for λ. This produced the results given in Table 10.

The Table 10 suggests that initial parameter values which are within 30% of the true values are suitable for initial iterates, at least in the absence of noise in the data. This range of parameter values should be compatible with reasonable *a priori* knowledge of the parameters of a real material.

The inverse problem is then attempted in the presence of noise of uniform relative amplitude applied to the observed data in the manner described in Section 4.2 for the Debye problem. The initial values for the parameters are perturbed by 10% from the correct values (with one exception noted below) and the results of these simulations are given in Table 11.

We notice that the quality of the results deteriorates at 5.0% noise and that τ

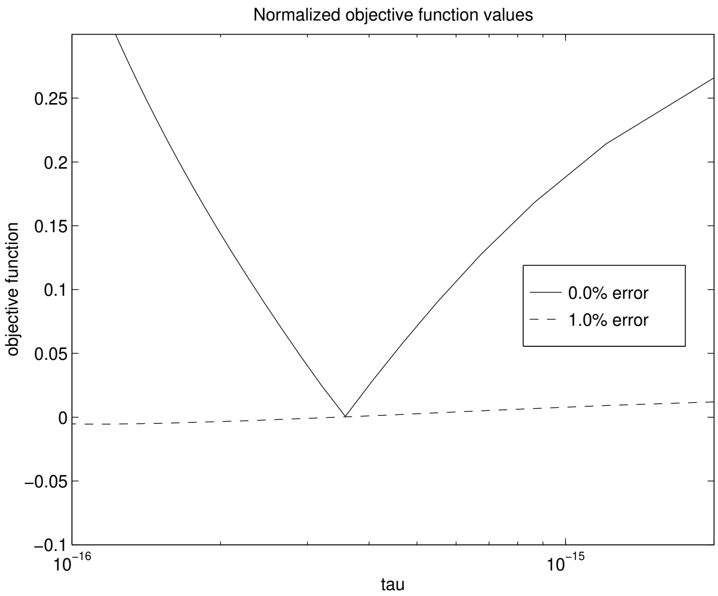

Figure 20: Plot of $J(\vec{q}) - J(\vec{q}^*)$ versus τ

is the most difficult of the parameters to recover accurately. When considered as a function of τ only, the objective function exhibits considerable sensitivity with respect to noise, as shown in Figure 20. Here, we can see that the objective function is much less sensitive to the value of τ even in the presence of a small amount of noise. The minimizing values of τ in the presence of various amounts of noise is given in Table 12.

% noise	estimated τ
1.0%	1.1291×10^{-16}
2.0%	6.1779×10^{-17}
3.0%	4.5353×10^{-17}
4.0%	3.6834×10^{-17}
5.0%	3.1432×10^{-17}
7.0%	2.4687×10^{-17}

Table 12: Results of identifying τ

4.5 Forward or Simulation Problem with General Polarization Models

We begin with the differential equation (8) and develop a variational form of the problem much as described in Section 4.1. The time and polarization variables are scaled in the same fashion, but we do not apply the method of mappings to scale the space variable. In order to model materials of various thicknesses, we allow the computational domain to be of arbitrary size, i.e., $\tilde{\Omega} = [0, l]$ for $l > 0$. (The right boundary of the material domain is also not required to be $z_2 = l$ but must coincide with one of the nodes in the spatial discretization. Hence, $z_2 = \bar{z}_R^N, \Omega = [\bar{z}_L^N, \bar{z}_R^N]$, and $\Omega_0 = \tilde{\Omega} - \Omega$. For our examples we will always take $z_2 = l$.) We allow a more general problem by considering both the supraconductive boundary condition at $z = l$ or allowing an absorbing boundary condition like the one at $z = 0$. Although it is not a generally used part of these models, we also retain the possibility of instantaneous polarization. Hence, $\epsilon_r \geq 1$. Also, we will assume a zero initial condition for the electric field.

Our more general weak form of the equation is

$$
\begin{aligned}
&\langle \mu_0 \epsilon \ddot{E}, \phi \rangle + \langle \mu_0 \sigma \dot{E}, \phi \rangle + \langle \mu_0 \ddot{P}, \phi \rangle \\
&\quad + \langle E', \phi' \rangle + \frac{1}{c} \dot{E}(t, 0) \phi(0) + \frac{1}{c} \dot{E}(t, l) \phi(l) = -\langle \mu_0 \dot{J}_s(t, \cdot), \phi \rangle
\end{aligned}
$$

The new term is a contribution of the absorbing boundary condition at $z = 1$ and the inner product has been redefined as $\langle \psi, \phi \rangle = \int_0^l \psi(z) \phi(z) dz$.

The Galerkin finite element approximation proceeds as in Section 4.1. Our two cases for the boundary condition at $z = l$ are implemented by either retaining or omitting the function $\phi_N^N(z)$ from the finite dimensional space of test functions. Let $\bar{N}$ denote the index of the highest test function included and $V^{\bar{N}} = \text{span}\{\phi_0^N, \phi_1^N, \ldots, \phi_{\bar{N}}^N\}$ be the space spanned by these functions. The supraconductive boundary is implemented with $\bar{N} = N-1$ while the absorbing boundary condition is implemented with $\bar{N} = N$.

For polarization, we use the weak form of equation (11). Applying the same scaling as before ($\tilde{t} = ct, \tilde{P} = P/\epsilon_0$) and using the approximation of E in equation (61) we obtain the following variational equations:

$$\sum_{i=0}^{\bar{N}} \ddot{e}_i(t)\langle \epsilon_r \phi_i, \phi\rangle + \langle \int_{-t}^{0} \alpha(s,\cdot) \sum_{i=0}^{\bar{N}} \dot{e}_i(t+s)\phi_i ds, \phi\rangle + \sum_{i=0}^{\bar{N}} \dot{e}_i(t)\langle \gamma\phi_i, \phi\rangle$$
$$+ \sum_{i=0}^{\bar{N}} e_i(t)\langle \phi_i', \phi'\rangle + \sum_{i=0}^{\bar{N}} \dot{e}_i(t)\phi_i\phi\Big|_{z=0,l} = -\eta_0\langle \dot{J}_s, \phi\rangle \tag{85}$$

We find the variational form of the equation by allowing $\phi = \phi_j$ for ϕ_j in $V^{\bar{N}}$, obtaining a system of size $\bar{N}+1$. For a function $\alpha(t,z)$ which varies in both variables, the integral term becomes:

$$\sum_i \int_{-t}^{0} \dot{e}_i(t+s)\langle \alpha(s)\phi_i, \phi_j\rangle ds$$

We make the following definitions:

$$\begin{aligned} M_{ij}^r &= \langle \epsilon_r \phi_i, \phi_j\rangle \\ \hat{M}_{ij} &= \langle I_\Omega(\eta_0\sigma(\cdot) + g(0,\cdot))\phi_i, \phi_j\rangle + \phi_i\phi_j|_{z=0,l} \\ K_{ij} &= \langle \phi_i', \phi_j'\rangle \\ A(t)_{ij} &= \langle I_\Omega \alpha(t,\cdot)\phi_i, \phi_j\rangle \end{aligned} \tag{86}$$

Note that $A(t) = [A(t)]_{ij}$ is a time-varying matrix-valued function, while $M^r, \hat{M}$ and K are constant matrices of size $\bar{N}$. We can now write our system as:

$$M^r\ddot{e} + \hat{M}\dot{e} + \int_{-t}^{0} A(s)\dot{e}(t+s)ds + Ke = f(t) \tag{87}$$

and $f(t) = -\eta_0\dot{J}_s(t)\hat{e}_1$ where $\hat{e}_1$ is the unit vector with 1 in the first component.

4.5.1 Galerkin Methods for the History Approximation

We choose a method for approximating the history of $\dot{e}(t)$ which maintains the same order of accuracy as the discretization of the rest of the problem. This is because the order of the accuracy of the solution is limited by the lowest order in accuracy of each of its parts. To do this, we use a Galerkin discretization of the history variable on a finite domain with a degree matching the degree of the discretization in the space variable z. For all of the results presented here, we use degree one elements for each approximation. We can limit the history variable to a finite domain because the hysteresis models of interest to us are all fading memory models, i.e., the kernel function α decays to zero as $s \to -\infty$. The integral over the history of the electric field with this kernel function can be well approximated by truncating it to a sufficiently long interval.

We consider an abstract problem with the appropriate conditions to approximate the history. Let $u(t,s)$ denote the solution to this problem and represent the truncated history of $\dot{e}$ with finite duration r via $u(t,s) = \dot{e}(t+s)$ for $(t,s) \in [0,\infty) \times [-r,0]$. By its relationship to $\dot{e}$, we see that $u(t,s)$ satisfies,

$$\frac{d}{dt}u(t,s) = \frac{d}{ds}u(t,s) \tag{88}$$

The appropriate initial condition is $u(0,s) = 0$ since $\dot{e}(s) = 0$ for all $s < 0$. For boundary conditions, we suppose that the state variable $\dot{e}(t)$ is known at all times t, and we can thus impose the boundary condition $u(t,0) = \dot{e}(t)$. Since it is a first order hyperbolic problem, there is a unique solution specified by $u(t,s) = 0$ when $t < -s$ and $u(t,s) = \dot{e}(t+s)$ when $t > -s$.

We create a Galerkin finite element approximation in the history variable s, much as done for the space variable z in Section 4.1. Let ψ_i^M be continuous basis functions defined on the interval $[-r,0]$ with inner product $\langle \psi_i, \psi_j \rangle = \int_{-r}^{0} \psi_i(s)\psi_j(s)ds$. There are a number of choices one might make for these elements, e.g., piecewise linear, quadratic, or higher order polynomial elements. Since our space variable approximations were made with piecewise linear elements, we chose the same type of elements here for compatibility of order. These functions are defined on the uniform grid $\bar{s}_i = -r + \frac{r}{M} i$ for $i = 0, \ldots, M$ where $\psi_i(\bar{s}_j) = \delta_{ij}$.

The past history of $\dot{e}$ is approximated as an element of the space spanned by these basis functions:

$$u(t,s) \approx u^M(t,s) = \sum_{i=0}^{M} u_i(t)\psi_i(s). \tag{89}$$

Recall that $\dot{e}$ is a vector of size $\bar{N}$, and so each of the u_i are vectors of the same size. Let the matrix U denote these unknowns taken together as rows:

$$\begin{aligned} U(t) &= \begin{bmatrix} u_0(t) \\ u_1(t) \\ \vdots \\ u_M(t) \end{bmatrix} \\ &= \begin{bmatrix} u_0^{(1)}(t) & u_0^{(2)}(t) & \cdots & u_0^{(\bar{N})}(t) \\ u_1^{(1)}(t) & u_1^{(2)}(t) & \cdots & u_1^{(\bar{N})}(t) \\ \vdots & \vdots & \ddots & \vdots \\ u_M^{(1)}(t) & u_M^{(2)}(t) & \cdots & u_M^{(\bar{N})}(t) \end{bmatrix} \end{aligned} \tag{90}$$

Storing the coefficients u_i as rows in this matrix means that the operators we will derive for the history-evolution are applied on the *left* side of U. This was deliberately chosen to simplify the numerical implementation, since one of these operators needs to be inverted, and the available linear-algebra routines work with matrices applied on the left. Matrices representing operators in the space variable will be applied to the right side of U or to the left side of U^T.

4.5.2 Approximating the history of $\dot{e}(t)$

We consider two different methods for finding approximate solutions to equation (88) which differ in their variational form of the expression and how the boundary condition is imposed. The first method is to use a variational form which implies no boundary conditions, consider its resulting finite dimensional approximation, and then use the approximate boundary condition to eliminate an equation and unknown from the system. We will see that this approach has a particularly simple implementation. The second is to write a variational form of the equation which imposes the boundary condition in a weak sense. Care must be taken in this approach not to introduce a spurious boundary condition at the other boundary $s = -r$.

Imposing $\mathbf{u(t,0)} = \mathbf{\dot{e}(t)}$ exactly: Consider the trivial variational form:

$$\langle u_t, \psi \rangle = \langle u_s, \psi \rangle \tag{91}$$

No boundary conditions are implied in a variational sense by this equation, since no integration by parts is performed in order to relate it to the original PDE (88). We create a finite-dimensional version by restricting ψ to members of the basis set ψ_i in equation (91) and using the approximation (89) The following system of equations results:

$$\mathcal{M}\dot{U} = WU \tag{92}$$

where $\mathcal{M}_{ij} = \langle \psi_i, \psi_j \rangle$ and $W_{ij} = \langle \dot{\psi}_i, \psi_j \rangle$.

This system is determined in the sense that the derivative is well-defined, but it is not clear which PDE it approximates, since it has nothing to say about the boundary condition necessary in a well-posed continuous problem. We consider the system of equations (92) too large by one equation and one unknown, which we eliminate with the auxiliary condition arising from the boundary data. Using the same approximation (89) for $u(t, s)$ we find,

$$\sum_{i=0}^{M} u_i(t)\psi_i(0) = \dot{e}(t). \tag{93}$$

We assume that $\psi_M(0) \neq 0$ (which is the case for the piecewise linear spline approximations used here) and solve for the coefficient $u_M(t)$. We obtain

$$u_M(t) = \frac{1}{\psi_M(0)} \left(\dot{e}(t) - \sum_{i=0}^{M-1} u_i(t)\psi_i(0) \right). \tag{94}$$

For the elements we use in the numerical simulations, this reduces to $u_M(t) = \dot{e}(t)$ because $\psi_i(0) = \delta_{0i}$.

We seek a simple way of implementing the removal of the coefficient $u_M(t)$ from the system of equations (92). We can use Gaussian row-reduction to eliminate $\dot{u}_M$ from the left-hand side, and then substitute the expression (94) wherever $u_M(t)$ appears on the right. This produces a smaller system of the form: $\bar{\mathcal{M}}\dot{\bar{U}} = \bar{W}\bar{U} + v\dot{e}(t)$, where v is a vector of coefficients.

We avoid this process by noting that the same process of Gaussian operations can be applied just as well to both sides of equation (92) after performing the matrix-vector multiplication, as they can to the matrix system itself. This allows us to substitute the value of $u_M(t)$ in equation (94) before the elimination operations.This yields the following procedure for evaluating the derivative of the reduced system (which is missing $u_M(t)$).

1. Compute the correct boundary value of $u_M(t)$ from (94)

2. Compute $\dot{U}$ from equation (92) using the entire state $u_i, i = 1, \ldots, M$.

This also produces a value for $\dot{u}_M(t)$ which we ignore as the evolution of this term is determined by the boundary condition.

Another possible advantage of this method is that the boundary condition is satisfied exactly, instead of in a weak sense. The effects of this on the quality of the rest of the approximation are not known. Since the above method departs from the standard finite-element approach, we can no longer say that our approximation of u is the least-squares projection into the finite-dimensional subspace. For this reason we consider another approximation scheme which imposes the boundary condition as part of the weak form.

Imposing the Condition $\mathbf{u(t,0)} = \dot{\mathbf{e}}\mathbf{(t)}$ weakly: As the variational formulation of the problem we choose,

$$\langle u_t, \psi \rangle = -\langle u, \psi_s \rangle - \psi(-r)u(-r) + \dot{e}(t)\psi(0) \tag{95}$$

This implies that $u_t = u_s$ and $u(0) = \dot{e}(0)$ under the standard variational arguments. Notice that the term $-\psi(-r)u(-r)$ cancels a term which would otherwise yield the condition $u(-r) = 0$ after integration by parts.

In the usual manner, we find a system of differential equations from the variational form (95).

$$\begin{aligned}\sum_{i=0}^{M} \dot{u}_i(t)\langle \psi_i, \psi_j \rangle = &-\sum_{i=0}^{M} u_i(t)\langle \psi_i, \dot{\psi}_j \rangle \\ &-\sum_{i=0}^{M} u_i(t)\psi_i(-r)\psi_j(-r) + \dot{e}(t)\psi_j(0).\end{aligned} \tag{96}$$

We define the matrices $\mathcal{M}, \mathcal{W}$ by $\mathcal{M}_{ij} = \langle \psi_i, \psi_j \rangle$ and $\mathcal{W}_{ij} = \langle \psi_i, \dot{\psi}_j \rangle + \psi_i(-r)\psi_j(-r)$, then express the system of differential equations (96) in matrix form as

$$\mathcal{M}\dot{U}(t) = -\mathcal{W}U(t) + \Psi \dot{e}(t)^T \tag{97}$$

where $\Psi(0) = (\psi_0(0), \psi_1(0), \ldots, \psi_M(0))^T$. We note that the $M+1$ rows of U are vector valued functions in $\mathbb{R}^{1\times \bar{N}+1}$. This differs from the convention of treating e and $\dot{e}$ as column vectors, hence, the appearance of $\dot{e}^T$ in equation (97).

The matrix equation (97) is appropriate for implementation, however we seek to simplify the implementation further. Through integration by parts we find

$$\begin{aligned}\mathcal{W}_{ij} &= \langle \psi_i, \dot{\psi}_j \rangle + \psi_i(-r)\psi_j(-r) \\ &= -\langle \dot{\psi}_i, \psi_j \rangle + \psi_i \psi_j|_{-r}^{0} + \psi_i(-r)\psi_j(-r) \\ &= -W_{ij} + \psi_i(0)\psi_j(0) \\ &= -W_{ij} + \Psi \cdot \Psi^T\end{aligned}$$

where $W_{ij} = \left\langle \dot{\psi}_i, \psi_j \right\rangle$ and equation (97) becomes:

$$\begin{aligned}\mathcal{M}\dot{U} &= WU - \Psi\Psi^T U + \Psi \dot{e}(t)^T \\ &= \hat{W}U + \Psi \dot{e}(t)^T\end{aligned}$$

where $\hat{W}_{ij} = W_{ij} - \psi_i(0)\psi_j(0)$. This equation can also be written as: $\mathcal{M}\dot{U} = WU + \Psi(\dot{e}(t)^T - \Psi^T U)$. Here we can more clearly see the presence of the boundary condition in the weak form. The boundary condition can itself be expressed as $\dot{e}(t)^T = \sum_{i=1}^{M} \psi_i(0) u_i = \Psi^T U$.

Note that the time varying terms in equation (97) are very few provided that for only a few i, $\psi_i(0) \neq 0$. For the standard first-order splines we use, $\psi_i(0) = \delta_{iM}$ so only one element is non-zero.

4.5.3 Implementing the Hysteresis Term

We express the integral term in equation (87) in terms of the Galerkin approximation. We have

$$\begin{aligned}\int_{-t}^{0} A(s)\dot{e}(t+s)ds &\approx \int_{-r}^{0} A(s)u(t,s)^T ds \\ &\approx \int_{-r}^{0} A(s)u^M(t,s)^T ds \\ &= \int_{-r}^{0} A(s)\sum_{j=0}^{M} u_j^T(t)\psi_j(s)ds\end{aligned}$$

$$
\begin{aligned}
&= \sum_{j=0}^{M} \int_{-r}^{0} A(s)\psi_j(s)ds\, u_j^T(t) \\
&= \sum_{j=0}^{M} A^j u_j^T(t) \qquad (98)
\end{aligned}
$$

where $A^j = \int_{-r}^{0} A(s)\psi_j(s)ds$. Recall that $A(s)$ is a matrix function, and so the A^k are matrices of size $\bar{N}+1 \times \bar{N}+1$, where the ij element of A^k is:

$$
A_{ij}^k = \int_{-r}^{0} \langle A(s,\cdot)\phi_i, \phi_j\rangle \psi_k(s)ds. \qquad (99)
$$

This gives us the complete discretization of the history terms in the second order system of equations (87), which we now can write as:

$$
\begin{aligned}
M^r \ddot{e} + \hat{M}\dot{e} + \sum_{k=0}^{M} A^k u_k^T + Ke &= f(t) \\
\mathcal{M}\dot{U} + \mathcal{W}U &= \Psi \dot{e}^T
\end{aligned}
$$

where $f(t) = -\eta_0 \dot{J}_s(t)\hat{e}_1$ and $\Psi = (\psi_1(0), \psi_2(0), \ldots, \psi_M(0))^T$. We convert this system to first order by letting $x = e$, $y = \dot{e}$.

$$
\begin{aligned}
\dot{x} &= y \\
M^r \dot{y} &= -\hat{M}y - Kx - \sum_{k=0}^{M} A^k u_k^T + f(t) \qquad (100) \\
\mathcal{M}\dot{U} &= -\mathcal{W}U + \Psi y^T. \qquad (101)
\end{aligned}
$$

The state variables of the system we need to solve are the length $\bar{N}+1$ vectors x,y and the $M+1 \times \bar{N}+1$ matrix U. The matrices A^k, K, M, and $\hat{M}$ are as defined in equations (86). The matrices $\mathcal{M}$ and $\mathcal{W}$ and the vector Ψ depend only on the basis functions chosen for the history approximation, while $M^r, \hat{M}$ and the A^ks depend on physical parameters we will want to estimate.

4.5.4 Specific Implementation: Constant Material Parameters

We consider the special case of materials which are homogeneous throughout the domain Ω. Functions which describe dielectric properties of these materials are constants modulated by the indicator function of the domain Ω. These are given by

$$\begin{aligned}
\sigma(z) &= \sigma I_\Omega(z) \\
\epsilon_r(z) &= 1 + I_\Omega(z)(\epsilon_r - 1) \\
\alpha(s, z) &= \alpha(s) I_\Omega(z) \\
g(0, z) &= g_0 I_\Omega(z)
\end{aligned} \tag{102}$$

We have introduced new parameters σ and g_0 for the conductivity and zero value of g, and the kernel function $\alpha(s)$.

As in Section (4.1), we further assume that the boundaries of the material coincide with the domains which define the test functions. This way, the material parameters are constant over each domain over which an integral is evaluated. The matrices in (86) become

$$\begin{aligned}
M^r &= M + (\epsilon_r - 1) M_\Omega \\
\hat{M} &= (\eta_0 \sigma + g_0) M_\Omega + B \\
A(s) &= \alpha(s) M_\Omega
\end{aligned}$$

where

$$\begin{aligned}
M_{ij} &= \langle \phi_{i-1}, \phi_{j-1} \rangle \\
M_{\Omega ij} &= \langle I_\Omega \phi_{i-1}, \phi_{j-1} \rangle \quad \text{and} \\
B_{ij} &= \phi_{i-1}(0)\phi_{j-1}(0) + \phi_{i-1}(1)\phi_{j-1}(1),
\end{aligned}$$

representing the contributions of the boundary conditions. For the case of a supracondicting boundary at $z = 1$ then $B_{ij} = \phi_{i-1}(0)\phi_{j-1}(0)$ and the space of test functions is reduced to $V_R^N = \mathrm{span}\{\phi_0^N, \ldots, \phi_{N-1}^N\}$.

We use equation (99) to find the specific form of the matrices A^k:

$$A_{ij}^k = \int_{-r}^{0} \langle \alpha(s, \cdot)\phi_i, \phi_j \rangle \psi_k(s) ds$$

$$
\begin{aligned}
&= \int_{-r}^{0} \alpha(s) M_{\Omega ij} \psi_k(s) ds \\
&= M_{\Omega ij} \int_{-r}^{0} \alpha(s) \psi_k(s) ds
\end{aligned}
$$

So

$$A^k = M_\Omega \alpha_k$$

where $\alpha_k = \int_{-r}^{0} \alpha(s)\psi_k(s)ds$. Letting $\alpha = (\alpha_0, \ldots, \alpha_M)^T$ we can express the approximation of the hysteresis approximation in equation (98) as

$$
\begin{aligned}
\int_{-r}^{0} A(s)\dot{e}(t+s)ds &= \int_{-r}^{0} A(s)u(t,s)^T ds \\
&\approx \sum_{j=0}^{M} \alpha^j u_j^T(t) \\
&= \sum_{j=0}^{M} M_\Omega \alpha_j u_j^T \\
&= M_\Omega U^T \alpha.
\end{aligned}
$$

The full system of equations (100) is now:

$$
\begin{aligned}
\dot{x} &= y \\
(M + M_\Omega(\epsilon_r - 1))\dot{y} &= -((\eta_0\sigma + g_0)M_\Omega + B)y - Kx - M_\Omega U^T \alpha + f(t) \\
\mathcal{M}\dot{U} &= -\mathcal{W}U + y\Psi^T
\end{aligned} \tag{103}
$$

where the last equation may still be replaced with:

$$\mathcal{M}\dot{U} = \hat{W}U + \Psi y^T.$$

4.6 Results of Simulations with the General Model

4.6.1 Hysteresis Representation of Debye Model

We measure the accuracy of solutions to the general polarization model by comparing them with those obtained from the differential Debye model of Section 4.1. The correct function to be used in the general polarization model to represent a Debye material is found from the variation of constants solution to the differential equation.

In the scaled version of the equations we have:

$$\dot{P} + \psi P = \epsilon_d \lambda E.$$

Use of an integrating factor yields:

$$P(t) = \int_0^t g(t-\xi)E(\xi)d\xi$$

where $g(s) = \epsilon_d \lambda e^{-\lambda s}$. From this we calculate:

$$\ddot{P}(t) = \int_{-t}^0 \dot{g}(-s)\dot{E}(t+s)ds + g(0)\dot{E}(t). \tag{104}$$

The function α which appears in the definitions (102) is $\alpha(s) = -\epsilon_d \lambda^2 e^{\lambda s}$ and the remaining parameters are: $\epsilon_r = \epsilon_\infty$, $g_0 = \epsilon_d \lambda$.

We compute the solution to a test problem using both the differential and hysteresis Debye polarization models. The results are summarized in Table 4.6.1. The physical parameters are $\sigma = 0.0, \epsilon_\infty = 5.5, \epsilon_s = 80.1$ and $\tau = 8.1 \times 10^{-12}$ and the simulation is run to $t = 1.67 \times 10^{-9}$. The boundaries of the material medium are $z_1 = 0.005$ and $z_2 = 0.1$. The discretization in space is a first-order finite element approximation with $N = 100$ in for both the differential and hysteresis models. The hysteresis simulations also use a first-order finite element approximation in the history variable. That is, the functions ϕ_i and ψ_i are both piecewise linear functions defined on discretizations of the intervals $z \in [0, l]$ and $s \in [-r, 0]$ respectively.

The maximum difference is computed as $\|e_d - e_h\|_\infty$ and the percent difference is $\|e_d - e_h\|_\infty / \|e_d\|_\infty$, where e_d and e_h are the solutions obtained from the differential and hysteresis models respectively. The last column is an average value of the actual computer time in seconds taken to solve the test problem. These figures should be contrasted with the 6.65 seconds time for the differential Debye simulation using the

r	M	Δs	Max Difference	% Difference	execution time
0.02	5	4.0×10^{-3}	0.4038	1.04	36.08
0.02	7	2.86×10^{-3}	0.5705	1.47	40.27
0.02	10	2.0×10^{-3}	0.6824	1.76	46.09
0.02	20	1.0×10^{-3}	0.6662	1.73	68.29
0.03	7	4.28×10^{-3}	0.4011	1.04	40.13
0.03	10	3.0×10^{-3}	0.1119	0.29	45.79
0.03	15	2.0×10^{-3}	0.0149	3.84×10^{-2}	56.3
0.03	30	1.0×10^{-3}	0.0120	3.10×10^{-2}	91.13
0.04	10	4.0×10^{-3}	0.3101	0.801	45.92
0.04	13	3.08×10^{-3}	0.1117	0.289	51.93
0.04	20	2.0×10^{-3}	0.0223	5.94×10^{-2}	67.75
0.04	40	1.0×10^{-3}	0.0016	4.24×10^{-3}	113.44

Table 13: Comparison of General and Differential Debye Simulations

same discretization in the space variable. We see that agreement between the two methods is very good when sufficiently accurate discretizations of the history variable are used. This requires that a sufficiently long history be retained in the simulation (as measured by r) and a sufficiently fine discretization of this interval (measured by $\Delta s = r/M$). The results show that a history duration of at least $r = 0.03$ (about 10 ns, in the unscaled time variable) is necessary for results with small relative error.

Comparing results from the table, we see that similar results are obtained by $M = 10, r = 0.03$ and $M = 13, r = 0.04$ while the computation with $M = 13$ takes about 14% longer to execute. Although more accurate results are obtained for higher values of M with $r = 0.04$ than with $r = 0.03$, these are only incremental improvements in the quality of the simulation. Since we are interested in the inverse problem which requires repeated simulations of the system, the time of execution is a primary concern.

We show graphically in Figure 21 the close fit of results generated with the two formulations (i.e., differential Debye versus hysteretic Debye polarization models).

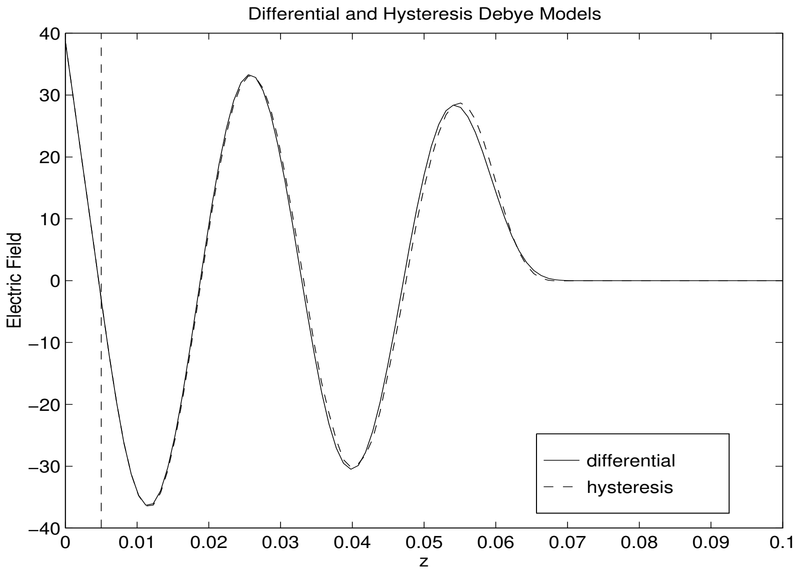

Figure 21: Results from Differential and Hysteresis Debye Models

This plot is for $M = 4$ and $r = 0.03$ in the hysteresis formulation. For more accurate simulations the graphs are indistinguishable in the plot. Figure 22 exhibits a case where an insufficiently refined discretization of the history variable leads to a very poor approximation. This result was computed with $M = 3$ and $r = 0.03$.

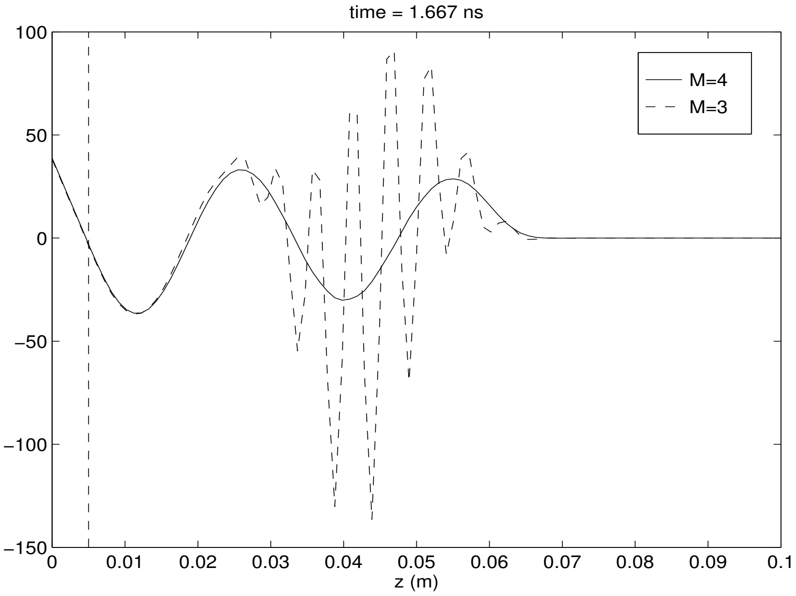

Figure 22: Breakdown of Hysteresis Debye Model

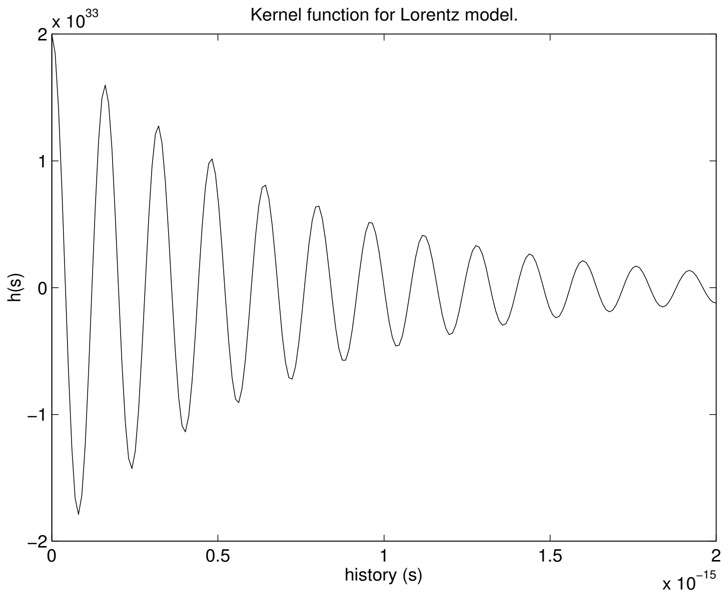

Figure 23: Hysteresis kernel for Lorentz model with $\tau = 3.57 \times 10^{-16}$

4.6.2 Hysteresis Representation of Lorentz Model

The representation of the Lorentz model of polarization is plagued by computational difficulties which make it impractical for simulations.

The plot of the hysteresis kernel using the parameter values used in the inverse problem of Section 4.4 is given in Figure 23. This function is the derivative of the impulse response function which appears in the variation of constants solution to the differential equation. Because of the oscillatory nature of the function, a much finer approximation of the history variable is required, making the size of the resulting system of equations prohibitively large. For example, the plot of the kernel function in Figure 23 suggests that a history duration of $r = 2 \times 10^{-15}$ is necessary before the kernel function drops to a level where it can be neglected. This includes twelve complete oscillations. To approximate this function accurately would require on the order of 36 basis elements in the Galerkin discretization of the history variable, allowing for a meager three elements per cycle.

Furthermore, stability requirements limit the discretization in time of the entire system to being no larger than the discretization of the history variable. This arises from the discretization of the evolution equation of u in equation (88). The resulting discretizations in equations (92) and (97) are subject to a stability condition which limits the size of the discretization in time. Since we do not want the propagation speed of the numerical scheme ($\Delta s/\Delta t$) to be faster than the actual propagation speed of the solutions (1, in the scaled variables), the time step can be no larger than the discretization used in the history variable. In the example considered here, the resulting discretization in the history variable would be approximately $\Delta s = 5.6 \times 10^{-17}$, suggesting a time step of similar size. (The similar differential problem in Section 4.3 required an even smaller step size of 1.0×10^{-17} for an accurate result.) A simulation of duration 6.67×10^{-14} (as used in the inverse problem of Section 4.4) would require about 1200 steps. Because of the large number of basis elements in the history variable, the resulting computation is prohibitively expensive.

4.7 Inverse or Estimation Problem with General Polarization Model

Having successfully duplicated the quantitative behavior of the Debye model of polarization with a hysteretic polarization model, we turn to using this method of simulation in an inverse problem. Different inverse problems can be formulated in this way depending on the way in which the hysteresis kernel depends on the set of parameters being optimized. One option is to express the kernel as a function of the same set of parameters which appear in the differential equation, $\sigma, \epsilon_d, \epsilon_\infty$ and τ and hence in the variation of constants solution. For the Debye differential equation, this function was computed in Section 4.6.1 as $g(s) = \epsilon_d \lambda e^{-\lambda s}$ and the kernel function is

$\alpha(s) = -\epsilon_d \lambda^2 e^{\lambda s}$. As noted in Section 4.2 optimizing over the parameter $\lambda = 1/c\tau$ instead of τ in the differential Debye polarization model improved the performance of the optimization problem.

As an alternative to representing the Debye kernel as a function of the Debye physical parameters, we can attempt to reconstruct it directly. From equation (12) we see that recovering the hysteresis function $g(t)$ can only be done through identifying a suitable finite dimensional approximation of its derivative α, which appears in the integral term, and its value at zero, which appears in the damping term. Since we're interested in the case where $E(0,z) = 0$, the term κ is zero. Furthermore, in this case, the only appearances of the conductivity σ and the parameter $g(0)$ are both in the damping term. Therefore we do not expect to be able to recover these parameters separately. For the remainder of this problem, we consider $\sigma = 0$ and let $g(0)$ represent whatever actual conductivity the material may have.

To reconstruct the hysteresis kernel α we attempt to find optimal values for the coefficients in a Galerkin finite element approximation of this function. This Galerkin approximation is performed over a discretization of the history exactly as described in Section 4.5.1. To simplify the computations, the same basis elements are used to approximate the kernel function for the purpose of identification as are used in the simulation. Hence, the coefficients we seek to identify are directly related to the ones used in the forward simulation. Using the notation established in Section 4.5.1, $\mathcal{M}$ is the mass matrix arising from pair-wise inner products of the basis functions: $\mathcal{M}_{ij} = \langle \psi_{i-1}, \psi_{j-1} \rangle$. The values which appear in the forward simulation are $\alpha_k = \int_{-r}^{0} \alpha(s)\psi_k(s)ds$ and the coefficients of the Galerkin approximation of α are given by $h = \mathcal{M}^{-1}\alpha$, where the vector α is $\alpha = \langle \alpha_0, \alpha_1, \ldots, \alpha_M \rangle$ and $h = \langle h_0, h_1, \ldots, h_M \rangle$

We adopt a standard test problem for comparing the relative ease of reconstructing the hysteresis function through the Debye physical parameters and through Galerkin coefficients. The true values for the physical parameters are $\sigma = 0.0$, $\epsilon_\infty = 5.5$,

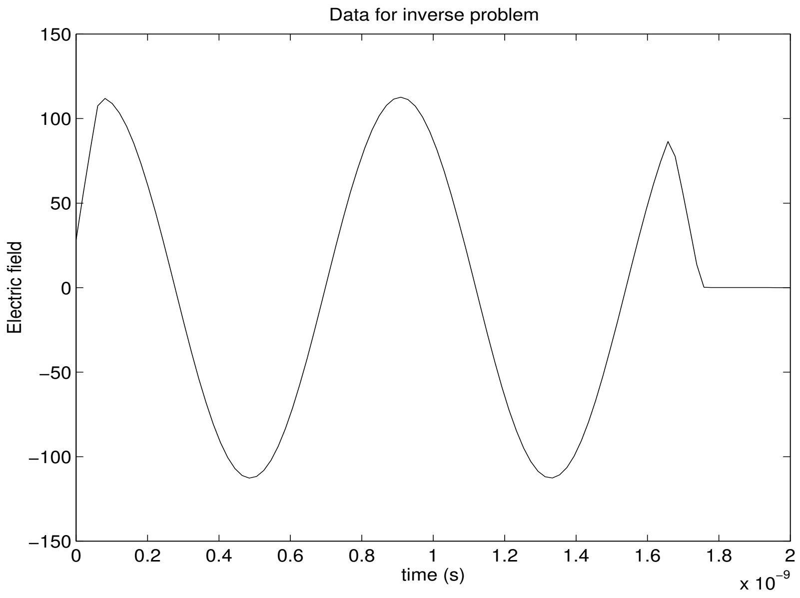

Figure 24: Data for Debye Test Problem

$\epsilon_s = 80.1$ and $\tau = 8.1 \times 10^{-12}$ (Again, these are the typical values for water). The data is gathered from a forward simulation of the problem using the differential Debye polarization model and is depicted graphically in Figure 24.

We attempt two inverse problems over different sets of parameters using this test problem. These different sets of parameters arise from the different ways of representing the Debye kernel function, either as a function of the Debye parameters or through the coefficients of a Galerkin approximation. Both of these inverse problems use the result of a forward simulation from the differential Debye model to provide the data. Since no noise is added, we expect to be able to reproduce the parameter values with a high degree of accuracy, depending on the precision of the hysteresis approximation. We do not attempt to identify the parameters σ and ϵ_∞. In Section 4.2 the low sensitivity of the objective function to these parameters was established. Instead, each of these parameters have their values fixed at the value used in generating the

M	estimated ϵ_s	estimated τ	residual	iterations
True values:	80.100	8.1000×10^{-12}		
Initial values:	83.8300	7.7142×10^{-12}		
4	81.3481	8.2190×10^{-12}	1.14808	14
5	79.7209	8.8766×10^{-12}	0.37468	11
6	80.4458	7.9891×10^{-12}	0.30911	9
7	79.9598	8.3541×10^{-12}	0.13821	10
8	80.2243	8.0389×10^{-12}	0.11429	8
9	80.0418	8.1978×10^{-12}	5.83645×10^{-2}	12
10	80.1558	8.0660×10^{-12}	5.19723×10^{-2}	14

Table 14: Results of estimating hysteresis Debye model from differential Debye data

data.

The results of fitting the hysteresis Debye model to data generated by the differential Debye model are summarized in Table 14. All of these attempts used $r = 0.03$ for the duration of the history approximation. The initial values for the two parameters were $\tau_0 = 7.7142 \times 10^{-12}, \epsilon_{s0} = 83.83$. These results demonstrate that a sufficiently accurate hysteresis implementation of the Debye model yields reasonable estimates for the parameter values in an inverse problem.

The identification of the Galerkin coefficients proved to be considerably more difficult than identification of the Debye model parameters. The "true" values for the parameters are found by taking the vector of coefficients α which are computed to perform the forward simulation and computing the coefficients of the Galerkin approximation h. These true values are then perturbed by 10% to generate the initial values used in the optimization. As summarized in Table 15, attempts to identify all of the coefficients h and the value of $g(0)$ generally failed to converge in a reasonable number of iterations. The results for $M = 4$ and $M = 6$ were taken before the program terminated and indicated convergence. (At the time that the values were taken, both programs had been running continuously for at least nine days.) We

M	h_0	$g(0)$	residual	Iterations
True values:	—	2264.20		
Initial values:	$h_0^* \times 1.1$	2490.63		
4*	-683759	2336.54	2.159×10^{-1}	900
5	-765083	2365.97	1.645×10^{-2}	188
6*	-809484	2349.39	1.323×10^{-1}	829

Table 15: Results from estimating all coefficients of kernel.

M	True h_0	Initial h_0
4	-640889	-704978
5	-706575	-777233
6	-753628	-828991

Table 16: True and initial values of h_0 for various M

report the values of the two parameters $g(0)$ and the first coefficient of the Galerkin approximation of the kernel h_0. Since the value h_0 depends on the discretization, its true and initial value both vary with M. These values are summarized in Table 16. This result strongly suggests that the problem is over parameterized. To alleviate this problem, we note that h_0 is considerably larger than the other coefficients, owing to the decaying exponential form of the kernel function. This parameter, along with the value of $g(0)$ are likely to have the most influence over the objective function, with the remaining coefficients playing minor roles. We attempt to identify just these two most significant parameters while holding the others fixed at their true values.

This smaller optimization problem also proved to be very difficult, although acceptable results were eventually obtained, as indicated by the results in Table 17. We see that this problem required a much larger number of iterations to attain convergence than the two parameter Debye estimation problem summarized in Table 14. One possible cause of the very slow convergence is suggested by the objective function. Figure 25 is a plot of the logarithm of the objective function over a narrow (5%)

M	h_0	$g(0)$	residual	iterations
True Values:	—	2264.20		
Initial Values:	$h_0^* \times 1.1$	2490.63		
4	-640888	2264.20	1.15539×10^{-5}	83
5	-706574	2264.20	1.63708×10^{-5}	80
6	-753625	2264.20	1.98944×10^{-5}	95

Table 17: Results of estimating $g(0)$ and h_0

range of reach of these parameters. We see that the minimizer lies at the bottom of a narrow trench. This is likely caused by the two coefficients g and h_0 being nearly interdependent in their influence on the solution. On one side of the trench we see that the values of the objective function rise slowly, while on the other they increase exponentially fast.

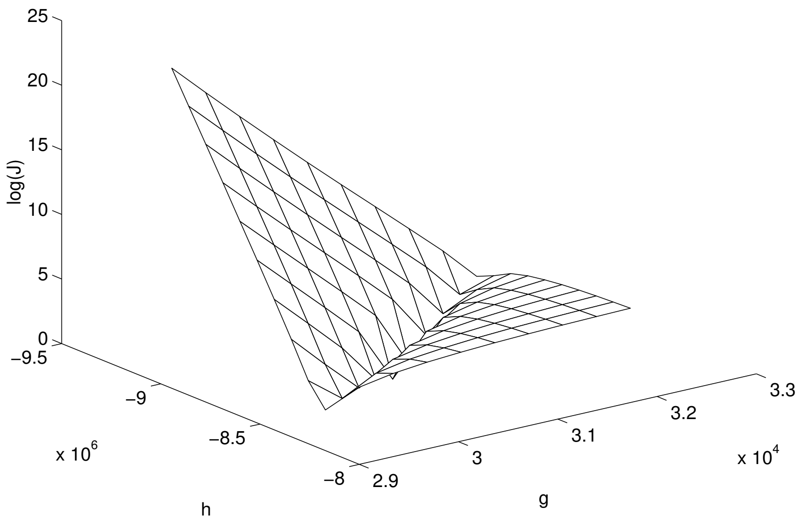

Figure 25: $\log J(g(0), h_0)$ for $M = 4$

Acknowledgment:

Both authors gratefully acknowledge Dr. Richard Albanese, U.S. Air Force Research Laboratory, Brooks AFB, San Antonio, TX for his continual encouragement and numerous specific technical discussions throughout the course of the research discussed in this report. His many suggestions and questions provided significant impetus for our research efforts.

References

[APM] R. Albanese, J. Penn and R. Medina, Short-rise-time microwave pulse propagation through dispersive biological media, J. of Optical Society of America A, **6** (1989), pp. 1441–1446.

[Bal] C.A. Balanis, *Advanced Engineering Electromagnetics,* J. Wiley & Sons, New York, 1989.

[Blo] F. Bloom, *Ill-Posed Problems for Integrodifferential Equations in Mechanics and Electromagnetic Theory,* SIAM Studies in Applied Math., Vol 3, SIAM, Philadelphia, 1981.

[BFW1] H.T. Banks, R.H. Fabiano and Y. Wang, *Estimation of Boltzmann damping coefficients in beam models,* Proceedings of COMCON Workshop on Stabilization of Flexible Structures, A.V. Balakrishnan and J.P. Zolesio, eds., Optimization Software Inc., New York, (1987) pp. 13-35.

[BFW2] H.T. Banks, R.H. Fabiano and Y. Wang, Inverse Problem Techniques for beams with tip body and time hysteresis damping, Mathematical Applications and Computations, **8** (1989), pp. 101-116.

[BSGII] H.T. Banks, D.S. Gillian and V.I. Shubov, Global solveability for damped abstract nonlinear hyperbolic systems, Differential and Integral Equations **10** (1997), pp. 309–332

[BIW] H.T. Banks, K. Ito and Y. Wang, Wellposedness for damped second order systems with unbounded input operators, Differential and Integral Equations **8** (1995), pp. 587–606.

[BJ] H.T. Banks and M.Q. Jacobs, The optimization of trajectories of linear functional differential equations, SIAM J. Control **8** (1970), pp. 461–488.

[BKo] H.T. Banks and F. Kojima, Boundary shape identification problems in two dimensional domains related to thermal testing of materials, Q. Appl. Math **47** (1989), pp. 273–293.

[BKoW] H.T. Banks, F. Kojima and W.P. Winfree, Boundary Estimation problems arising in thermal tomography, Inverse Problems **6** (1990) pp. 897–921.

[BMZ] H.T. Banks, N.G. Medhin and Y. Zhang, A mathematical framework for curved active constrained layer structures: Wellposedness and approximation, Numer. Funct. Anal. **17** (1996), pp. 1-22.

[BSW] H.T. Banks, R.C. Smith and Y. Wang *Smart Material Structures: Modeling Estimation and Control,* Masson/J. Wiley, Paris/Chichester, 1996.

[BZ] H.T. Banks and J. Zou, Regularity and approximation of systems arising in electromagnetic interrogation of dielectric materials, Technical Report CRSC-TR98-33, Center for Research in Scientific Computation, North Carolina State University, September 1998.

[BK] R.S. Beezley and R.J. Krueger, An electromagnetic inverse problem for dispersive media, J. Math. Phys. **26** (1985), pp. 317–325.

[BF] J.G. Blaschak and J. Franzen, Precursor propagation in dispersive media from short-rise-time pulses at oblique incidence, J. Opt. Soc. Am. A **12** (1995) pp. 1501–1512

[Bri] L. Brillion, *Wave Propagation and Group Velocity*, Academic, New York, 1960.

[Bui] D.D. Bui, On the well-posedness of the inverse electromagnetic scattering problem for a dispersive medium, Inverse Problems **11** (1995), pp. 835–863.

[Buk] M. Buksas *Modeling, Analysis and Implementaion of Forward and Inverse Problems in One Dimensional Electromagnetic Scattering with Differential and Hysteretic Polarization Models,* Doctoral Thesis, College of Physical and Mathematical Sciences, North Carolina State University, Raleigh, 1998

[CM] D. Colton and P. Monk, The detection of leukemia by electromagnetic waves, preprint

[CS] J. Corones and Z. Sun, Simultaneous reconstruction of material and transient source parameters using the invariant imbedding method, J. Math. Phys. **34** (1993), pp. 1824–1845

[Deb] P. Debye, *Polar Molecules*, Chem. Catalog Co., New York, 1929.

[FI] R.H. Fabiano, K.I. Ito, Semigroup theory and numerical approximation for equations in linear viscoelasticity, SIAM J. Math. Anal. **21** (1990), pp. 374-393.

[HFL] S.He, P. Fuks and G.W.Larson, An optimization approach to time-domain electromagnetic inverse problem for a stratified dissipative slab, IEEE T. Att. Prop. **44** (1996), pp. 1277–1282.

[HS] S. He and S. Ström, The electromagnetic scattering problem in the time domain for a dissipative slab and a point source using invariant imbedding, J. Math. Phys. **32** (1991), pp. 3529–3539.

[Hop] 1877

[Jac] J. D. Jackson, *Classical Electrodynamics,* 2nd Ed., J. Wiley & Sons, New York, 1975.

[Kri] K.L. Kreider, Time dependent direct and inverse electromagnetic scattering for the dispersive cylinder, Wave Motion **11** (1989), pp. 427–440.

[KK] G. Kristenson and R.J. Krueger, Direct and inverse scattering in the time domain for a dissipative wave equation. I. Scattering operators, J. Math. Phys. **27** (1986), pp. 1667–1682

[KK2] G. Kristenson and R.J. Krueger, Direct and inverse scattering in the time domain for a dissapative wave equation. II. Simultaneous reconstruction of dissipation and phase velocity, J. Math. Phys **27** (1986), pp. 1683–1693

[KK3] G. Kristenson and R.J. Krueger, Direct and inverse scattering in the time domain for a dissapative wave equation. III. Scattering operators in the presence of a phase velocity mismatch, J. Math. Phys **28** (1987), pp. 360–370.

[KK4] G. Kristenson and R.J. Krueger, Direct and inverse scattering in the time domain for a dissapative wave equation. Part 4. Use of phase-velocity mismatches to simplify inversions, Inverse Problems **5** (1989), pp. 375–388.

[Kru] R.J. Krueger, An inverse problem for a dissapative hyperbolic equation with discontinuous coefficients, Q. Appl. Math **34** (1976), pp. 129–147.

[Kru2] R.J. Krueger, An inverse problem for an absorbing medium with multiple discontunities, Q. Appl. Math **36** (1978), pp. 235–253.

[Kru3] R.J. Krueger, Numerical Aspects of a dissapative inverse problem, IEEE Trans. Att. Prop. AP-29 (1981), pp. 253–261.

[Ler] I. Lerche, Some singular, nonlinear integral equations arising in physical problems, Q. Appl. Math. **44** (1986), pp. 319–326.

[Lions] J.L. Lions, *Optimal Control of Systems Governed by Partial Differential Equations*, Springer-Verlag, New York, 1971.

[Paz] A. Pazy *Semigroups of Linear Operators and Applications to Partial Differential Equations,* Springer-Verlag, New York, 1983

[Pi] O. Pironneau, *Optimal Shape Design for Elliptic Systems*, Springer-Verlag, New York, 1983.

[PTVF] W.H. Press, S.A. Teukolsky, W.T. Vetterling, B.P. Flannery, *Numerical Recipies in Fortran*, 2nd Ed. Cambridge University Press, Cambridge, 1994.

[RGKM] V.G. Romanov, J. Gottlieb, I. Kabankhin and S.V. Martakov, An inverse problem for special dispersive media arising from ground penetrating radar, J. Inv. Ill-Posed Problems **5** (1997), pp. 175–192.

[St] J.A. Stratton, *Electromagnetic Theory,* McGraw-Hill, New York, 1941.

[Sun] Z. Sun, Direct scattering and reconstruction of internal sources, Wave Motion **16** (1992), pp. 249–263.

[VH] A.R. von Hippel, *Dielectric Materials and Applications*, J. Wiley, New York, 1954.

[Wloka] J. Wloka, *Partial Differential Equations*, Cambridge University Press, Cambridge, 1987.

[Wes] V.H. Weston, On the inverse problem for a hyperbolic dispersive partial differential equation, J. Math. Phys. **13** (1972), pp. 1952–1956.

[Wes2] V.H. Weston, Factorization of the dissapative wave equation and inverse scattering, J. Math. Phys. **29** (1988), pp. 2205–2218.

[Wol] L.V. Wolfersdorf, On an electromagnetic inverse problem for dispersive media, Q. Appl. Math. **49** (1991), pp. 237–246.